THE UNIVERSITY *of* EDINBURGH

THERE AND BACK AGAIN

A stretch receptor's tale

by

Thomas Suslak

School of Informatics

THE UNIVERSITY
of EDINBURGH

2015

"It's a pop song, it's not a doctoral thesis."

Sir Bob Geldof

(responding to criticism of Band Aid 30)

Ex sapientia ad ignorantiam

1. Abstract

Mechanotransduction is fundamental to many sensory processes, including balance, hearing and motor co-ordination. However, for such an essential feature, the mechanism(s) that underlie it are poorly understood. The mechanotransducing stretch receptors that relay information on the tonicity and length of skeletal muscles have been well-defined, particularly at the gross anatomical level, in a wide variety of species, encompassing both vertebrates and invertebrates. To date, there exists a wealth of data describing them, anatomically, as well as good electrophysiological data from stretch receptors of some larger organisms. However, comparatively few studies have succeeded in identifying putative mechanotransducing molecules in such systems. Nonetheless, this class of sensory mechanotransducers perhaps offer the best means of identifying molecules that permit the stretch-sensitivity of such endings, revealing new information about the underlying mechanisms of stretch receptors, and mechanoreceptors more generally.

However, a different approach is clearly needed; a theoretical approach, utilising mathematical modelling, offers a powerful means of pooling the current wealth of knowledge on the reported electrophysiological behaviour of muscle stretch receptors. This study, therefore, develops an extended theoretical model of a stretch receptor system in order to reproduce, *in silico*, the reported behaviour of both vertebrate and invertebrate stretch receptors, within the same modelling environment, thus enabling the first quantitative framework for comparing these data, and moreover, making predictions of the likely roles of specific molecular entities within a stretch receptor system.

Subsequently, this study utilises a model *in vivo* system to test these theoretical predictions. The genetic toolbox of *D. melanogaster* offers a wide range of tools that are extremely suitable for identifying mechanotransducing molecules in stretch receptors. However, very little is currently known about such endings in this organism. This study, therefore, firstly characterises a putative stretch receptor organ in larval *Drosophila,* the *dbd* neuron, via a novel experimental approach. It is shown that this neuron exhibits known properties of stretch receptors, as previously observed in other, similar organs. Furthermore, these observations bear out the predictions of the mathematical model.

Having defined the *dbd* neuron as a muscle stretch receptor, pharmacological and genetic assays in this system, combined with predictions from the mathematical model, identify a key role for the recently-discovered DmPiezo protein as an amiloride-sensitive,

mechanically-gated sodium channel (MNaC) in *dbd* neurons, with TRPA1 also acting in this system in a supporting role. These data confirm the essential role of an MNaC in mechanosensory systems, but also supply important evidence that, whilst the electrophysiological mechanisms in stretch receptors are remarkably similar across *taxa*, different species likely employ various molecular mechanisms to achieve this.

Acknowledgements

The following people and groups assisted this work and merit special mention for their contributions, without which this would not have been possible:

Douglas Armstrong [DTC/IANC, University of Edinburgh, UK] and Andrew Jarman [CIP, University of Edinburgh, UK] supervised this Ph.D.

Guy Bewick [IMS, University of Aberdeen, UK] proposed me for this Ph.D. and has collaborated with me, throughout, producing mammalian data, assisting in setting up the patch-clamp protocol and provided opportunities for lab visits to develop mechanostimulation.

Rod Scott [IMS, University of Aberdeen, UK] assisted in setting up the patch-clamp protocol, which was integral to this project.

Sonia Watson and Karen Thompson [Ph.D. students, IMS, University of Aberdeen, UK] greatly assisted me during my visits to the Bewick lab and have been valuable collaborators.

S.E. Kim [Scripps Research Institute**,** CA., USA] kindly donated fly lines for *DmPiezo* experiments.

B. Rydqvist [Karolinska Institutet, Stockholm, SWE] kindly made available software code for initial programming of the mechanotransduction model.

Jack McKay-Fletcher [4th year Honours student, Informatics, University of Edinburgh, UK] devised the novel analysis software, NEOX, enabling some of the data analysis.

Richard Ribchester [CIP, University of Edinburgh, UK] provided early support in acclimatisation to electrophysiology in *Drosophila*, including access to lab space and equipment.

Mike Shipston [CIP, University of Edinburgh, UK], kindly provided lab space for conducting the majority of my electrophysiological experiments.

This Ph.D. was supported in part by grants EP/F500385/1 and BB/F529254/1 for the University of Edinburgh School of Informatics Doctoral Training Centre in Neuroinformatics and Computational Neuroscience (www.anc.ac.uk/dtc) from the UK Engineering and Physical Sciences Research Council (EPSRC), UK Biotechnology and Biological Sciences Research Council (BBSRC), and the UK Medical Research Council (MRC).

Many thanks to the various members of the Jarman and Armstrong labs (past and present) for their friendship, support and purchases of cake.

Thanks also to my many and various colleagues in the School of Informatics and Centre for Integrative Physiology, and to my family and friends for their support and forbearance – you all know who you are. Special thanks are due to my long-suffering and ever-baking wife, although, in fairness, she knew what she was letting herself in for.

Declaration of Own Work

I confirm that all this work is my own except where indicated, and that:

1. I have read and understood the plagiarism rules & regulations in the research students' Code of Practice;
2. I have clearly referenced / listed all sources as appropriate;
3. I have referenced and appropriately indicated all quoted text of more than three words (from books, web, *etc*.);
4. I have given the sources of all pictures, data *etc*. that are not my own;
5. I have not made any use of the essay(s) of any other student(s) either past or present;
6. I have not submitted for assessment work previously submitted for any other course, degree or qualification, except as specified;
7. I have not incorporated any work from or used the help of any external professional agencies other than extracts from attributed sources;
8. I have acknowledged in appropriate places any help that I have received from others (*e.g.*, fellow students, teachers in schools, external sources);
9. I understand that any false claim for any of the above will mean that the relevant piece of work will be penalised in accordance with the University regulations;

Signed: _____ Date: _____

Thomas Suslak

List of contractions

2P: two-pore (of ion channels)

4-AP: 4-aminopyridine, a voltage-gated potassium channel blocker

Ca_v: voltage-gated calcium (channel)

Ch: chordotonal (organ), a fly mechanoreceptor

CNS: central nervous system

da: dendritic arborisation (neuron)

dbd: dorsal bipolar dendritic (neuron)

dbp: dorsal bipolar (neuron), another term for a *dbd* neuron

DEG/ENaC: degenerin/epithelial sodium (channel)

dNTP: deoxyribonucleotide triphosphate

DRG: dorsal root ganglion/ganglia

EGTA: ethylene glycol tetraacetic acid

EIPA: ethyl isopropyl amiloride, an MSC-blocker

HEPES: (4-(2-hydroxyethyl)-1-piperazine ethane sulfonic acid)

HMA: hexamethylene amiloride, an MSC-blocker

K_{Ca}: calcium activated potassium (channel)

md/MDN: multi-dendritic (neuron)

mGluR: metabotropic glutamate receptor

MKC: mechanosensory potassium channel

MNaC: mechanosensory sodium channel

MS: mechanosensitive (as descriptive of *e.g.*, proteins or a receptor organ)

MSC: mechanosensitive ion channel

MscK: a bacterial mechanosensory potassium channel

n.d.: no date (in citations)

NMDG: N-methyl-D-glucamin

n.s.: not significant (of statistical differences)

PLD: phospholipase-D

PNS: peripheral nervous system

SLV: synaptic-like vesicle

SRO: stretch receptor organ, a type of mechanoreceptor in arthropods

TEA: tetra-ethyl ammonium, a voltage-gated potassium channel blocker

TTX: tetrodotoxin, a voltage-gated sodium channel blocker

VKC: voltage-gated potassium channel

VNaC: voltage-gated sodium channel

List of tables and figures

Contents

1. Introduction

1.1. Overview of mechanosensation

Mechanotransduction, at a gross level, can be generally defined as the means by which kinetic stimuli, such as pressure, torsion, shear stress, stretching or physical pain are received by specialised receptors and converted to electrical impulses to the nervous system. These mechanoreceptors are diverse and each variety is specific to the sensory modality to which it pertains. Perhaps the most obvious means to illustrate the diversity of mechanoreceptors is to consider the specialised cells in human skin, which are utilised to sense what can be broadly categorized as Aristotelian touch [Aristotle, *n.d.*].

Delmas *et al.*, [2011] provide a useful summary of the various types of touch-sensitive cells found within the human dermis. These include the Pacinian corpuscles, which detect vibration of the skin, and Ruffini corpuscles, which detect dermal stretching. Whilst these are both varieties of touch sensation, these sensations are distinct, and thus, specialised receptors exist to detect each one [see **Fig. 1**]. Differences between these receptors are apparent at the anatomical level, as well as at a functional level, *e.g.*, variations in output spiking patterns, via which the detected stimuli are encoded, and it has long been known that the unique anatomy of a given receptor type is essential for specific information-coding [Weddell & Miller, 1962].

Thus, the laminar capsule of the Pacinian corpuscle plays an important role in reducing the sensitivity of that type of ending to static stimuli, ensuring its detection of rapid, dynamic vibrations are specific [Mendelson & Loewenstein, 1964] and it is only the encapsulated area of the corpuscle that is mechanosensitive [Ishiko & Loewenstein, 1959]. Furthermore, the activation of the corpuscle by a mechanical stimulus facilitates further activation, thus enabling Pacinian corpuscles to be effective vibration detectors [Loewenstein, 1958a; 1958b].

However, skin is far from the only site of mechanoreceptors. The sense of hearing also relies upon mechanosensory apparatus. Sound waves enter the ear and cause vibrations of the tympanum. These are transmitted, via the auditory ossicles, to the fluid of the cochlear duct, where they generate a mechanical force that stimulates mechanoreceptors [Marcotti, 2012]. In the inner ear, these mechanoreceptors are hair cells. Hair cells are specialised epithelial cells, each of which possess a mechanosensory stereocilium, projecting from the

apical membrane [Furness *et al.*, 2010]. Auditorily-generated waves in the fluid of the cochlear duct displace the basilar membrane, which vibrates to cause deflection of the hair cells. Each cell is tuned to detect a specific frequency, as determined by its position along the basilar membrane [Phillips *et al.*, 2008].

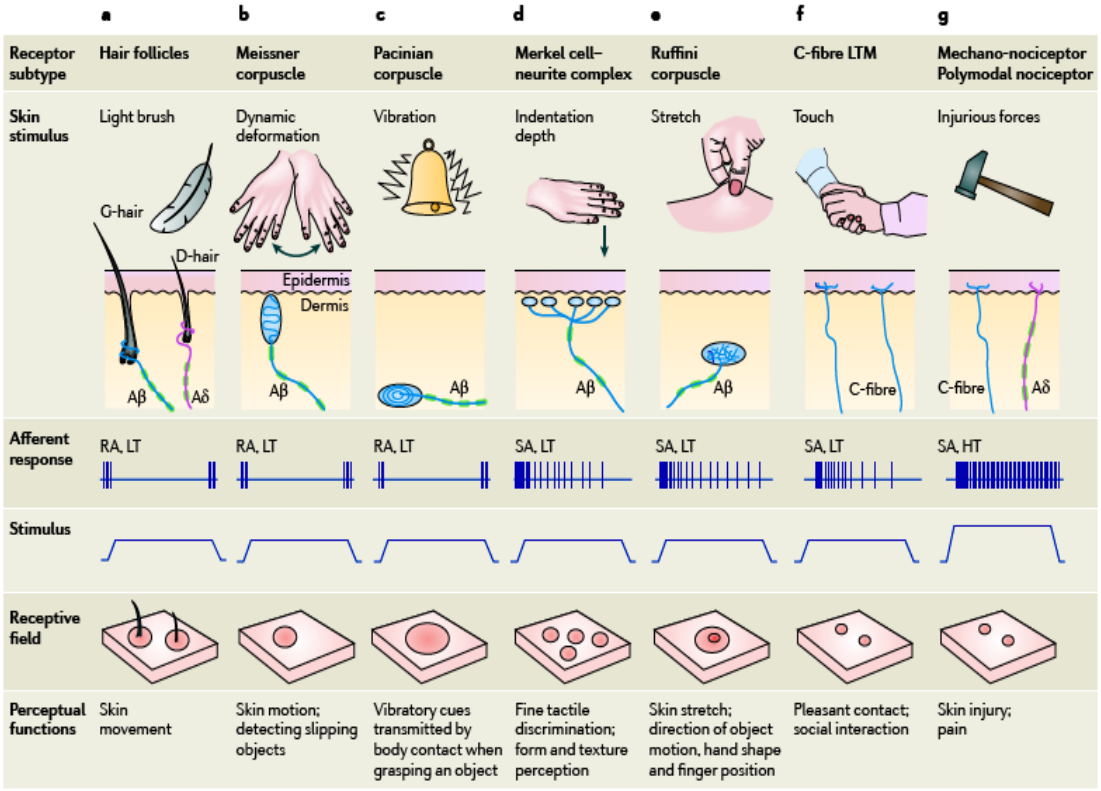

Figure 1: Mechanoreceptors are a diverse class of sensory endings, responsible for a wide range of sensory inputs. Many mechanoreceptors are found in the skin, where they are responsible for detecting the full gamut of external touch inputs that can be registered by the nervous system. Different sensations are registered by distinct receptor types, which vary in terms of gross anatomy and position within the skin, among other physical features. Additionally, the particular electrophysiological properties of each receptor type are largely unique, as typified by whether they are rapidly or slowly adapting (RA or SA, respectively) and whether their afferent spike generation is mediated by a high or low spiking threshold (HT or LT, respectively) [taken from Delmas *et al.*, 2011].

In addition to these various examples of mechanotransduction, it is also worth noting, briefly, that mechanosensitivity, as distinct from a neurological transduction process, can occur in other tissues, for example, the distension of the lungs, or vascular vessels, or digestive tract can be detected by the endothelial cells of these structures. Intracellular processes can then be triggered by detection of mechanical forces by endothelial cell

membranes [for example, see Chatterjee *et al.*, 2008]. However, such processes are not especially pertinent to the nature of the current enquiry and are merely mentioned here for the sake of completeness.

Unsurprisingly, then, mechanotransduction is a fundamental process that is important in all organisms. Mechanotransducers have been extensively studied in a variety of model species, including *D. melanogaster* and *C. elegans* [Goodman *et al.*, 2004; Kernan, 2007; Lumpkin *et al.*, 2010]. Within each species, an array of sense organs exist to detect the various kinetic stimuli that are important to that organism. Mechanosensation is also a feature of prokaryotes, which can sense osmotic pressure through mechanosensory mechanisms [Levina *et al.*, 1999]. This is vital in unicellular organisms, which maintain their membrane integrity in variable external environments, detecting osmotic pressure to regulate ion balance via downstream processes.

1.2. Muscle stretch receptors

In mammals, an important group of organs of homeostasis are the muscle spindles, which are essential for balance and proprioception. Each muscle spindle comprises a fibrous capsule, which encloses a section of muscle (the intrafusal muscle fibres), along with the sensory terminals of groups I and II afferent neurons and an associated motor neuron [see **Fig. 2**]. These organs form the sensory end of a proprioceptive feedback loop which regulates muscle tonicity, in order to maintain balance, *etc.* [Hunt, 1990].

In mammals, muscle spindles are located in all skeletal muscles, with the known exceptions of the lateral pterygoid and posterior digastric muscles [Lennartson, 1980]. Within the mass of the muscles, sections of between two and ten muscle fibres are enclosed by the fibrous capsule of the muscle spindle, delineating the intrafusal fibres. The capsule further encloses the afferent terminals of myelinated 1a afferent neurons. The stretching of the intrafusal fibres stimulates these nerves, which relay information regarding muscle length and tonicity to the CNS [Fitz-Ritson, 1982].

The electrical properties of muscle spindles, first demonstrated in frog, have been well documented since the 1930s [Matthews, 1931a; 1931b]. At rest, the afferent neuron associated with a muscle spindle fires spikes at a regular, basal rate. Upon application of a dynamic stretch stimulus of regular rate, the afferent neuron exhibits a burst of action potentials. As extension ceases and the muscle enters a state of static stretch, being held in a

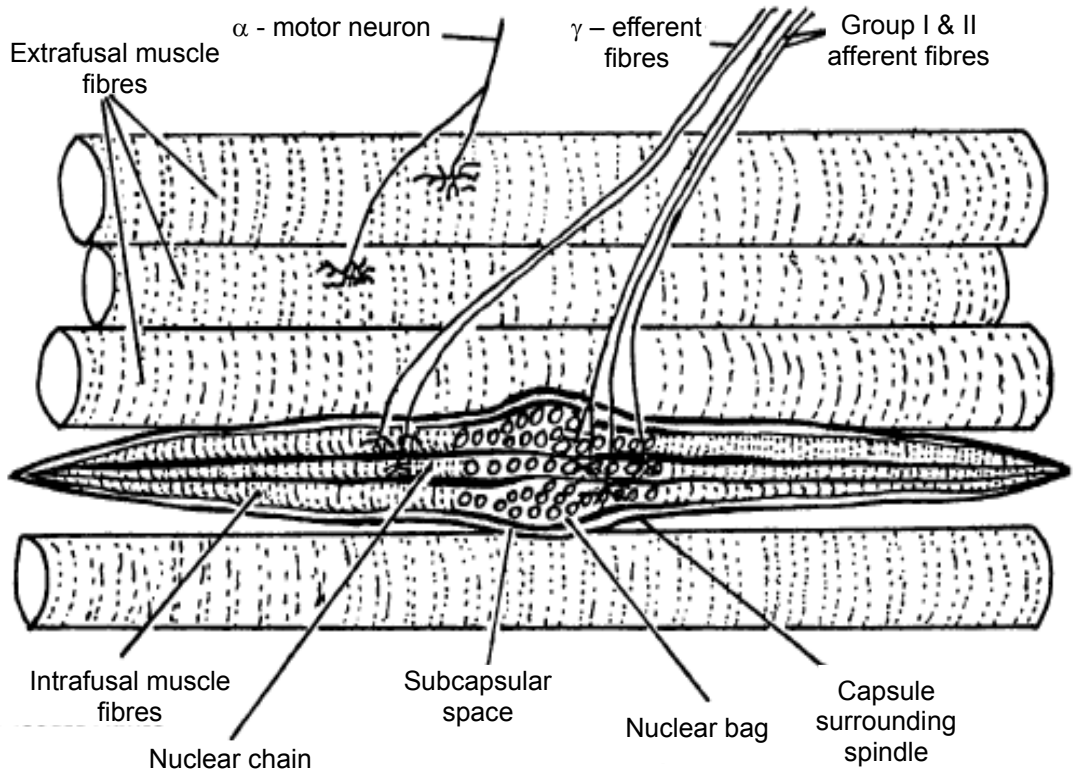

Figure 2: The anatomy of a muscle spindle. The neuromuscular spindles (muscle spindles) are fusiform in shape and widely scattered in the fleshy bellies of skeletal muscles. Each spindle consists of 2-10 slender, striated muscle fibres, enclosed within a thin connective tissue capsule, and attached at both ends to the epimysium or ordinary striated muscle. These slender muscle fibres, innervated by gamma (g) fibres (3-7mm) are known as intrafusal fibres, and they are tiny compared with the extrafusal fibres that produce contractile tension within a muscle. Intrafusal muscle fibres are of two distinct sizes: one is of smaller diameter (10-12mm), is shorter in length (3-4mm) and has a single chain of central nuclei; the second or larger spindle fibres are about 2.5mm in diameter, are 7-8mm in length and in the equatorial region are enlarged to accommodate an area of numerous small nuclei (nuclear bag). The smaller intrafusal fibres are known as "nuclear chain fibres" and the larger fibres are designated "nuclear bag fibres". The ends of the nuclear chain fibres are attached to the polar parts of the longer nuclear bag fibres. There are usually two of the longer fibres and five of the smaller fibres in each spindle, but these numbers are variable. A nuclear bag fibre with its capsule and associated sensory and motor nerve endings is shown. Two or more myelinated afferent fibres enter each spindle. A thick primary afferent fibre forms a spiral, branching and reticulated ending within the nuclear bag area (primary, annulospiral or nuclear bag ending) [taken from Fitz-Ritson, 1982].

state of increased length, the afferent neuron ceases bursting and resumes a steady firing rate. This firing rate is higher than the basal rate, by degrees proportional to the extension of the muscle fibre. Dynamic relaxation of the muscle again elicits a burst of firing from the afferent neuron, which reverts to tonic firing upon resumption of a new static muscle length. Once more, the tonic firing rate is proportional to the degree of muscle stretch in the steady state [Hunt, 1990].

Non-spiking electrophysiological adaptation of these neurons has also been observed and documented. Hunt *et al.* [1978] recorded 'receptor potentials' from the axons of muscle spindle afferents, after injecting TTX, to block action potential generation. These receptor potentials were evoked in response to stretch stimuli that were similar to those outlined above. A dynamic stretch 'ramp' was applied to the muscle, followed by a 'hold' at the extended length, before the muscle was released. This 'ramp-and-hold' protocol elicited a receptor potential, characterised by a large, rapid initial depolarisation during dynamic stretching, followed by a second after-depolarisation. Subsequently, upon entering the hold phase, the ending partially repolarised to a 'hold potential', which was maintained throughout static stretching. Finally, upon release, the ending hyperpolarised, before returning to rest [see **Fig. 3**].

Hunt *et al.* [1978] further demonstrated that the amplitude of the initial dynamic component (1-2 in **Fig. 3**) did not significantly vary over differing pre-stimulus muscle lengths, and thus over various pre-stimulus resting membrane potentials. They laid out detailed evidence of the ionic dependence, especially of the dynamic component of the stretch response, which was seen to be largely sodium-dependent, but which also displayed a smaller contribution by calcium. It was also shown that the resting potential of the spindle afferent could be varied by changing the extracellular potassium concentration, whilst chloride concentration had little effect.

That study is perhaps the seminal work on electrical adaptation of muscle spindle afferents in response to stretch stimuli. As such, the results of that study will be used extensively in order to evaluate some of the results achieved in my research. Thus, greater detail will be provided on the data of Hunt *et al.* [1978], along with the appropriate analysis, at relevant points [see **Ch.2.2.1**., **Ch.3.2.4**].

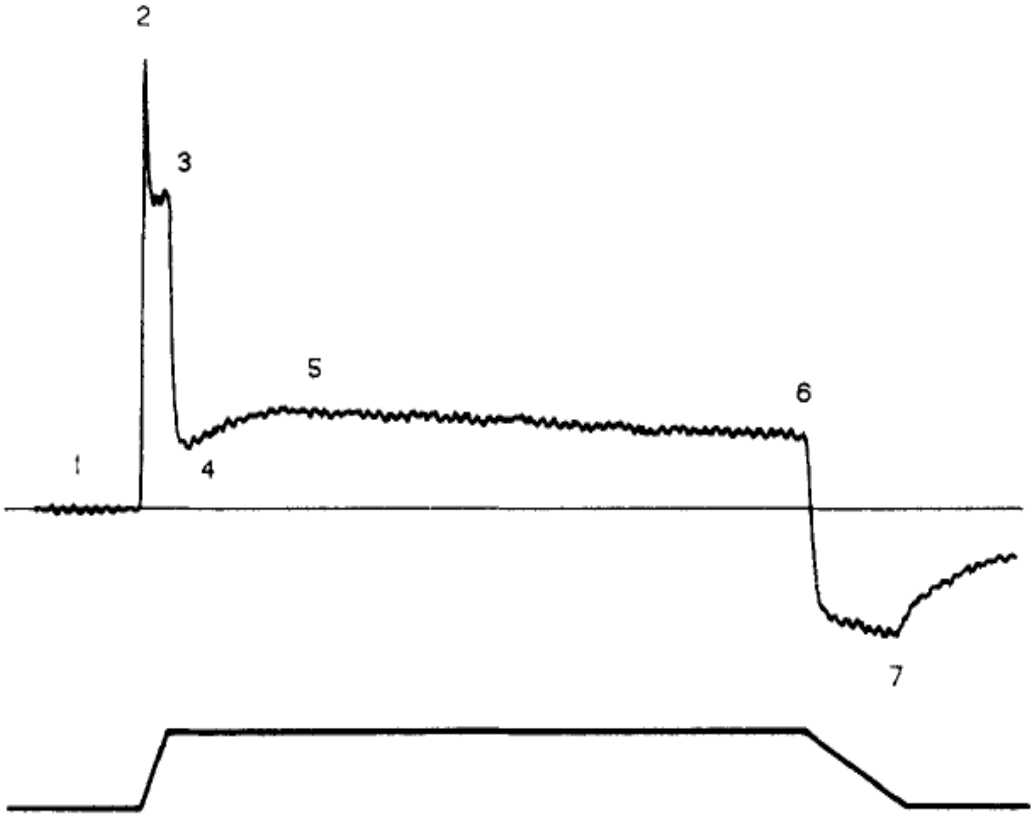

Figure 3: Receptor potential of a primary ending of an isolated, decapsulated spindle, recorded in a flow chamber. Upper trace: potential recorded from primary axon. Lower trace: length change. (1) Base line; (2) peak of initial dynamic component; (3) peak of late dynamic; (4) postdynamic minimum; (5) static maximum; (6) end static level; and (7) postrelease minimum. Sweep duration: 1.5 s [taken from Hunt *et al.*, 1978].

1.3. *Drosophila* mechanosensation

As with mammals, lower organisms are also highly dependent upon mechanosensation for normal functioning. Thus, they exhibit a similarly large variety of mechanoreceptors, in order to detect the wide range of kinetic stimuli they experience. The fruit fly, *Drosophila melanogaster*, has long been studied as a model species and typifies this range of mechanosensation. Kernan [2007] helpfully summarises the many and various behaviours of the fly that rely upon some degree of mechanotransduction, including grooming, courtship, gravitaxis and proprioception. He groups these sensations according to the anatomical class of the receptor that is utilised in its detection, *i.e.*, ciliated and non-ciliated endings [see **Fig. 4**].

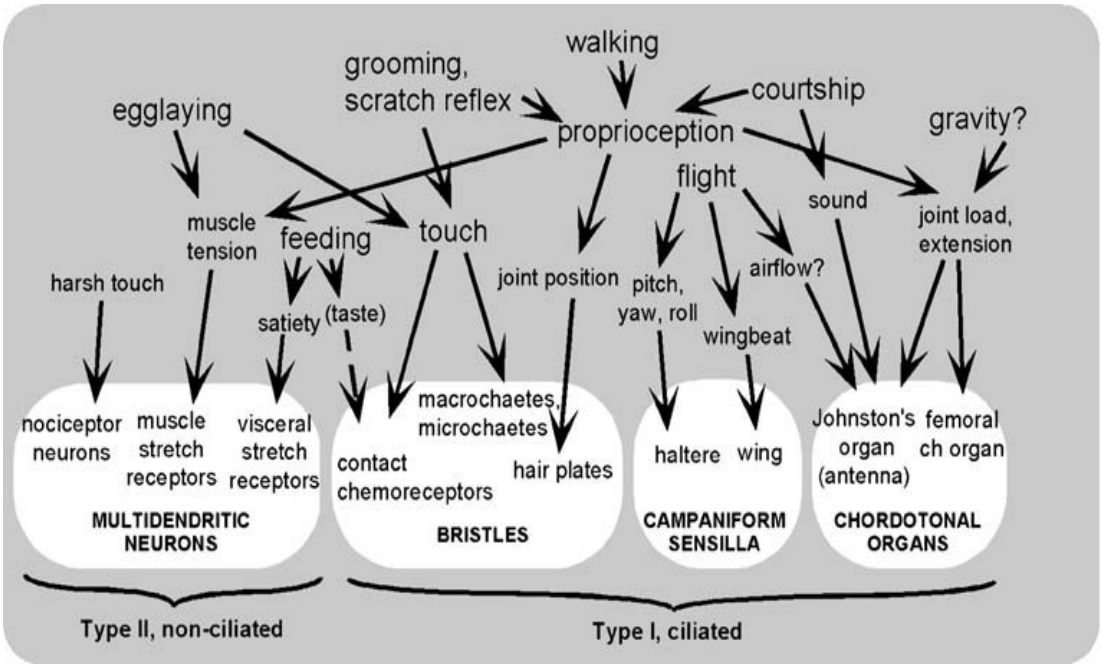

Figure 4: *D. melanogaster* exhibit a number of mechanosensory endings, which can be broadly grouped into two sub-types. Flies depend heavily on mechanosensation and possess a large number of different receptor varieties. These can be sub-divided in to two groups, based on their anatomy. Type 1 endings possess mechanosensory cilia, which detect stimuli via the mechanical force produced by the deflection of these projections. Type 2, non-ciliated endings detect stimuli via dendritic deformation, typically due to stretching [taken from Kernan, 2007].

By far the largest group of mechanoreceptors in *Drosophila* are the ciliated mechanosensors, which include the chordotonal (Ch) organs. These ciliated mechanoreceptors play various roles in locomotion, in both larvae and adults, as well as fulfilling important sensory roles in adult courtship [Kernan, 2007]. The largest of the fly's Ch organs is Johnston's Organ, which is involved in hearing in adult *Drosophila*, where it detects sound-wave vibrations [Bennet-Clark, 1971].

Ch organs themselves are comprised of 'scolopidial units', which are made up of four cells: the chordotonal neuron itself and three supporting glial cells, which are required for the function of the chordotonal organ. [Carlson *et al.*, 1997; Eberl *et al.*, 2000]. The chordotonal neuron is the principal mechanosensory component of the Ch organ. This neuron is characterised by a mechanosensory primary cilium, which projects from the tip of the neuron. The distal end of the cilium is then connected to the cap cell - one of the three glial cells [Carlson *et al.*, 1997]. It is interesting that, in general appearance, this could be

described as somewhat reminiscent of the arrangement of the mammalian hair cell, mentioned above.

1.4. Muscle stretch detection in *Arthropoda*

As is the case in mammals, arthropods also require mechanisms to detect the length and tonicity of their muscles. Many larval insects, for example, possess dorsal abdominal stretch receptors that closely associate with body wall muscles, which provide proprioceptive feedback in response to the contraction of muscle fibres [Finlayson & Lowenstein, 1958]. In the case of the body wall muscles in larval *Drosophila*, this information may be relayed by the dorsal bipolar dendritic (*dbd*) neuron (sometimes referred to as *dbp* - dorsal bipolar neuron [see **Fig. 5C**]). Two *dbd* neurons are located in the dorsal body wall of each larval abdominal segment, between the muscle layer and the external cuticle. They are immediately distinguishable by their two, longitudinally-projecting dendrites, which extend from the cell body of the neuron along the long axis of the larva, into the underlying horizontal muscles [Scrader & Merritt, 2007]. The axon of neuron projects perpendicularly to the CNS, giving the neuron a distinctive T-shape. To date, there has been minimal research into the role of these neurons. Thus, they have not been definitively characterised as muscle stretch receptors. However, the similarity of their gross anatomy to stretch receptor organs (SROs) in hawkmoth caterpillars had previously suggested that they may perform an analogous function in fly larvae [Schrader & Merritt, 2007; Nair *et al.*, 2010; see also **Fig. 5A & C**].

The SRO of hawkmoth (*Manduca sexta*) caterpillars had earlier been identified as a putative organ of muscle stretch sensation [Levine, 1984; Tamarkin & Levine, 1996]. These stretch receptors are paired neurons, common to caterpillar species, which are located in each segment of the dorso-lateral body wall of caterpillars, spanning their respective segments [Libby, 1961]. SRO neurons synapse with both ipsilateral and contralateral motor neurons that innervate the muscle fibres associated with the SRO segment, forming a feedback loop that regulates peristaltic movement in crawling [Tamarkin & Levine, 1996; Simon & Trimmer, 2009].

At the gross anatomical level, *dbd* neurons appear highly similar to SRO neurons, and also to stretch receptors in larger arthropods [see **Fig. 5**]. Muscle stretch receptors in crayfish species (*Astacus astacus* and *Pacifastacus leniusculus*) have been extensively described [reviewed in Rydqvist *et al.*, 2007]. Anatomically, these receptors exhibit similar shape and orientation, relative to the striated muscle fibres with which they interface, to the putative

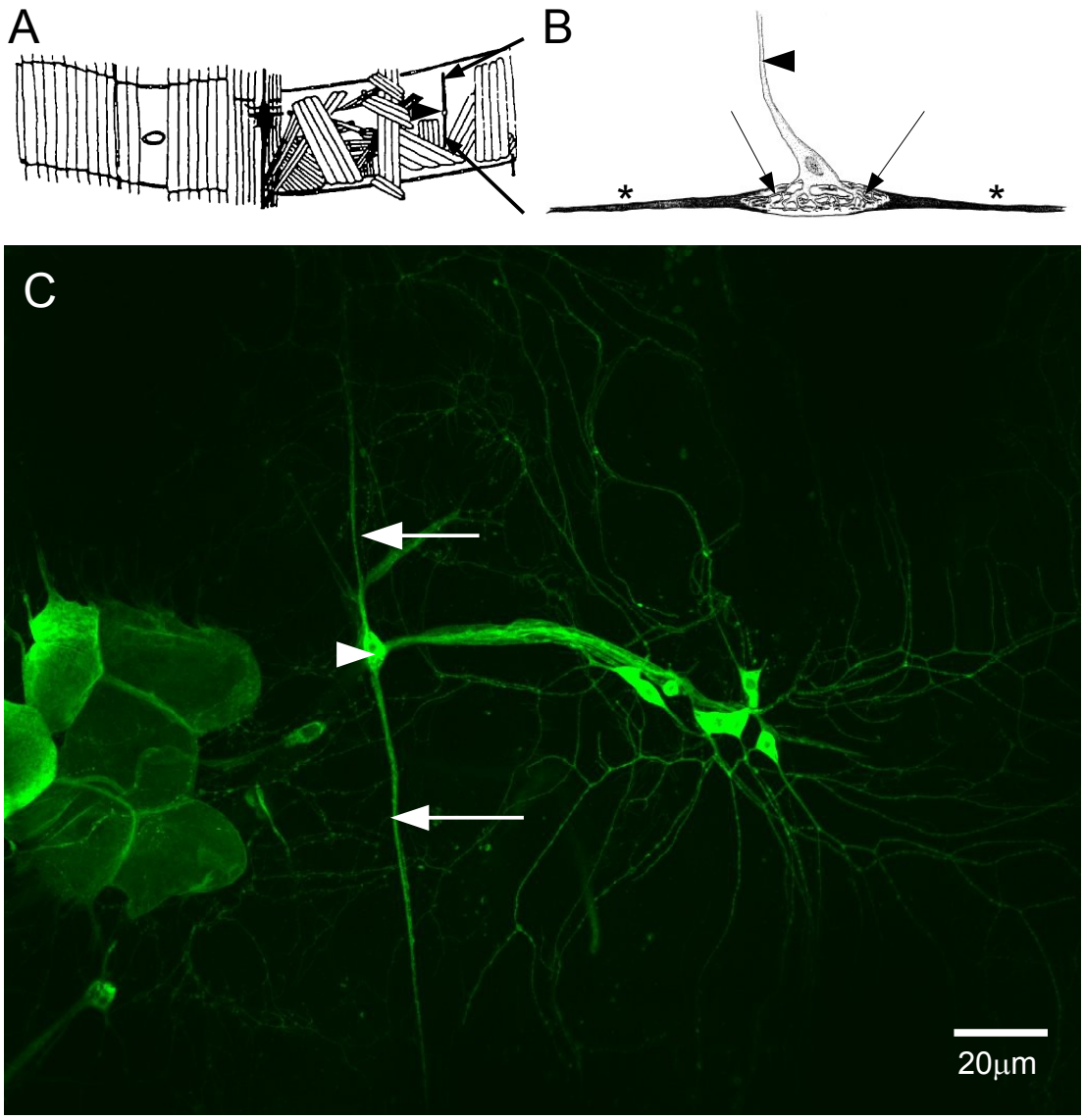

Figure 5: The stretch receptor organ (SRO) in *Manduca sexta* is anatomically equivalent to the *dbd* neuron in *D. melanogaster* and to muscle stretch receptors in crayfish. (A) Diagram of a dissected segment of the larval *Manduca sexta* is shown, opened dorsally, with the ventral nerve cord in the centre. The intersegmental muscles are shown on the left and dissected away on the right. The SRO in *Manduca sexta*, embedded in the external dorso-lateral musculature (arrowhead), can be easily distinguished by its morphology: two, longitudinal dendrites (arrows), extending along the long axis of the organism, spanning one segment in the larva [taken from Levine, 1984]. (B) A micrograph of the PNS of a *D. melanogaster* larval segment, with labelling of neuronal tissue. The *dbd* neuron can be seen (labelled as above), located in an analogous position and orientation to the SRO. (C) A similarly annotated muscle stretch receptor of *A. astacus*, also indicating the associated muscle fibres (*) [taken from Swerup & Rydqvist, 1996].

muscle stretch receptors in smaller arthropods [see, for example, Swerup & Rydqvist, 1996]. The confirmed role of these receptors in larger arthropods further suggests a probable similar role for the anatomically similar receptors of their smaller cousins.

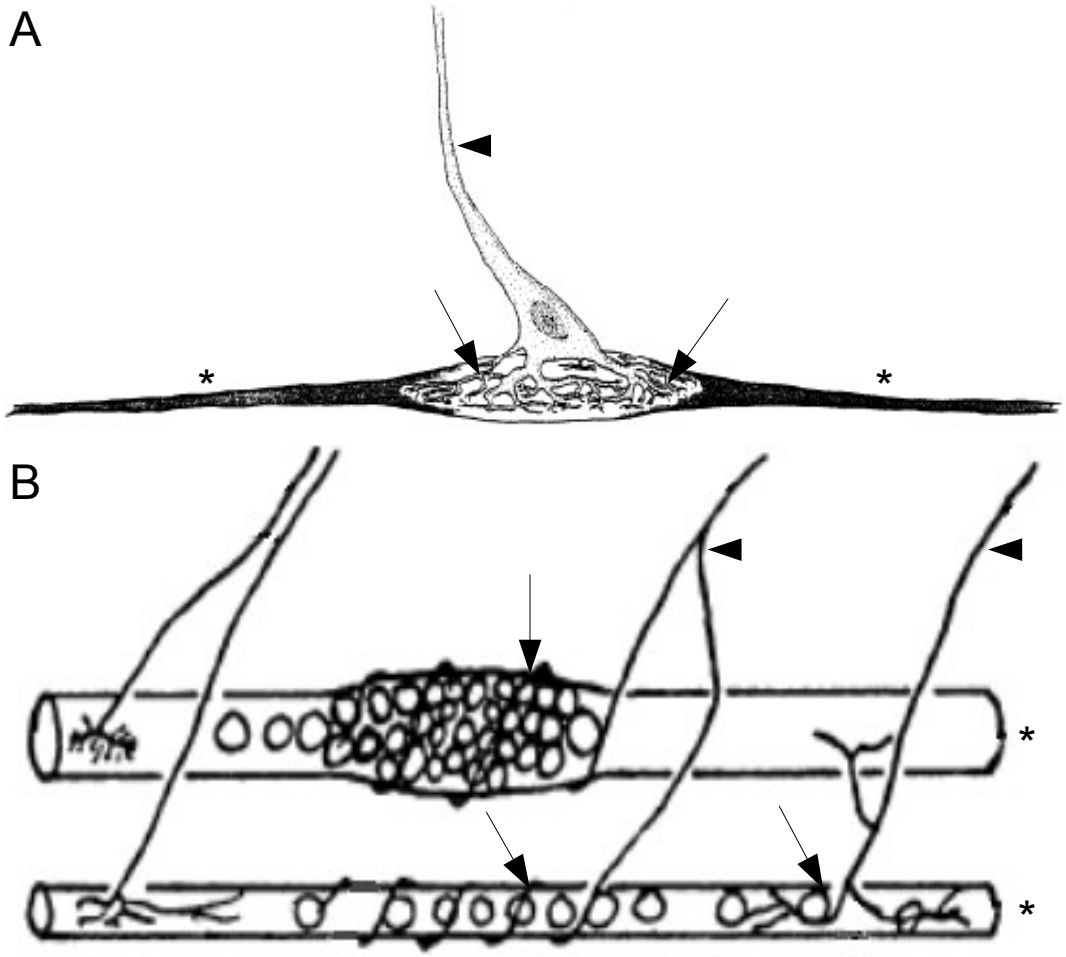

Figure 6: Comparative gross anatomy of arthropod and mammalian muscle stretch receptors. (A) A muscle stretch receptor of *A. astacus*, labelled to show the axon (arrowhead) and the dendrites (arrows), which project perpendicularly and detect stretching in the the associated muscle fibres (*) [taken from Swerup & Rydqvist, 1996]. (B) Diagrammatic representation of a mammalian muscle spindle, indicating the intrafusal fibres (*), afferent endings (arrows) and the projections to the CNS (arrowheads) [taken from Fitz-Ritson, 1982]. All three endings are identifiable by their longitudinal afferent terminals, along the line of the muscle, with the afferent dendrite projecting to the CNS at right angles.

Of particular interest is the additional, behavioural data that have been collected from crayfish stretch receptors, *i.e.*, electrophysiological recordings of the stretch-evoked responses – data that are much less characterised in, for example, the *dbd* neuron of

Drosophila. Extensive characterisation of receptor potentials, ionic currents and firing properties of crayfish stretch receptors have been reported [Edwards *et al.*, 1981; Ottoson & Swerup, 1985a; Ottoson & Swerup, 1985b; Kaila *et al.*, 1987; Kaila *et al.*, 1992]. In terms of the receptor potential, crayfish stretch receptors display a large, sharp initial depolarisation in response to dynamic stretch. During static stretch, this is followed by rapid adaptation, resulting in a smaller after-depolarisation, before a static, depolarised, steady state (a 'hold' potential) is attained. Termination of the stimulus then results in recovery to its pre-stimulus baseline, with an initial, rapid repolarisation, followed by a slower decline to baseline [Ottoson & Swerup, 1982]. It could be considered that identification of similar responses in the putative stretch receptors of *Drosophila* would be strong evidence of their functional role, in support of the apparent anatomical homology.

1.5. Comparisons between stretch receptors of mammals and arthropods

Of note is the observation that the anatomy of muscle stretch receptor organs seems to show remarkable similarity across species [Suslak *et al.*, 2011]. In particular, at the gross anatomical level, muscle spindles share common anatomical features, essential to their function, with muscle stretch receptors in a variety of invertebrates [see **Fig. 6**]. For example, both mammalian and arthropod muscle stretch receptors are immediately recognisable by their T-shaped configuration of longitudinal dendrites, which project along the contractile axis of their associated muscles, and a perpendicular projection to the CNS [see **Fig. 6**; see also Fitz-Ritson, 1982; Swerup & Rydqvist, 1996; Schrader & Merritt, 2007].

Whilst there are inter-species differences, particularly the presence of more accessory structures in higher organisms, the visual similarity is still apparent. Thus, the principal sensory neural component of muscle spindles comprises the annulospiral dendrite of a 1a afferent neuron, circumventing the intrafusal muscle fibre [Matthews, 1964; see also **Fig. 6B**]. Likewise, the *dbd* neurons of larval *Drosophila* are distinguished by their dendritic configuration, after which they are named. The two dendrites of *dbd* project longitudinally, in the rostro-caudal axis, from the cell body to the horizontal peristaltic muscles, along the contractile axis of the muscles [Schrader & Merritt, 2007]. This morphology is also consistently visible in the muscle stretch receptors of other arthropod species [Swerup & Rydqvist, 1996; Tamarkin & Levine, 1996].

Additionally, studies in *Manduca* show evidence of a sensory-motor feedback loop, connecting SROs with associated motor neurons [Levine, 1984; Tamarkin & Levine, 1996]. This resembles the association of muscle spindles with gamma motor neuron fibres, innervating the intrafusal muscle [Katz, 1949; Boyd, 1986; Banks, 1988]. Although no evidence has been put forward for similar connectivity in *Astacus*, *dbd* neurons in *Drosophila* do appear to be similarly connected [Hughes & Thomas, 2007].

Furthermore, a qualitative comparison of stretch-evoked receptor potentials that have been recorded in mammalian muscle spindles and arthropod stretch receptors indicates some apparent consistencies. Comparing data from muscle spindles, recorded by Hunt *et al.* [1978], with data from crayfish stretch receptors, obtained by Ottoson & Swerup [1982], reveals some key similarities. Both respond to dynamic stretch stimuli with large, rapid depolarising events that quickly inactivate; both sustain a steady, depolarised state throughout static stretch; and both ending types adapt upon release, before returning to rest [see **Fig. 7**].

Thus, given the anatomical and electrophysiological homology of mammalian muscle stretch receptors and crayfish stretch receptors, and given the further anatomical similarity of a putative *Drosophila* stretch receptor, it is likely that *dbd* neurons may, firstly, share similar electrophysiological properties as these two examples, and secondly, be muscle stretch receptors in fly larvae. Thirdly, if these hypotheses were to be confirmed, it may be that the fly stretch receptor system may be a suitable model system in which to identify a mechanism of stretch-activated mechanotransduction that would increase understanding of the more complex mammalian system.

1.6. Molecular mechanotransduction

All the diverse varieties of mechanosensory endings possess molecular machinery that enables them to convert mechanical stimuli to electrical impulses, or which initiates other cellular signalling processes, in both neurons and non-neural tissues. These mechanism(s) have yet to be completely characterised and stretch receptors in particular, especially in mammals, are very poorly understood [Lumpkin *et al.*, 2010; Delmas *et al.*, 2011]. It is, however, generally agreed that mechanosensitive ion channels play an important role in transduction [Hamill & Martinac, 2001; Hamill, 2006; Damann *et al.*, 2008].

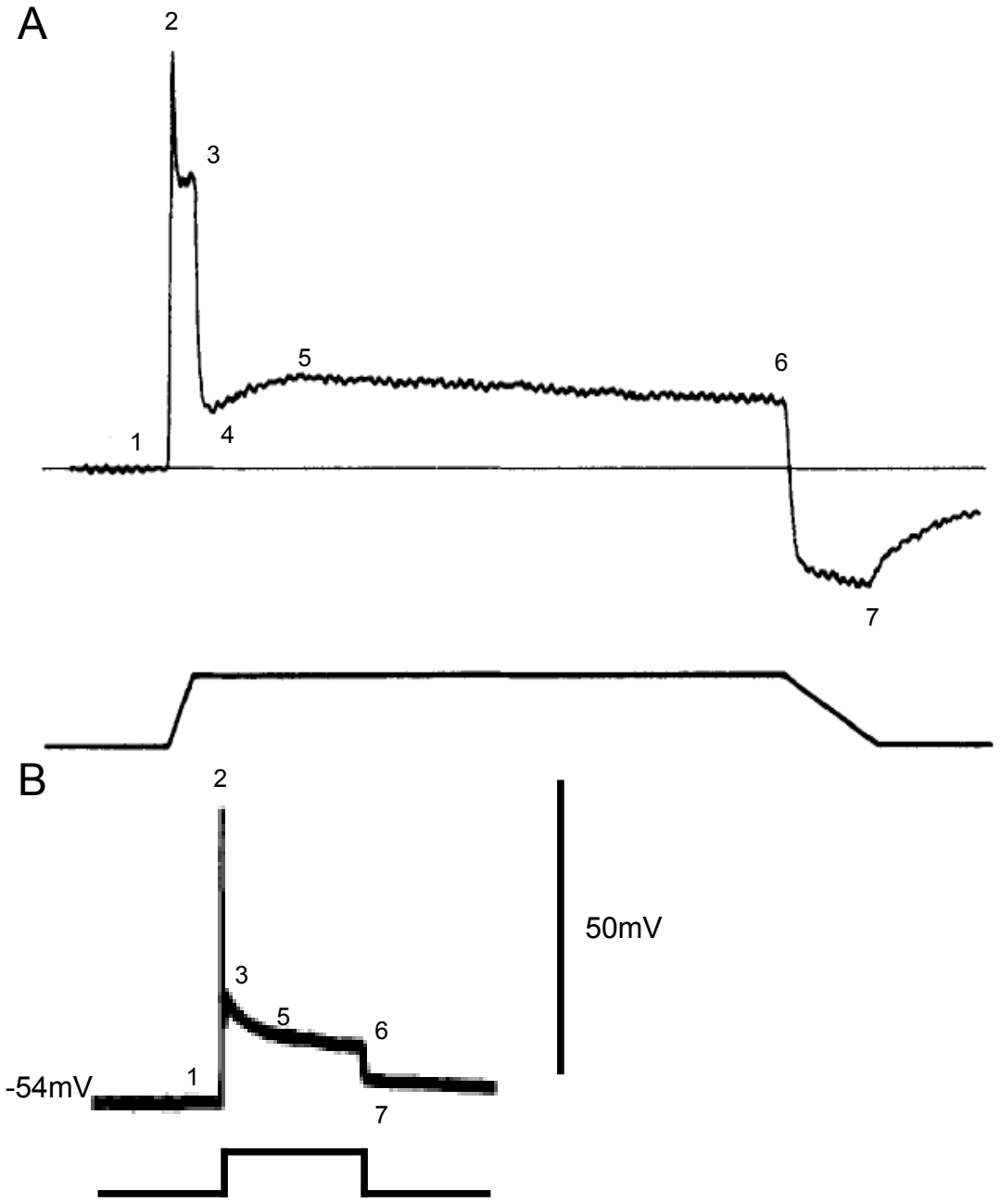

Figure 7: Receptor potentials of crayfish stretch receptors are, qualitatively, highly consistent with those of muscle spindles. (A) Receptor potential recorded from primary axon of a muscle spindle afferent, as in **Fig. 3** [taken from Hunt *et al*., 1978]. (B) A stretch-evoked receptor potential in *A. astacus* (lower trace: receptor length in arbitrary units) [adapted from Ottoson & Swerup, 1982]. With the exception of the postdynamic minimum (4) and the post-release minimum (7), all identified features of the muscle spindle response are readily identifiable in the crayfish data.

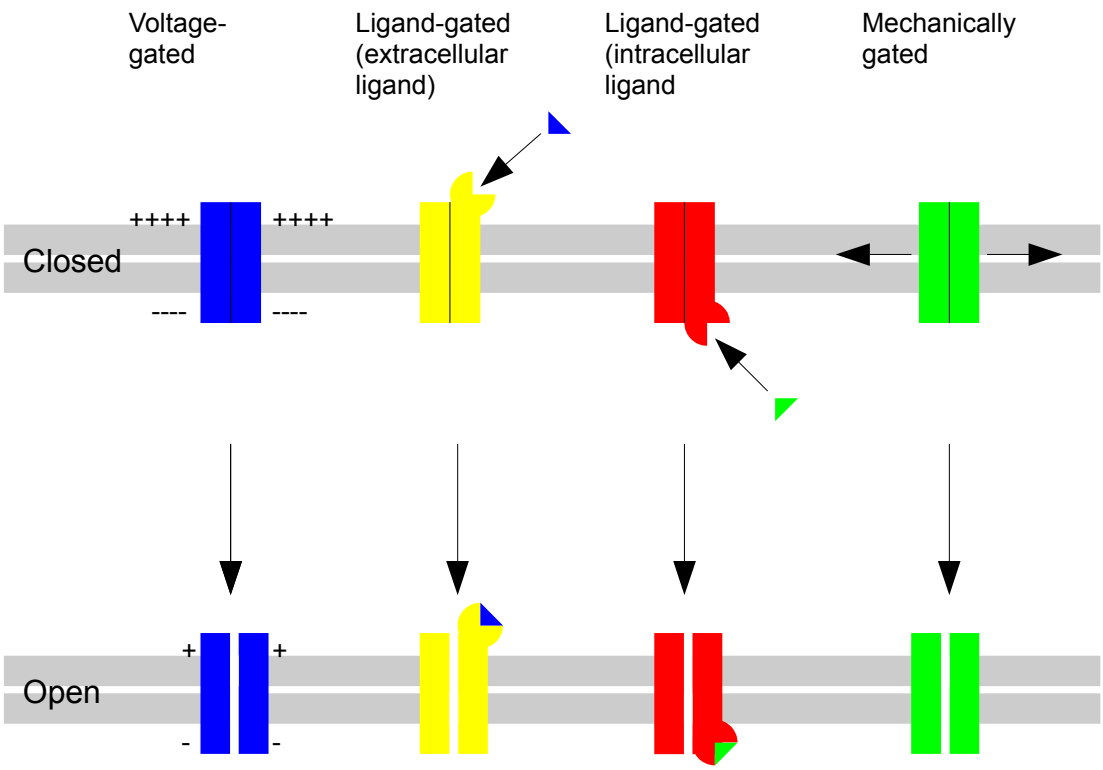

Figure 8: Mechanosensory endings depend upon activation of mechanically gated ion channels to relay sensory information. Many types of ion channel are expressed throughout the nervous system. In order for neurons to transmit information, ion channels within neurons are activated by specific stimuli, like voltage changes across the cell membrane or the binding of activating ligands. Mechanosensory neurons rely on mechanically gated ion channels, which are opened by the application of a tensile force to the cell membrane. This force directly alters the channel configuration from a closed to an open state, permitting ion flow [adapted from Kaplan, 2014].

Mechanosensitive ion channels (MSCs) broadly define all ion channels which are gated by kinetic forces, typically as experienced by cell membranes. Such channels open (or close) in response to the application of a mechanical force to the membrane – being distinct from channels gated by voltage or ligands [see **Fig. 8**] (although MSCs can also be gated, secondarily, by these) – and return to their resting state upon the removal of this force stimulus. Hamill & Martinac [2001] used the following definition, which it is useful to consider here:

"For a membrane protein to be directly MS [*mechanosensitive*], it must be sensitive to a membrane property that changes with mechanical deformation. For the specific case of a

simple two-state channel, a shift in the equilibrium between closed and open channel conformations may be caused by changes in bilayer tension, thickness, or local curvature or by direct "tugging" on the protein by cytoskeletal or extracellular tethers."

Both in this review [Hamill & Martinac, 2001] and Hamill's subsequent update on the state of the field of the study of MSCs [Hamill, 2006], MSCs are treated as 2-state channels, which are either open or closed, depending on the presence or absence of a mechanical force. This force may be either transduced to the channel protein, either directly via deformation of the phospholipid bilayer or via torsion along a protein-protein linkage between the MSC and one or both of the cytoskeleton or the extracellular matrix [see **Fig. 9**]. Single-channel recordings of various MSCs seem to support the 2-state model, with MSCs exhibiting unitary conductances, whilst populations display stimulus-dependent conductances [Hamill & McBride, 1995], suggesting that larger stimuli activate a larger population of identical channels.

Both Hamill & Martinac [2001] and Hamill [2006] note the presence of membrane "slack" in animal cells, such as the presence of microvilli or vesicles. The authors note that this feature of many animal cells, particularly receptors for mechanical stress, may provide a means of buffering the cell. Recently, this has been proposed as a potential means by which additional channels may become inserted into the membrane, to facilitate mechanoreception [Bewick & Banks, 2014].

Some circumstantial evidence for this may be inferred from muscle spindles, for example, where proposed MSCs appear to strongly colocalise with synaptophysin, a marker for vesicle sin these endings [Simon *et al.*, 2010], which may accord with evidence that syntaxin 1A inhibits currents medicated by the same putative MSCs, when both are co-expressed in oocytes [Qi *et al.*, 1999]. However, there remains no concrete evidence to confirm that this mechanism does occur. Thus, trafficking and replenishment of MSCs remains largely a mystery.

Nonetheless, MSCs have been identified and studied in a wide range of organisms, from *Archaea* to mammalian mechanotransducers. Interestingly, it has been proposed that mechanosensation may be an evolutionarily ancient ion channel function, with ion channels developing in unicellular organisms out of a biological necessity to regulate osmotic balance between the intra- and extra-cellular environments [Kung, 2005]. Membrane tension due to osmotic pressure could have been the original ion channel gating mechanism, with later channel varieties and gating mechanisms evolving from this origin [see **Fig. 10**].

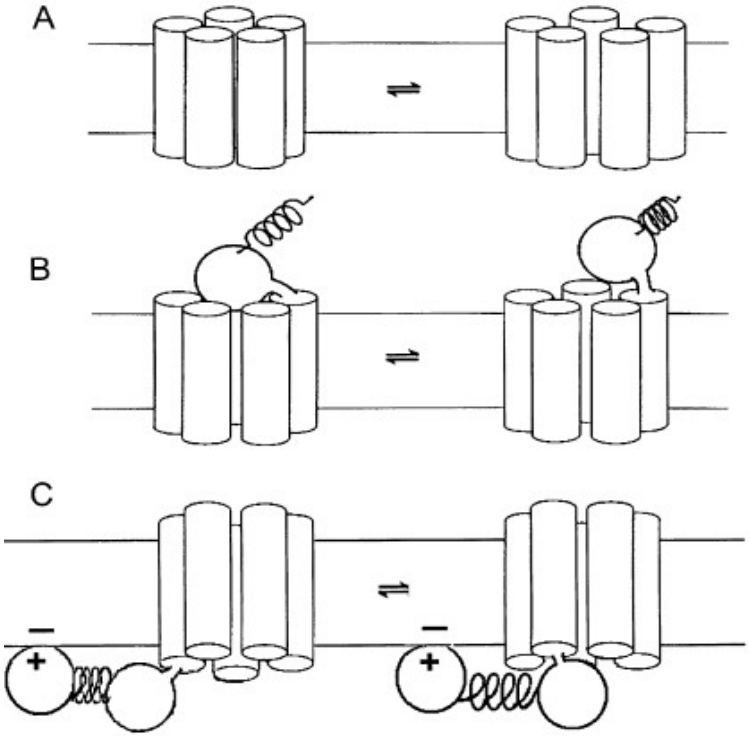

Figure 9: Three different models of mechanosensitive channel gating in a bilayer. (A) Mechanical forces are conveyed to the channel purely via the bilayer. Tension sensitivity occurs because of a difference in protein area (or hydrophobic thickness and/or lateral shape) between the open and closed channel conformations. (B) Extrinsic tether: tensions are exerted directly on the channel protein via extracellular or cytoskeletal elastic elements/gating springs. When tension is exerted on the gating spring, the open state is energetically more favourable. (C) Intrinsic tether (hybrid): In this model, the gating spring is one of the cytoplasmic domains that binds to the phospholipids and, in this way, becomes sensitive to membrane stretch [taken from Hamill, 2006].

Many channels are now known to be mechanosensitive. In both *Archaea* and bacteria, several channels have been identified that exhibit mechanical properties. These MS (mechanosensitive) channels are a diverse class of proteins that appear to primarily regulate osmotic pressure within the unicellular organism [Levina *et al.*, 1999; Kloda & Martinac, 2001].

However, all of the mechanically-sensitive channels that have currently been identified in flies and worms belong to only three families of ion channels – DEG/ENaC channels, TRP channels and Piezo channels [Goodman & Schwarz, 2003; Coste *et al.*, 2010]. With the

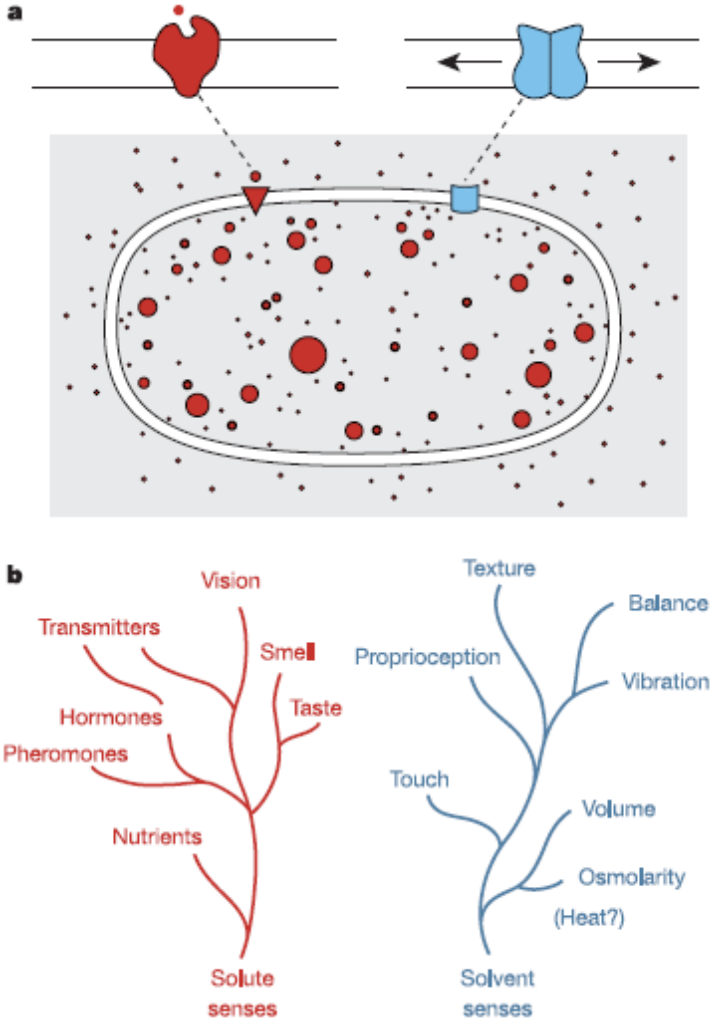

Figure 10: The disparate sensing of solutes and solvent. (a) A diagram of an imaginary early cell equipped with two types of receptors that are required to sense solutes and solvents — the two ingredients of life's chemistry. The dots in the grey background represent water molecules (the solvent) and the red circles represent solutes (molecules dissolved in water). When a cell accumulates solutes, the internal water concentration is reduced and the tendency of water to enter the cell results in a turgor. Both the lock-and-key type of receptors (red) for different solutes (ligands), as well as the turgor sensors (blue) for water (the solvent), are needed for even an early cell to survive. (b) A hypothetical diagram (not to be mistaken for phylogenetic trees) on the grouping of various senses that emphasises the discrete separations of the lock-and-key type of sensing of the solutes (red) from the force-from-bilayer type of sensing of the solvent (blue) [taken from Kung, 2005].

exception of the Piezo family, which are a small group of recently-identified channels [Coste *et al.*, 2010; Coste *et al.*, 2012], the other channels implicated in mechanosensory roles have generally been previously associated with other non-mechanosensory roles [*e.g.*, see Drummond *et al.*, 2008]. Here, an outline of these three channel families is provided, with details on what is currently known about their involvement in mechanotransduction in sensory endings.

1.6.1. DEG/ENaC channels

The degenerin/epithelial sodium channel (DEG/ENaC) family of ion channels (which also include acid-sensing ion channels – ASICs) is a large group of non-voltage-dependent sodium channels, associated with many physiological roles [Drummond *et al.*, 2008]. Principally, they had been associated with Na^+ absorption across endothelial membranes [Kellenberger & Schild, 2002], but more recently, they, along with their orthologues in *C. elegans*, have been implicated in mechanotransduction [Drummond *et al.*, 2001; Goodman *et al.*, 2002].

Mammalian ENaC is a heteromeric protein complex that may comprise α -, β-, γ-, and δ-subunits, with either an α- or δ-subunit being required to form an ion channel pore, although the exact stoichiometry is yet to be identified [Waldmann *et al.*, 1995; Simon *et al.*, 2010]. The channels themselves are blocked by amiloride and its analogues, including HMA (hexamethylene amiloride), EIPA (ethyl isopropyl amiloride) and benzamil (although Simon *et al.* [2010] noted that the dose-response profile of ENaC to HMA is different to the response to other amiloride analogues). All of the four subunits, as well as ASIC2, have been detected in mammalian muscle spindles, and have been shown to play a role in regulating stretch-evoked firing in these endings [Simon *et al.*, 2010].

Expression of other members of this family have been shown in both worms and flies. In *C. elegans*, proteins like MEC-4 and MEC-10 are ENaC homologues, both of which are known to be involved in touch sensation [Driscoll & Chalfie, 1991; Goodman *et al.*, 2002]. In *Drosophila*, the *pickpocket* (*ppk*) family of genes, of which there are 31 known members, diversely expressed across organ systems and developmental stages, are also ENaC homologues [Liu *et al.*, 2003]. However, only two of these *Drosophila* genes have thus far been implicated in mechanosensation. Kim *et al.* [2012] have linked expression of *ppk1* to mechanical nociception by *md* neurons in fly larvae, and it has also been linked to motor defects [Ainsley *et al.*, 2003]. Expression of *rpk* (*ripped pocket* – also referred to as *ppk2*)

has also been shown in mechanosensing neurons [Adams *et al.*, 1998].

1.6.2. TRP channels

The transient receptor potential (TRP) channel superfamily of ion channels is a large, heterogeneous group, comprising seven sub-families of ion channels – TRPC ('classical' or 'canonical'), TRPV ('vanilloid'), TRPM ('melastatin'), TRPN ('NOMPC'), TRPP ('polycistin'), TRPML ('mucolipin'), and TRPA ('ankyrin'). In general, TRP channels comprise six transmembrane domains and, whilst there are large degrees of conservation within sub-families, conservation between subfamilies is limited to the transmembrane domains and carboxyl terminal [Montell, 2001]. Primarily, though, there appears to be a high degree of conservation between mammalian and *Drosophila* TRP channels, with *Drosophila* expressing at least one of every type of TRP channel, whose roles, especially in sensation, seem consistent with their mammalian homologues [Montell, 2005]. These include the *Drosophila* channel protein, TRP, after which the family is named [Montell, 2001].

TRP channels have been observed to be expressed widely, in various tissues, fulfilling a range of roles, with homologues in a variety of species, including many roles in mechanosensation. The *C. elegans* TRPV homologue, OSM-9, has been implicated in mechanosensation and olfaction [Colbert *et al.*, 1997], whilst its mammalian counterpart, vanilloid receptor 1 (VR1), has been shown to mediate heat-induced pain responses [Caterina *et al.*, 1997]. TRPA1 has been linked to mechanosensation in vertebrate auditory hair cells [Farris *et al.*, 2004], and NOMPC (the eponymous TRPN, found in *Drosophila*) is required for mechanosensory signalling in Ch neurons [Walker *et al.*, 2000].

1.6.3. Piezo channels

The third known family of mechanically-gated ion channels is the recently-discovered Piezo family. First identified in 2010 by Coste *et al.*, Piezo1 (*Fam38A*) and Piezo2 (*Fam38B*) are two, distinct, novel, mammalian ion channels that are mechanically activated [Coste *et al.*, 2010]. Like TRP channels, Piezo channels are non-selective cation channels, permeable to both sodium and calcium. Both are also similarly blocked by such agents as ruthenium red and gadolinium [Coste *et al.*, 2012]. Piezo2 has recently been shown to be essential for conferring mechanosensitivity on Merkel cells [Woo *et al.*, 2014].

A Piezo homologue has also been identified in *Drosophila*, which has only a single *Piezo*

gene – *dmpiezo* – that has been shown to be essential for mechanical nociception in *md* neurons [Coste *et al.*, 2012; Kim *et al.*, 2012]. Additionally, a zebrafish (*Danio rerio*) homologue, *Piezo2b*, has been shown to regulate responses to light touch stimuli [Faucherre *et al.*, 2013]. However, direct evidence for a role for Piezo in these cases is still absent and it remains to be seen how, precisely, Piezo functions within mechanosensory apparatus.

1.6.4. Ion channel summary

The field of mechanosensitive ion channels is clearly broad, containing many entities that may mediate mechanotransduction. The addition of the novel Piezo proteins has added yet more potential mediators to the already considerable number of known mechanically-gated channels. Importantly, however, in the field of stretch-activated mechanosensors, little is known about what entities may be acting [Tobin & Bargman, 2004]. Tentative steps have been taken in analyses of muscle spindles and baroreceptors that point to roles for DEG/ENaCs in these receptors [Drummond *et al.*, 2001; Simon *et al.*, 2010], and whilst these have been shown to be important for mediating stretch transduction in these endings, it is still unclear where these channels fit, in terms of constructing a complete model of the mechanotransducing apparatus of stretch receptors. Furthermore, the quantity of additional, known MSCs counteracts any simple means of deconstructing such an apparatus purely by current, experimental means.

It has previously been suggested that a common mechanism may underlie mechanotransduction, at the receptor level [Benos, 2004]. To what extent this hypothesis holds remains to be seen. It is clear, from the literature, that disparate receptor types are unlikely to share common, molecular mechanisms, as, by way of example, in *Drosophila*, NOMPC is essential for Ch neuron mechanoresponses, while *md* neurons require the expression of *ppk1* [*cf.* Walker *et al.*, 2000 and Kim *et al.*, 2012]. However, as has been indicated, electrophysiological data from anatomically similar stretch receptors show strong similarities [*cf.* Hunt *et al.*, 1978 and Ottoson & Swerup, 1982]. Consequently, it may be that these endings do share a common molecular mechanism.

Alternatively, it may be that the hypothesis of Kung [2005] could be borne out in this case. Kung postulated that all ion channels may share a common ancestor, and that mechanosensitivity might be the original gating mechanism of this 'ancestor channel'. Thus, it could be conceived that, whilst mechanoreceptors may share common behaviours, at an

electrophysiological level, these need not be due to the same channels. Rather, the same behaviour could be produced by different channel combinations, due to shared characteristics between mechanically-gated channels, which trace back to their common origins (note, however, that this does not necessarily contradict Benos' hypothesis).

1.6.5. Other components of mechanotransduction

Apart from MSCs, there are other aspects to the mechanotransduction process. Indeed, from the extant analyses of the receptor potential of muscle spindles, it is clear that stretch-evoked receptor potentials require a number of ionic currents [Hunt *et al.*, 1978]. Additional research in *C. elegans* also highlights the need for further factors that support the formation of MSCs [Goodman *et al.*, 2002]. Of particular interest to the field of stretch-activated endings, perhaps, is the work of Bewick *et al.* [2005], in which a novel, autocrine vesicular mechanism was discovered within the sensory terminals of the afferent fibres, themselves. These vesicles, which were shown to be glutamate-containing, are released from the afferent ending and subsequently act back upon that same ending to increase afferent firing during stretch. A similar mechanism has also been shown in lanceolate endings of mammalian hair follicles, where it has been confirmed that the action of this autocrine glutamate is through a novel, phospholipase-D-coupled, metabotropic glutamate receptor [Banks *et al.*, 2013].

1.7. Aims

Thus, a number of questions are left unanswered by the current literature:

1. What mechanisms underlie stretch transduction?
2. Are these mechanisms shared by anatomically similar stretch receptors of different species?
3. To what extent does similarity of electrophysiological behaviour correlate with similarity of molecular mechanism?

Specifically, this study will look at the molecular level to determine how a particular mechanosensitive ending – the *dbd* neuron of *D. melanogaster* – transduces stretch; it will aim to identify stretch sensitive ion channels that mediate their receptiveness. This study will look to examine the electrical responses of such stretch receptors, to characterise these and

determine the nature of their relationship to relevant stimuli, thus providing a means whereby the 'normal' behaviour these receptors can be identified and subsequently challenged, in order to specify the roles that specific ion channels may play in their responsiveness.

Furthermore, this study will look to compare the data obtained from *dbd* neurons with extant understanding of stretch receptors in other organisms. By doing so, this study will look to determine whether the *dbd* neuron might be suitable as a model system for examining stretch receptors – whether it will exist as a simple, tractable and accessible model of this receptor-type, in order to promote a further understanding of the means by which such neurons sense and transduce mechanical stimuli.

The following chapters will discuss the approaches that were taken in order to address these unanswered questions. Firstly, a theoretical approach is discussed. An *in silico* representation of stretch-evoked receptor potentials is developed, based upon existing electrophysiological data. This model aims to reduce the apparent complexity of mechanotransduction apparatus by identifying the necessary components of such a system and providing a framework for comparing electrophysiological data from stretch receptors of different species, finally allowing predictions of the effects of perturbing a stretch receptor system to be made, which will allow putative system components to be assayed.

Secondly, the development of a novel recording technique for studying receptor potentials in a *Drosophila* muscle stretch receptor system is presented. This technique combines previous methods of *Drosophila* electrophysiology, mammalian mechanoreceptor assays, and the “awesome power of *Drosophila* genetics” [A.P. Jarman, 2014 (personal communication)], resulting in a powerful tool for identifying molecular mediators of mechanotransduction.

Thirdly, these two models – both *in silico* and *in vivo* – are utilised to identify molecular components of the transduction apparatus. The *in silico* model is used to predict the role of individual transduction components on the electrophysiological responses of stretch receptors. The *in vivo* model is then challenged with the inhibition of putative components of the transduction apparatus and, by comparing the effect on electrophysiological responses of pharmacological and genetic challenges with predictions from the *in silico* model, components of the transduction mechanism are identified.

2. An *in silico* model of stretch receptor mechanotransduction

2.1. Introduction

Although mechanotransduction has long been identified as key to the sensations of touch and other mechanical inputs, classical, experimental approaches have thus far failed to elucidate the mechanisms underlying these processes [Suslak *et al.*, 2011]. Many studies have been undertaken to probe mechanosensory endings via physio-pharmacological means, to attempt to isolate key molecules that fulfil the role of mechanotransducers in these endings [Rydqvist & Swerup, 1991; Goodman & Schwarz, 2003; Farris *et al.*, 2004; Goodman *et al.*, 2004; Simon *et al.*, 2010]. Currently, research has proposed many candidate channels which could mediate mechanotransduction [as described in **Ch.1**], but it is still unclear what is necessary to comprise a mechanotransduction system, how many distinct channels are required and what interactions there might between these components. Research has mainly focused on candidate channels for primary mechanotransduction, but the identity of any system remains unclear.

The bulk of current research has aimed to begin with the primary mechanotransduction channel, which would initiate mechanoresponses. Some studies consistently point to the presence of a DEG/ENaC family member in mechanosensory endings [Drummond *et al.*, 2001; García-Añoveros *et al.*, 2001; Bianchi & Driscoll, 2002; Drummond *et al.*, 2008; Simon *et al.*, 2010], others indicate roles for TRP channels [Walker *et al.*, 2000; Corey *et al.*, 2004; Lumpkin *et al.*, 2010]. Furthermore, the emergence of the *Piezo* family as a third alternative [Coste *et al.*, 2010], as well as a general lack of agreement as to the overall mechanotransduction process and its potential mediators, have created a situation in which many channel types could potentially contribute primary MSCs. Thus, the process(es) of mechanotransduction at the molecular level is still complicated and largely unknown.

The main problems inherent in the classical approaches to probing mechanotransducers are the lack of information about what systems may underlie the process, and the debate as to how similar different receptors are likely to be, in terms of their molecular composition. One school of thought holds that the basic process of mechanotransduction is inherently uniform [Benos, 2004; Hamill, 2006]. The theory goes that all mechanoreceptors utilise the same basic system, but there is modulation at a secondary level, which furnishes receptors with

diversity. However, the fact that different studies in different mechanosensory endings have highlighted the presence of different molecules, whilst failing to find previously identified ones [see above] would suggest that not all mechanosensors utilise the same, molecular mechanism of transduction.

A similar, but distinct, theory proposes that mechanoreceptors may share a common biophysical mechanism, but this mechanism can be mediated by distinct molecular entities [Kung, 2005]. This theory proposes that ion channels may all share an evolutionarily ancient connexion in their gating properties, *i.e.*, mechanical gating may be the original ion channel gating mechanism, with such mechanisms as ligand gating and voltage-dependence evolving later. Such a theory is partially harmonious with that of Benos [2004] and Hamill [2006], but does not necessitate a common molecular mechanism. Whether this latter theory can shed light on the processes of mechanotransduction remains to be seen. In particular, though, it appears that classical, experimental approaches have distinct limitations in addressing the large knowledge-gap in this field. A novel approach to this problem, however, may be found in a theoretical approach.

Mathematical modelling in the neurosciences is not new. The first statistical description of afferent firing patterns in a neuron was published in 1946 [Brink *et al.*, 1946]. Following this, decoding of spike patterns via statistical methods led to a new field of computational analysis of neurons [Moore *et al.*, 1966]. This diverse field has since contributed much to our knowledge of neural connectivity in the brain [*e.g.*, Girardi-Schappo *et al.*, 2013], how we understand consciousness [*e.g.*, Josipovic, 2014], the classification of neuron sub-types [*e.g.*, Kepecs & Fishell, 2014], and how the brain processes information [*e.g.*, Prescott *et al.*, 2014], to name but a few areas in which mathematical approaches have contributed to the study of neuroscience.

However, modelling in the field of mechanosensation is a relatively unexplored avenue of investigation. Mechanoreceptors, like all neurons, produce electrical outputs in response to stimuli. The key difference between mechanosensitive neurons and 'classical' neurons is the nature of their stimuli. Whilst a typical neuron receives a chemical stimulus from a synapse, the mechanoreceptor receives a mechanical input at the sensory terminal. Constructing a model of mechanoreceptors, based on experimental data of their electrical behaviour, provides a means to examine what components are required to function in a mechanosensitive ending in order to produce the observed electrical responses.

Such an approach may provide a suitable framework within which to compare the behaviour of a range of receptor types, in order to examine the likelihood of a common,

biophysical mechanism. Furthermore, a theoretical model of stretch-activated neuronal adaptation may provide a clear means of predicting the roles of specific channel types, providing a suitable screening parameter for identifying the involvement of candidate channels.

In 1996, Swerup & Rydqvist produced a mathematical description of primary mechanotransduction in a stretch receptor of the crayfish, *Astacus astacus* [Swerup & Rydqvist, 1996]. More recently, two reviews of the theory of intracellular adaptation in response to mechanical distortion have been compiled [Hoffman & Crocker, 2009; De *et al.*, 2010]. However, these reviews do not concern themselves with electrogenesis, only summarising effects of mechanical tension on a cell, as concerning the physics of cellular distortion. Similarly, other attempts to employ mathematical modelling in addressing mechanosensitive processes, like vascular remodelling, have only examined anatomical adaptation [as in Members of the Sicilian Gambit, 2001]. Thus, Swerup & Rydqvist [1996] remains the only identifiable description of a mechanism by which stretch-evoked mechanotransduction could be initiated, prior to my research [Suslak, 2011].

The initial work to produce a mathematical model of stretch-activated mechanotransduction in afferent terminals began in an earlier MSc. project [Suslak, 2011]. The model presented here is based on this earlier work. A summary of relevant points from the previous project is therefore included here, by way of introduction.

2.1.1. Model origins – Swerup & Rydqvist, 1996

Swerup & Rydqvist [1996] developed a biophysical model of stretch transduction in the crayfish stretch receptor [see **Fig. 11A**], comprising the only prior attempt to define, mathematically, the relationship between stretch stimuli and evoked electrical activity in the receptor ending. The underlying premise for their model was that a mechanoreceptor, specifically a stretch-sensitive mechanoreceptor, experiences a mechanical extension (e), which evokes tension in the receptor ending (σ) [see **Fig. 11B**]. Based on the anatomy of a non-ciliated, stretch-sensitive neuron, the architecture of the model followed the form of a non-linear spring in series with a Kelvin-Voigt element [see **Fig. 11C**]. That is to say, the stretch-responsive ending that was utilised as a basis for the *in silico* model is comprised of both elastic and inelastic anatomical components. Thus, in the model, the simulated mechanical extension will act on both these components, resulting in the activation of two

tensile components, which contribute, separately, to the overall tension of the receptor (Eq. 1).

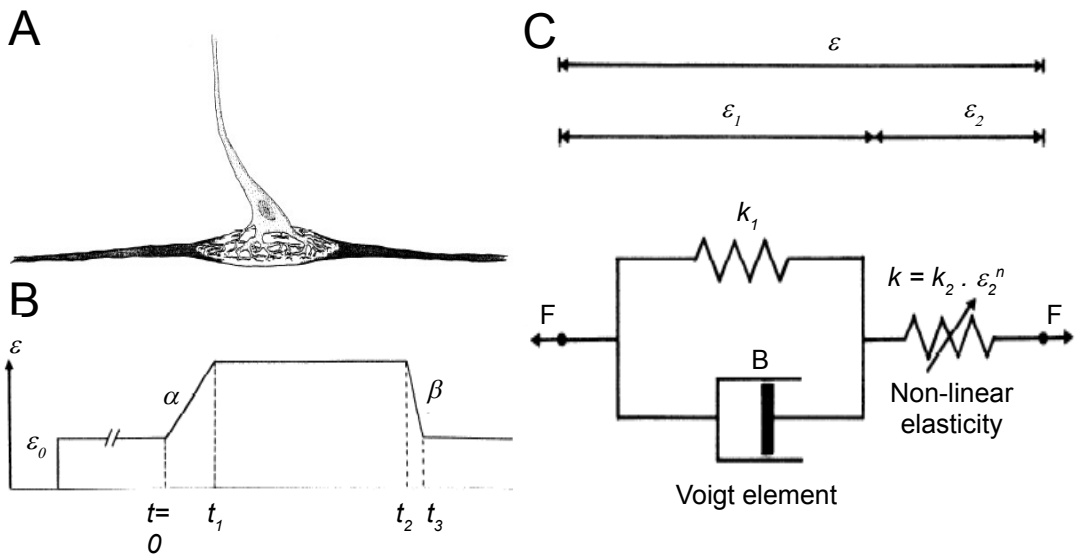

Figure 11: The basis of an earlier stretch-receptor model. An earlier receptor potential model was based upon experimental data, gathered from a slowly-adapting crayfish stretch receptor, which detects stretch and tonicity in skeletal muscle of *A. astacus* (A). The change in tonicity of these endings in response to a stretch-hold-and-release protocol (B) was hypothesized to be like that observed in this Kelvin-Voigt/non-linear spring arrangement (C), proportional to the extension applied (e_0=initial receptor length, *a*=extension rate, *b*=relaxation rate, *e*=overall extension, e_1=linear stretch component, e_2=non-linear stretch component, *F*=force, *B*=Dashpot constant, k_1=linear extension coefficient, k_2 non-linear extension coefficient, *n*=power constant, *t*=time) [taken from Swerup & Rydqvist, 1996].

(1) $$\sigma_m = k \cdot e_2 = k_2 \cdot e_2^{n+1} = k_1 \cdot e_1 + \frac{B \cdot de_1}{dt}$$

(2) $$P_O = \frac{1}{\left(1 + k_b \cdot \exp\left[-s \cdot \left(\frac{\sigma_m}{m}\right)^q\right]\right)}$$

(3) $$I_s = P_O \cdot g \cdot \left(E_{rest} - E_{srev}\right)$$

e_1 is the linear component of the extension, representative of the tension in the inelastic,

tendinous capsule of the receptor, e_2 is non-linear, representing the elastic components of the receptor, such as the membrane and muscle [$e = e_1 + e_2$]; k is a non-linear parameter relating tension and extension, k_2 is a non-linear spring constant, k_1 is a linear spring constant, B is the Dashpot constant of the Kelvin-Voigt element and n is a power constant for the non-linear spring.

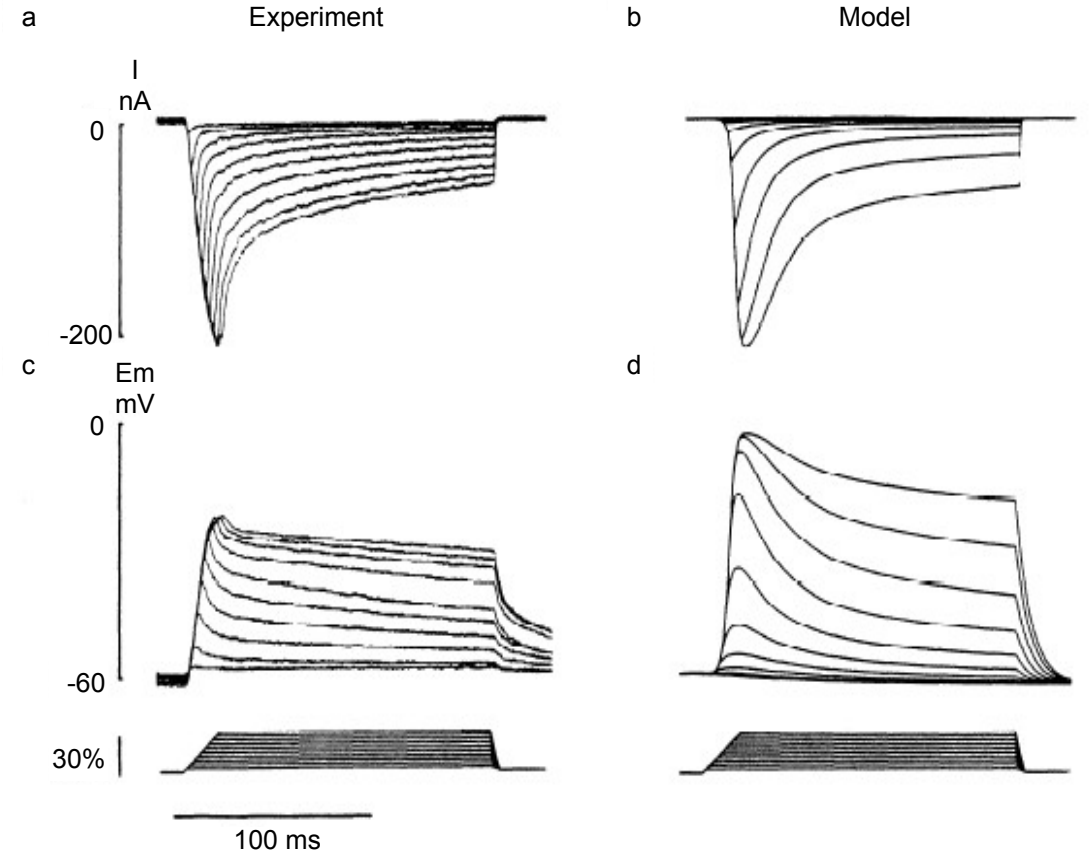

Figure 12: A biophysical model of stretch receptor electrophysiology faithfully reproduces the experimental results. Equations of motion were used to describe the properties of the stretch receptor. These were constrained by experimental data and combined with bio-electrical relations to reproduce the basic electrical behaviour of the receptor. Receptor current and receptor potential assuming MSC adaptation according to Eq. 2, using a time constant for adaptation (q) of 100 ms. **a** and **c**: experimental values from same cell in response to ramp-and-hold extensions (1500% s^{-1}, 3-30%). **b** and **d**: model receptor current and receptor potential, respectively, in response to identical extensions as in **a** and **c**.[taken from Swerup & Rydqvist, 1996].

This bivariate tensile force is hypothesized to gate an MSC, which opens in response to this tensile force, and permits a cation influx, which causes the depolarisation of the ending. The

tensile force is the sole variable that controls the open-probability (P_o) of the MSC (Eq. 2), which in turn governs the depolarisation of the ending (Eq. 3). All the parameters for this model were experimentally-derived in earlier studies [Brown *et al.*, 1978; Rydqvist & Zhou, 1989; Rydqvist *et al.*, 1990; Rydqvist & Swerup, 1991; Rydqvist & Purali, 1993][1].

This model was shown to faithfully reproduce the electrical activity observed in experimental data derived from a slowly-adapting stretch receptor in *A. astacus* [Swerup & Rydqvist, 1996; see **Fig. 12**]. These experimental data were obtained under conditions which eliminated all but the stretch-activated component of the stretch response, using TEA, 4-AP and TTX to block voltage-gated channels [see **Fig. 13**]. Thus, the model demonstrated how an MSC could operate in a stretch receptor to explain persistent ion channel activity in the presence of blockers of voltage-gated channels.

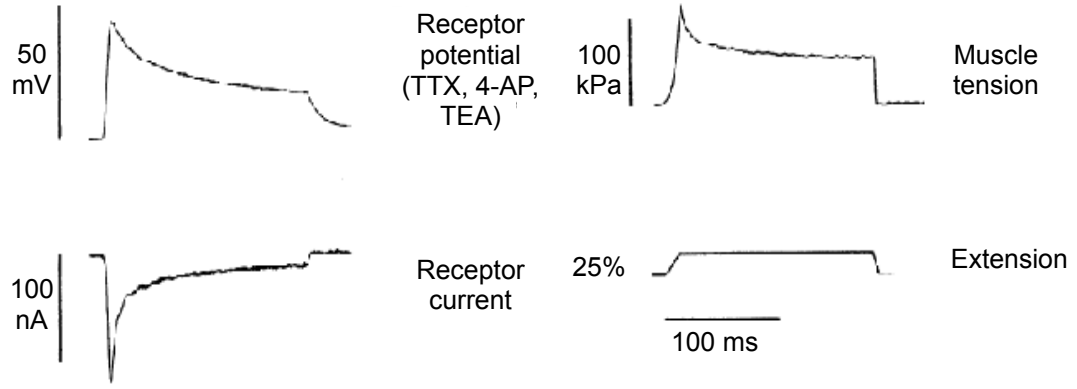

Figure 13: Recorded muscle tension, receptor current, and receptor potential in response to a ramp-and-hold extension in a slowly adapting stretch receptor. The muscle was extended by 25% (bottom-right) and the muscle tension (top-right), receptor current (bottom-left) and potential (top-left) were recorded (example traces shown). Receptor potential was obtained by blocking Na^+ and K^+ currents, using 0.6mM TTX, 10mM TEA, and 1mM 4-AP [taken from Swerup & Rydqvist, 1996].

2.1.2. Model origins – Suslak, 2011

Therefore, this model was used as the basis of an extended model of mechanoreceptor adaptation. The initial model only showed the contribution of an MSC to receptor adaptation. The scope of my MSc. project, which immediately preceded this study, encompassed an attempt to determine whether the original model could be extended, via the addition of

1 Values of all these experimentally-derived constants may be found in **Appendix i.i.**

voltage-gated channels, to reproduce experimental data obtained in the absence of blockers of voltage-gated channels.

$$P_V = \frac{1}{1+\exp\left(\frac{E_m - E_{act}\cdot \sigma_{Na}}{k_{Na}}\right)} \quad (4.1)$$

$$g_{Na} = \frac{P_V \cdot (NaE_{rev} - E_m) + g_{leak} \cdot (E_{leak} - E_m)}{C_m \cdot E_m} \quad (4.2)$$

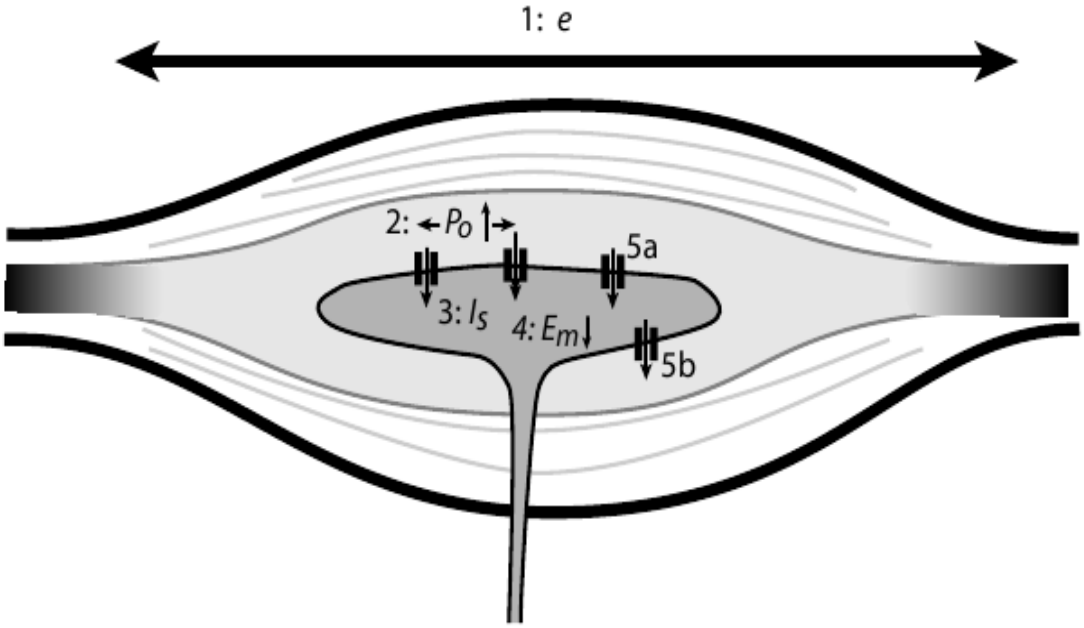

Figure 14: Diagrammatic representation of the stretch receptor model. When a stretch stimulus is applied, the muscle extends by length *e* (1) and the afferent ending experiences a proportional tensile force. Mechanosensory sodium channels (MNaCs) in the ending are gated according to this tension, with higher tensions increasing MNaC open probability. As the open probability increases, more MNaCs are likely to be open (2). As more MNaCs open, sodium enters the ending generating a mechanosensory current (3) and depolarising the ending (4). This depolarisation activates voltage-gated sodium channels in the ending (5a) and voltage-dependent potassium channels (5b), which are downstream components of the stretch-initiated response [taken from Suslak *et al*., 2011].

By way of summary, and to introduce the modelling work carried out in this project, the previous project demonstrated that, by gating both voltage-activated sodium channels

(VNaC) and voltage-activated potassium channels (VKC) with the change in membrane potential induced by MNaC activation (Eq. 4.1), additional currents could be generated in the ending (Eq. 4.2), and thus, *in vivo* recordings of crayfish stretch receptor potential electrical behaviour, recorded in the absence of TTX and TEA, could be reproduced (where E_{act} is the VNaC activation potential, k_{Na} is a VNaC activation constant, σ_{Na} is a function of the VNaC time constant, τ_{Na}, NaE_{rev} is the VNaC reversal potential, g_{leak} is the VNaC leak conductance, E_{leak} is the membrane leak potential and P_V is the VNaC open probability; similar relations were also included which describe a VKC, with appropriate substitutions of constants and nomenclature.)[2]. These currents inactivate when time (t) > τ. This model is summarised, diagrammatically, in **Fig. 14**.

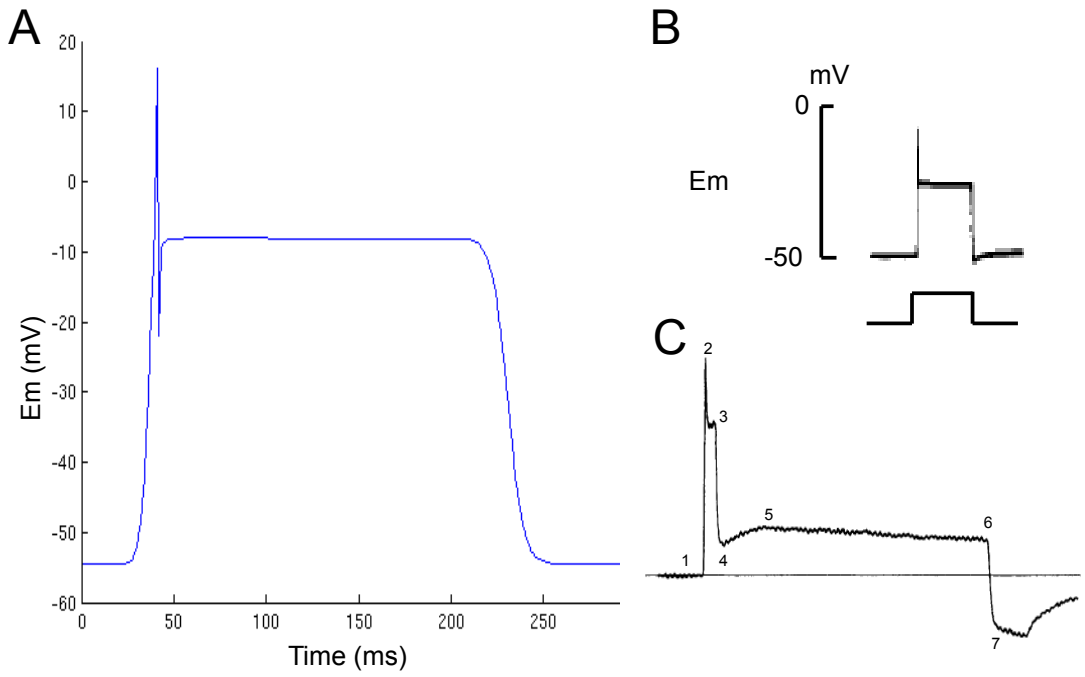

Figure 15: Previous work showed that a more complete stretch receptor model could be built from the initial MNaC model. Extending the MNaC model with voltage-gated channels (A) reproduced slowly-adapting crayfish stretch receptor responses under drug-free conditions (B). These responses also showed some qualitative similarities with prior recordings from mammalian muscle stretch receptors (C) [B – adapted from Ottoson & Swerup, 1985a; C – adapted from Hunt *et al.*, 1978; full figure taken from Suslak, 2011].

Additionally, that project noted that, with some modifications a similarity might exist between the modelled behaviour and that which had been previously observed in mammalian

2 Values used for these constants are given in **Appendix i.ii.**

stretch receptors, indicating that some commonality may exist between the crayfish and mammalian systems [see **Fig. 15**].

The following sections examine work that was carried out, as part of this project, to determine, firstly, whether further additions to the model could enable it to fully reproduce the behaviour of non-crayfish muscle stretch receptors, *e.g.*, that of the muscle spindle, and secondly, what such a model might be able to predict about the role that component channels may play in the adaptation response of muscle stretch receptors.

2.2. Modelling general stretch-dependent mechanotransduction

The model that had thus far been produced [Suslak, 2011] successfully recapitulated recordings from crayfish stretch receptors, via a reimplementation and extension of a previous model of stretch-dependent membrane potential [Swerup & Rydqvist, 1996]. The results from the model indicated that it could potentially describe the complex response of a mammalian stretch receptor – the muscle spindle – if it were suitably extended and modified to fit muscle spindle data.

The model, at this stage, exhibited three areas of clear divergence from muscle spindle experimental data. During the transition from dynamic stretching to static stretch, the muscle spindle exhibits an intermediate, partial repolarisation before settling to a stable hold potential [see 3 in **Fig. 15C**], which the model omits. Next, the hold potential during static stretch was noticeably higher in the model than in the muscle spindle recording, and finally, the model did not describe the post-release hyperpolarisation that occurs during dynamic relaxation of the spindle ending [see 7 in **Fig. 15C**].

2.2.1. Characterising mammalian data in the *in silico* model

It was apparent, even at a qualitative examination of the model at this stage, that three, clear areas of divergence existed between the model and experimental data. Two of these areas – in particular the hold-potential disparity and the lack of a post-release hyperpolarisation – were visually obvious. Solutions were proposed to these two disparities, which are discussed in this section.

Firstly, the issue of the hold-potential amplitude was addressed. This phenomenon appeared to lend itself to a simple solution, as it appeared, from the data, to be a direct consequence of

the transition from dynamic to static stretching and, furthermore, remained unaltered throughout static stretching, suggesting a simple mechanism, relying on the alteration of a single variable, namely the perturbation of charge flux balance. In the model, as it stood [Suslak, 2011], the hold potential was erroneously high. In order to correct this, it was hypothesized that the homeostatic balance point required re-setting to a lower value.

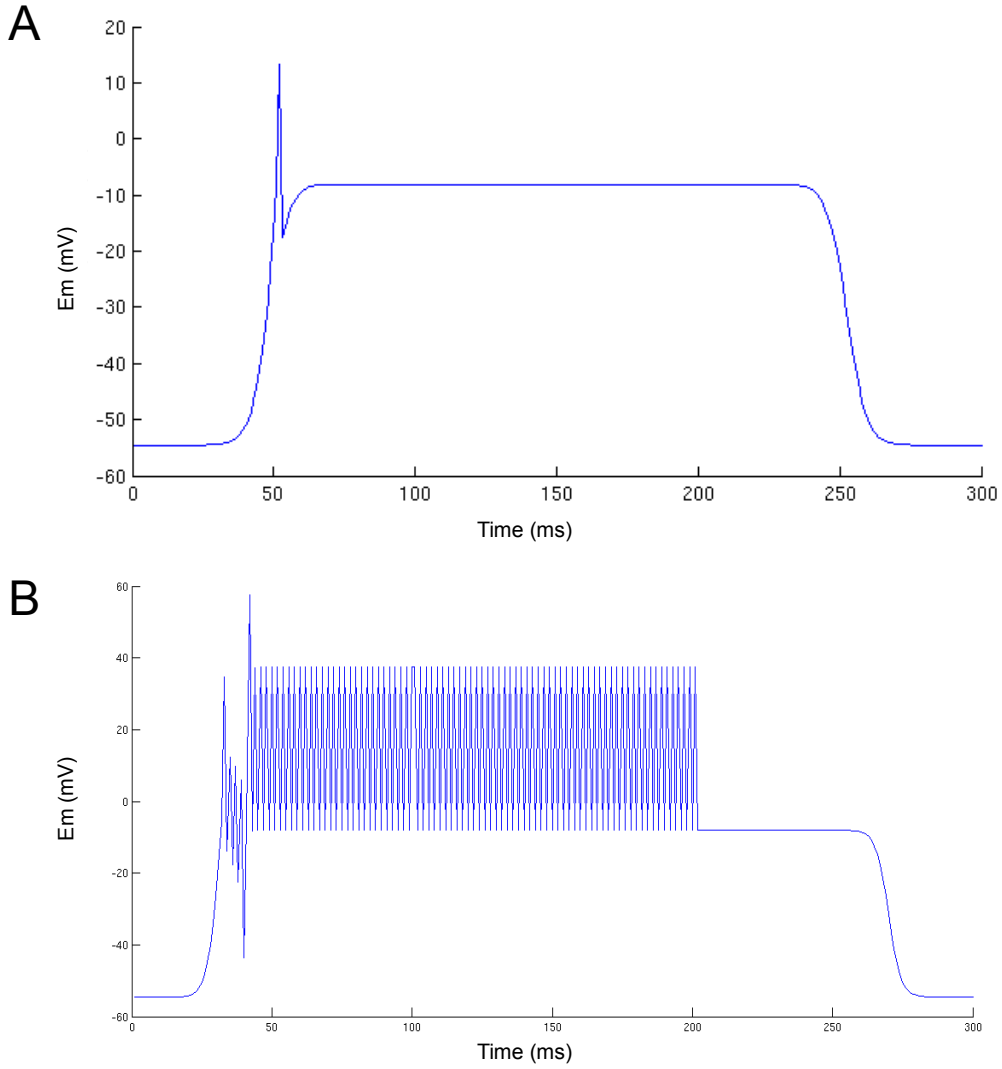

Figure 16: Additional voltage-dependent parametrisation was ineffective at rectifying the hold-potential disparity. (A) The previous model faithfully reproduced the initial, dynamic stretch response of stretch-sensitive afferent endings. However, upon transition to static stretch, a disparity between *in silico* and *in vivo* reporting of hold potentials was apparent [figure as in **Fig. 15A**]. (B) De-limiting the inactivation of VK channels could not correct this disparity, instead generating a spiking behaviour in the model.

As the original model [Swerup & Rydqvist, 1996] based the characterisation of the MNaC

on experimental data, this component of the model was considered immutable, as alteration of the modelled MNaC would remove the experimental basis of the model. However, both the VNaC and VKC components that had been added to the model, notwithstanding that their inclusion enabled the model to more faithfully reproduce *in vivo* data, were considered less concrete features, as their addition to the model was based on qualitative, as opposed to quantitative parity with *in vivo* data. As the model aimed to reduce the receptor potential to the simplest configuration of components, *i.e.*, the least possible number of different current types, modifying one of these unverified currents, rather than building in an additional channel, would, if successful, be the most expedient route.

In order to lower the hold potential to that seen in *in vivo* recordings, the hold phase of the model required an increase in net efflux of positive charge[3]. The simplest means of achieving this appeared to be the lengthening of the duration of the VKC component. Thus, the time constant of VKC (τ_K) was increased by 50% to 15ms, to delay the inactivation of the current, which occurs at time > τ_K. However, persistence of the voltage-gated current, rather than correcting the hold-potential disparity, promoted a spiking-like behaviour, which was undesirable [see **Fig. 16**].

Clearly, additional voltage-mediated currents could not correct the observed disparity. In addition to the generation of a spiking-like behaviour, the transient functionality of voltage-gated channels make them unsuitable for the long-term maintenance of depolarisation, as seen in the hold phase responses, observed *in vivo*. A persistent – or slowly-inactivating – system was required, which could reduce the net influx of charge or promote a counterbalancing efflux. Importantly, this could not be accomplished through reduced activation of the MNaC, as the MNaC activation within the model had already been experimentally verified. Thus, the model required an additional component that could mediate sustained net charge efflux, *i.e.*, a potassium or chloride channel.

Stretch-activated potassium channels are an established feature of the literature, with many K^+ channels exhibiting mechanical gating properties [comprehensively reviewed in Sackin, 1995; Patel *et al.*, 2001; Gautam *et al.*, 2006; Hamill, 2006; del Valle *et al.*, 2012]. However, little remains known about whether similar properties exist in chloride channels. Accordingly, a tension-gated potassium current was postulated. The characterisation of this channel followed the same form as that of the modelled MNaC (Eq.1-3), with modified parameters to reflect its hypothesized K^+ conductance: k_0=10kPa, k=120kPa, τ=150ms,

3 The model does not address any anion flow, for simplicity. Additionally, there has been no evidence yet put forward for any mechanosensitive chloride channels.

I_{smax}=100nA, E_{srev}=-100mV, g=1μS [after Conti *et al.*, 1976; Berntson & Walmsley, 2008]. As such, these parameters essentially encode a "reverse" MNaC, with physical properties that closely resemble the MNaC, but with the electrical properties of a K^+ channel, similar to the VKC.

Such a current would necessarily be activated at a higher tension than the MNaC-dependent current. If this were not the case, these currents would cancel out, preventing activation of the ending. Accordingly, a tension threshold was set for the 'mechanosensitive'[4] potassium current (MKC) at σ_m>66kPa, with the channel only being active at tensions above this value, which represents the tension in the ending that is exceeded as the system enters static stretch, and that is 90% of the maximum tension evoked. The result of the addition of a channel was a correction of the hold potential in the model to a close approximation of *in vivo* recordings [see **Fig. 17A**].

However, despite the addition of this MKC, the model persisted in failing to produce a hyperpolarisation upon release of stretch-evoked tension. This presented a puzzling issue as the model, to date, possessed both MNaC, MKC, VKC and VNaC components. Hyperpolarisation could not be brought about via reducing the influx of positive charge. This is due to the fact that, as tension is reduced in the model, the MNaC inactivates, reducing the Na^+ current to zero as tension is abolished. No other inward current is still active as the release phase is entered, as the VNaC component is rapidly-inactivating. Thus, the causative agent of hyperpolarisation must be an as yet unaccounted for persistent, or additional outward current.

This constraint suggested that, in order to create the net efflux of positive charge required for hyperpolarisation, persistence of the MKC current, or an increase in its net amplitude would be required. In practice, a tension-dependent increase in K^+ efflux would result in hyperpolarisation. Thus, an augmentation of the MKC current was proposed. This augmentation is in the form of an additional MKC term, identical to the first except for its gating parameter. This MKC (hereafter referred to as the putative MKC2) is gated by sensing decreasing tension, activating when σ_m declines below 50kPa. The result of this addition is a voltage trace that strongly resembles the *in vivo* data of Hunt *et al.* [1978] [see **Fig. 17**]. It should be noted, however, that although these parameters frame a model that reproduces experimental data, they are hypothetical and require *in vivo* validation of the proposed system components. Interestingly, both of these MKC components are required.

4 This channel need not be mechanosensitive (see **p.35**).

Incorporation of either one without the other cannot fully account for the profile of the *in vivo* data [see **Fig. 17A & B**].

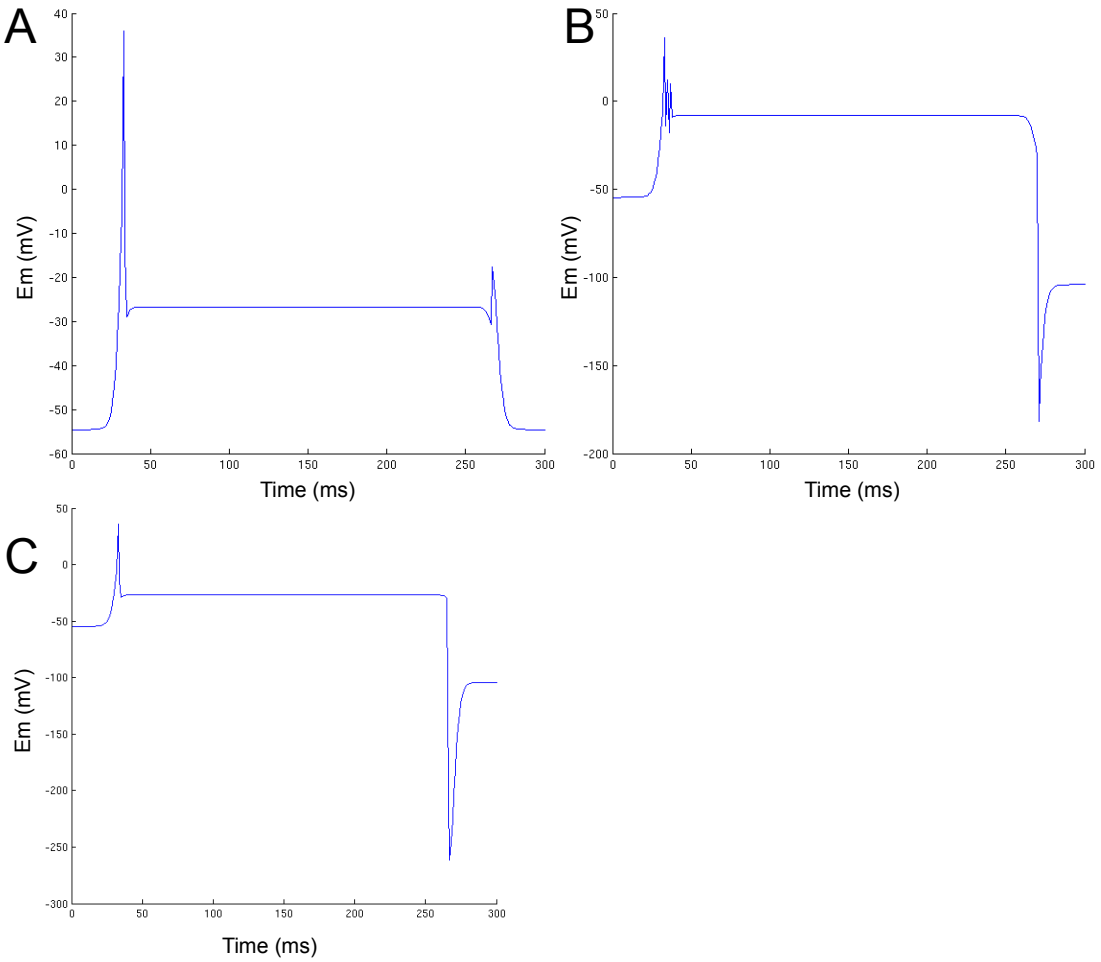

Figure 17: In order to model the post-release hyperpolarisation, it was necessary to account for a large net outward current. Following release, MNaC inactivates, leaving a K^+-mediated current as the sole ion flow in the model, causing hyperpolarisation. However, this overall K^+ current requires two, distinct components: (A) a high-threshold stretch-activated current lowers the hold potential but cannot produce a hyperpolarisation; (B) a delayed-activation (or "stretch-inactivating") K^+ current is required for hyperpolarisation, but does not act during the hold phase; (C) both the above are required to act in concert to reproduce a close approximation of a muscle spindle receptor potential recording [*cf.* Hunt *et al.*, 1978].

Two scenarios are suggested by this model. The first is direct, mechanical activation of the MKC (MKC1) and MKC2 components, with these two components each being highly attuned to specific levels of tonicity decline, thus re-setting the cell as they sense

corresponding declines in stimulus intensity. This scenario would suggest that these two K^+ components are distinct, given their different gating properties. Thus, an *in vivo* system that uses this scenario would require two types of MKC channels. Perhaps more likely is the hypothesis that one or both MKCs are calcium-dependent. In this scenario, stretch would need to induce some sort of calcium current, in addition to those currently modelled. This could be either a Ca^{2+} influx or intracellular release. Calcium gating of one or both MKC terms would maintain a degree of stretch-dependence, although this would now be indirect. Additionally, it would remove the need for differential stretch inactivation, as the off-switch for the MKC components could now be a decline in intracellular calcium, rather than membrane tonicity.

The model currently contains no Ca^{2+} component. However, this could occur via the "VNaC", if perhaps it were not a VNaC, but more like a voltage-gated Ca^{2+} (Ca_v) channel, or at least a non-selective channel. A simple modification of the model was therefore trialled, to determine whether substituting the VNaC for a Ca_v channel could feasibly be effected without disrupting the receptor potential profile significantly. To achieve this, no drastic alteration of the model architecture was required, as a cation current was already in place. All that was needed to convert this current from a Na^+-based conductance to a Ca^{2+}-mediated one was a modification of the electrical properties of the channel.

As described above, the VNaC conductance is described by 5 variables – activation potential, activation constant, reversal potential, time constant and leak conductance. With the exception of the reversal potential, these variables can be left effectively unchanged in order to switch from describing a sodium current to a calcium current. Interestingly, by modifying the reversal potential term for this channel from +50mV to +70mV, which is reported to resemble more closely the reversal potential for calcium in a high-Mg^{2+} extracellular environment [Campbell *et al.*, 1988], no appreciable variation in the stretch-evoked response of the model could be seen. This is unsurprising, as the effect of Na_{rev}, on conductance is several orders of magnitude below the effect of the other variables [see Eq. 4.1 & 4.2].

However, this simple variation accommodates a potential entry mechanism for calcium, which could begin to address the question of MKC gating. This Ca^{2+} could activate MKC1 near peak dynamic stretch, whilst also mediating some intracellular Ca^{2+} release. Intracellular calcium signalling would then help to maintain channel activity until it is either secreted, or reabsorbed by intracellular stores. As MKC1 activation, in this case, would be calcium-dependent, it would not be expected to inactivate upon stimulus removal, along with the

MNaC. Conversely, some intracellular mechanism might even promote more Ca^{2+} release upon sensing the additional stretch decline in the release phase, increasing MKC1 activation. Thus, MKC1 and MKC2 could, in fact, both be the same channel. The increase in current would be accounted for by the increase in intracellular signalling, brought about by tension release, activating further channels, or augmenting existing channel activity, both of which could increase conductance. The gradual return to baseline, seen in the post-hyperpolarisation of *in vivo* recordings also suggests the previously-documented physiology of K_{Ca} channels [Hicks & Marrion, 1998].

As yet, though, this mechanism remains hypothetical as there are no data to suggest how this calcium signalling could occur in sensory endings, or indeed whether it even occurs in the first place. Nonetheless, the model appears sufficiently complete to faithfully reproduce experimental data of stretch-evoked receptor potentials, although investigation of the role of calcium could iron out minor extant discrepancies, such as the persistent disparities in hyperpolarisation profile and the post-dynamic minimum between the model and *in vivo* recordings.

2.3. Deconstructing the role of the MNaC

The principal reason for constructing a model of stretch-activation in mechanosensory neurons was to access a simple approach to understanding and identifying the mechanisms by which mechanotransduction occurs in stretch receptors. This model has been shown to accurately reproduce the electrical behaviour of stretch-activated endings that are experiencing normal, physiological stimuli. It does so by presenting a simple system, involving the action and interaction of up to five ion-mediated current-types, which combine to reproduce experimental recordings of receptor potentials.

However, reproduction of normal physiology is not the limit of this model. By artificially reducing current activation terms within the model, predictions can be made with regard to likely *in vivo* responses to the inhibition of a putative ion channel in this system. It has already been shown, in the construction of this model, how the addition of novel conductances to the model has built it up from a basic, single-channel model to one which now faithfully reproduces *in vivo* electrophysiological results. Within the construction process, it was noted how certain channels, *e.g.*, VKC, were required in the initial dynamic stretch-response phase, but that their sustained activation could not account for hold-

potential repolarisation. Rather, this perturbation of the model evoked a "pathological" spiking behaviour [see **Fig. 16B**].

Similarly, now that the model has been fully constructed and can account for the entire stretch-hold-release response, by artificially deactivating a component of the model, its role in generating observed stretch-evoked responses can be predicted. Consequently, this model was manipulated to attempt to predict what differences might be observed between electrophysiological recordings from endings in normal conditions and recordings from endings where putative mechanotransduction components are impaired. Thus, the model could indicate the expected variations that should be observed in *in vivo* results where specific components of the mechanotransduction system are inhibited.

The model is based upon the assumption, indicated by the experimental data that inspired the original model [Swerup & Rydqvist, 1996], that a primary mechanosensitive sodium channel gates the transduction process that is evoked by a stretch stimulus. The effect of MNaC activation on the partial receptor potential, recorded in the presence of TTX, TEA and 4-AP, was reported in the original model paper [Swerup & Rydqvist, 1996]. However, the role of the MNaC in the generation of all the components of stretch activation could now be fully tested. Therefore, the predicted behaviour that inhibiting such a channel would evoke was determined, *in silico*, by "inhibiting" the model MNaC.

Within the model, the open probability of the MNaC (P_0) is dependent upon the tension that is evoked in the ending (σ_m), which, in turn, is a function of the rate of extension (a). Thus, the effect of "inhibition" of the MNaC was predicted by comparing evoked receptor potentials in the model for decreasing values of a. It should be noted that this "inhibition" would occur *in vivo* in two scenarios: (1) blockade of the MNaC, or (2) stimulating the ending with smaller stimuli. In the model, these two options are both represented by this mechanism and are indistinguishable.[5]

As the mechanism of hyperpolarisation generation is still poorly defined in the *in silico* model, due mostly to the remaining uncertainty surrounding its exact activation mechanism, the MKC components are not included in this section.

When stretch activation in the model is reduced in 2μm increments, via reduction of σ_m, a corresponding, non-linear reduction in the amplitude of all points of the corresponding voltage output is observed [see **Fig. 18**]. The model clearly indicates that a reduction in MNaC activation results in reduced receptor potential generation: that is to say that, in the

5 This phenomenon will be considered in greater detail in **Ch. 3.2.4 & Ch. 4.2.1.**

"inhibited" model, the amplitude of receptor depolarisation at any given point of the receptor potential profile is lower than in the control scenario.

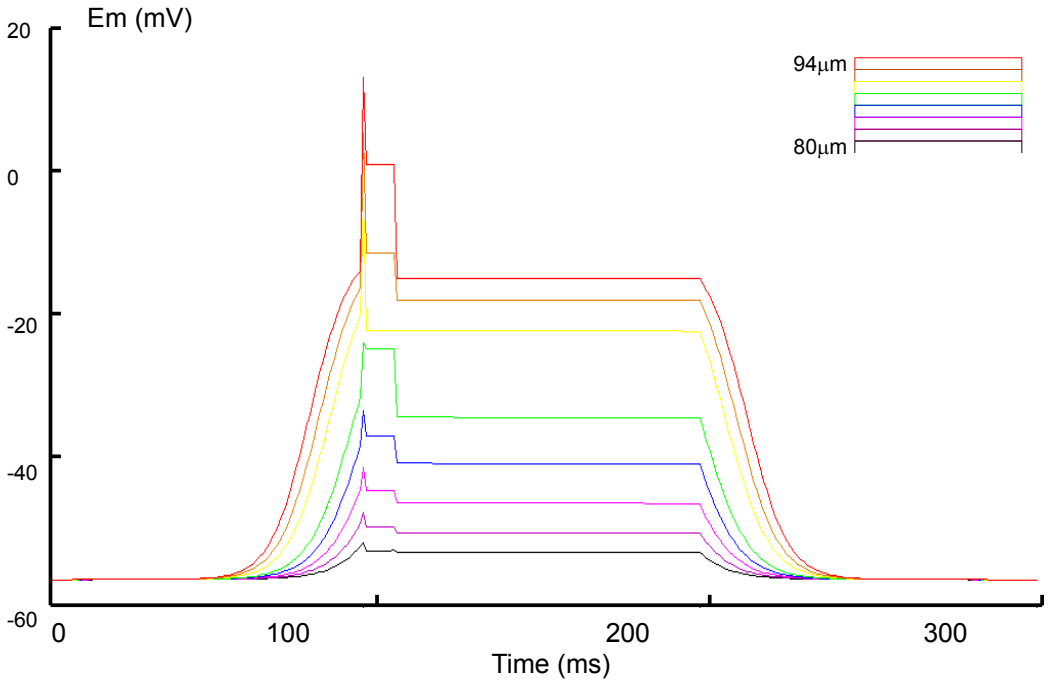

Figure 18: Modelling incremental inhibition of the mechanosensory sodium current proportionally inhibits all components of the receptor potential. MNaC activation is inhibited by the equivalent of 2mm increments with proportional inhibition of depolarisation (descending traces). The after-depolarisations (shoulder) and hold potentials are correspondingly reduced, as well. Mathematically, the model will not accept an activation value of 0, but as $MNaC_{Act} \rightarrow 0$, $E_m \rightarrow 0$mV. As the MNaC does not determine the post-release hyperpolarisation, and due to the incomplete modelling of the post-release behaviour, this has been omitted from this figure, for clarity.

This universal inhibition is unsurprising. All components of the model system require MNaC activation, so inhibition of the MNaC would be expected to produce an overall block. The non-linearity of the inhibition is also unsurprising, from a modelling point of view, as E_m varies in proportion to P_o, which is itself a function of an inverse variable with σ_m in the exponent, *i.e.*, $E_m \propto \frac{1}{a^{\sigma_m}}$, where a merely represents the other factors in the stretch-dependency relationships. What is particularly interesting about this result is how it relates to *in vivo* physiology. It has previously been reported that muscle spindles exhibit a sinusoidal

stretch-response modulation, which may appear linear over very short ranges [Hullinger *et al.*, 1977; Hunt & Wilkinson, 1980]. This would appear in accordance with the behaviour of the model, which shows a distinct sigmoidal curve to its stretch-response relationships.

2.4. Moving towards a more complete model – progress and limitations

Thus, the current state of stretch receptor modelling, as presented above, is a biophysical model of stretch receptor activation that accurately recapitulates the electrophysiological behaviour of a stretch-activated afferent ending, as observed in various examples of such an organ [Hunt *et al.*, 1978; Ottoson & Swerup, 1985a]. This model now represents the receptor potential of a stretch-activated neuron throughout a ramp-and-hold stretch protocol.

However, it can be seen that there are some characteristics, observed *in vivo*, that are not displayed in the model [see **Fig. 17**]. In particular, the repolarisation overshoot [4 in **Fig. 15C**], that occurs during the transition from dynamic to static stretch, is diminished in the model. Further, the release response [6-7 in **Fig. 15C**] in the model is very clearly an approximation. These incongruities would suggest that this model remains incomplete, or uses an over-simplified approximation to describe these phases.

The key issue that remains unaddressed in this model is that of a potential role for calcium. Currently, what was initially characterised as a VNaC [Suslak *et al.*, 2011] has now been repurposed as a Ca_v with no significant disruption to the receptor potential produced by the model. This results in a potential mechanism for calcium entry into the stretch response system. However, the transient opening of Ca_v channels does not provide enough calcium to activate K_{Ca} channels, like BK [Vergara *et al.*, 1998; Fettiplace & Fuchs, 1999]. Thus, some further calcium component must be required, such as intracellular store release, but it is currently unclear as to how that might be modelled.

Importantly, although the model generally reproduces the data for a number of different receptors, it does not imply that the same channels are used. The model does not specify channel species, merely the currents which are required to be permitted in order to reproduce the receptor potential profile. Therefore, in order to determine mediating components of stretch transduction, this model is limited in its use in that it requires extant expression data from the receptors of interest. Known expressed channels could be compared to the requirements of the model to support experimental evidence of their role in stretch transduction in afferent endings.

The absence of channel-type specification does allow the model to be employed as a general representation of what may underlie the overall behaviour of stretch receptors, or other receptor types that may exhibit similar electrophysiological properties. Whilst the model is non-specific in terms of ion channels, it does present a coherent model of the precise electrical behaviour, exhibited by a number of stretch receptors [Hunt *et al.*, 1978; Ottoson & Swerup, 1985a]. Thus, the utility of this model is not limited to identifying specific ion channels in an isolated system. Rather, its utility lies in predicting behavioural effects in a variety of endings that, overall, exhibit the same electrophysiological properties.

Interestingly, whilst the additional MKC solution resolves the hold potential disparity, it does not necessarily specify that this potassium current is required to be directly mechanically gated. Although that is the gating mechanism that has been suggested in the model (and indeed, that mechanism does work), the feature of this mechanism that is key is not its mechanosensitivity, so much as it is that it may be co-activated by the other model components. What this means is that, despite the possibility that the potassium current may be mechanically gated, it may also rely on some other activator, such as calcium. However, such upstream components must, themselves, be mechanically gated. Hence, this model works because the gating mechanism of this current must be mechanical at some level. This may either be direct, with an MKC that is gated at high tension, or it may be indirect, via a rapid, intracellular process that is also mechanosensitive. This would most likely involve intracellular calcium release, activating a Ca^{2+}-activated potassium channel.

There are numerous potassium channels in the literature that have been shown to be mechanosensitive, including bacterial MscK channels [Li *et al.*, 2007], and mammalian channels like TREK-2 [Bang *et al.*, 2000] and TRAAK [Maingret *et al.*, 1999; Lesage *et al.*, 2000], amongst other 2P domain K^+ channels [Patel *et al.*, 2001], M-type channels [Passmore *et al.*, 2012], and BK, IK and SK channels [Phillips & Arnolda, 2002; Hammami *et al.*, 2009]. These latter channels comprise the calcium-activated potassium channels [Berkefeld *et al.*, 2010], which are the most likely candidates for the MKCs proposed by the model.

The other important observation, at this point, is that the novel current component, due to its high activation threshold, has no appreciable effect on the dynamic stretch response. The initial depolarisation and after-depolarisation are still visible, as before. Thus, the major discrepancies between the model and *in vivo* data throughout the activation phases – dynamic and static stretch – have been resolved.

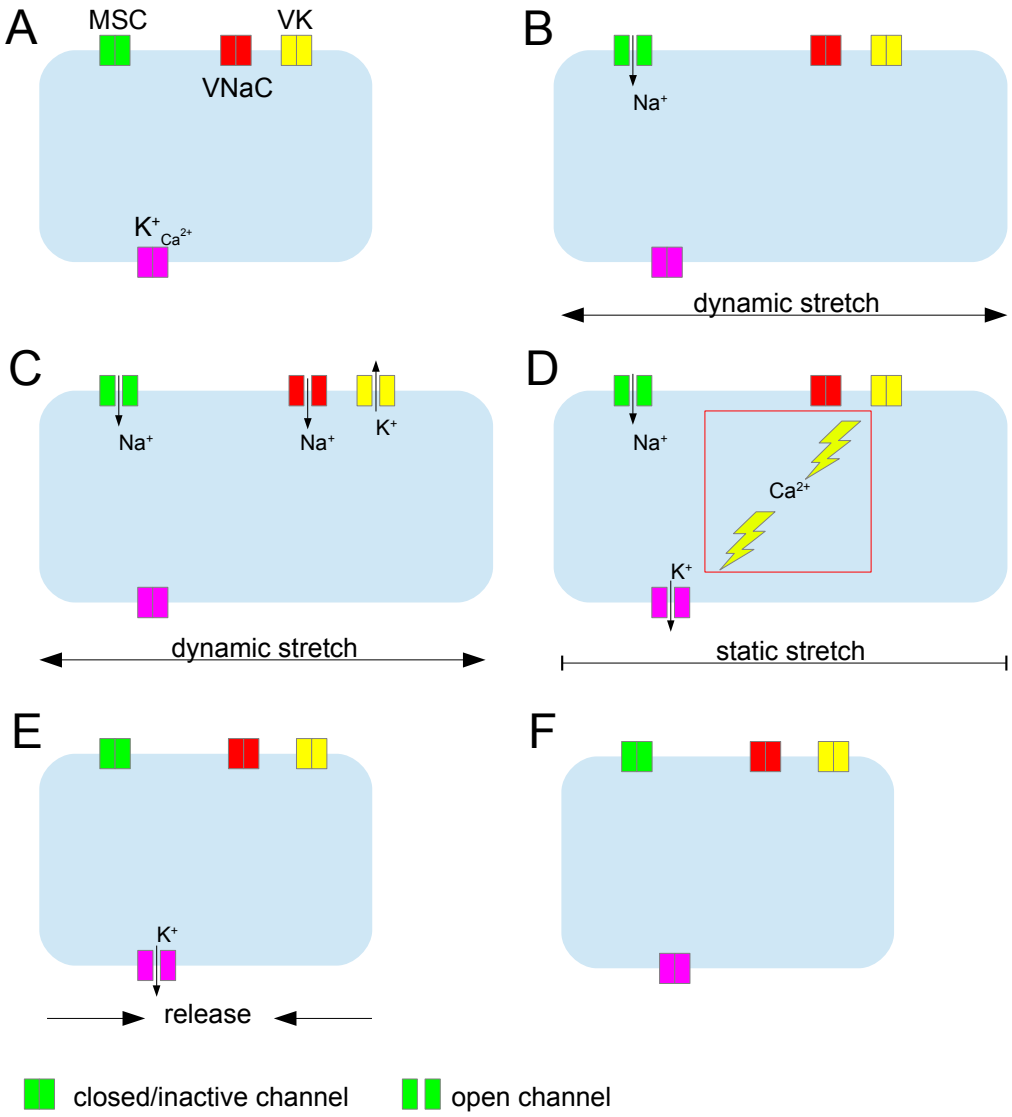

Figure 19: Diagrammatic representation of the predicted molecular model of stretch receptor activation. (A) The model predicts a minimum of four, essential components for stretch receptor activation. (B) When the ending is stretched, MNaCs open, allowing sodium-mediated depolarisation. (C) As dynamic stretching continues, voltage-gated Na^+ and K^+ channels open, transitively. (D) The voltage-gated channels deactivate rapidly and, upon transition to static stretch, additional K^+ channels are activated to repolarise the ending to its 'hold' potential. This is possibly a calcium-mediated mechanism, although that is still unconfirmed. (E) Once the tension is released, the ending contracts, closing MNaCs, but a potassium current persists, causing hyperpolarisation. (F) This current slowly decays as all tension is released and the ending returns to its resting state.

One consideration that must be made is that this model does not concern itself with non-ionic mediators of the stretch response. There may be additional modulators of stretch transduction, especially within static stretch, that have effects on the receptor potential, but which act via intracellular pathways, rather than directly through ion channels. For example, it has been proposed that phospholipase-D, coupled to a metabotropic glutamate receptor, may be implicated in the stretch response of muscle spindles [Bewick *et al.*, 2005]. The effect of this on the receptor potential, though, is unknown and, therefore, cannot be modelled at this stage.

Finally, it should be noted that, despite the success of this model in its ability to reproduce stretch-evoked receptor potential, the scale and style of this model are limited. This modelling approach was selected due to previous evidence of its utility [Swerup & Rydqvist, 1996]. However, such an approach is relatively high-level, and ignores such features as subcellular architecture of the receptor cell, or spatial organisation. Such considerations would be essential for the use of a model in determining, for example, the positioning of stretch transduction mediators within the cell, or elucidating the fine detail of the intracellular transduction pathway, with regard to molecular interactions.

A compartmental model, which can differentiate the dendritic and somatic contributions to mechanosensitive adaptation, may provide further detail in this area. However, in order to parametrise such a model, more information would be required on the location of ion channels within the cell, necessitating, perhaps high-resolution imaging data at the subcellular level.

2.5 Summary

Prior to this investigation, it was noted that a simple, biophysical model could potentially describe the pattern of a stretch-evoked receptor potential in a defined mammalian mechanoreceptor – the muscle spindle. However, it was noted that current work in this field fell short of a full recapitulation of same, limiting the utility of such a tool in the study of mechanoreceptor electrical adaptation.

This study successfully implemented modifications to a prior model, that had previously appeared suitable for modelling mammalian stretch receptor responses. By accounting for additional putative components of the proposed stretch receptor system, the current model can now accurately reproduce traces of muscle spindle receptor potentials. These additional components, previously absent from the model, are proposed to be a novel mechanosensory

potassium channel (which may also be modulated by calcium), and a transiently-active Ca_v channel, which replaces the proposed VNaC of the prior model.

This model does, however, rely upon the assumption, based upon evidence from the literature, that such components exist in a number of biological systems. The assumption is not the existence of these components *per se*, rather it is that these components all exist within the same mechanism [see **Fig. 19**]. As evidence of this, the model accurately reproduces *in vivo* observations and makes firm predictions about how this putative system should respond to certain, specific challenges, which could be easily tested within a suitable *in vivo* model system. Consequently, it remains to determine the accuracy of the predictions of the model as to whether the putative system components fairly correspond to an *in vivo* scenario[6]. It is hypothesized that an *in vivo* system will show the strong MNaC dependence of stretch activation that the model describes.

6 The full code for the complete model appears in textual form in **Appendix i**.

3. Establishing an *in vivo* model system

3.1. Identifying a model system

The receptor potential of stretch-activated, mechanosensory neurons had now been successfully modelled, *in silico*. This model faithfully reproduced previously observed recordings of receptor potentials in both vertebrates and invertebrates. However, this had only been shown qualitatively. In the absence of any contemporary, quantitative data, the model could not be fully verified, thus, any predictive power of the model could not be utilised. Therefore, it was necessary to obtain recordings of stretch-evoked receptor potentials that could be quantified and compared to the *in silico* model. However, in considering setting up a system for recording data to verify the model, importance was also placed upon other factors - principally the rapid acquisition of high-quality data and the ability to effectively test for the involvement of candidate channels by pharmacological and genetic means. Thus, a suitable model system would necessarily be readily amenable to both electrophysiological investigation and genetic assays.

Consequently, a return to the crayfish stretch receptor system was ruled out, due to a lack of experience in that system and lack of availability. Similar issues were raised with using the mammalian muscle spindle system. A lack of experience in preparing this system and a lack of local facilities and expertise working with muscle spindles effectively precluded their use. In addition, the difficulty in recording receptor potentials in that system, due to anatomical complexities of the endings, was a significant factor. The fibrous capsule that encloses the spindles presents a significant barrier to recording electrodes and disruption of that capsule risks changing the nature of the spindle, physically and electrochemically, such that any recordings thereafter achieved would not sufficiently reflect the *in vivo* scenario.

However, stretch receptors in some insect larvae had previously been studied. As illustrated in **Ch.1**, the SRO of hawkmoth caterpillars (*Manduca sexta*) had earlier been identified as a putative organ of muscle stretch sensation [Levine, 1984; Tamarkin & Levine, 1996]. Whilst a study of these neurons was ruled out, for similar reasons to the exclusion of crayfish, larval *Drosophila* possess an anatomically similar organ – the dorsal bipolar dendritic (*dbd*) neuron (sometimes referred to as *dbp* - dorsal bipolar neuron) [Bodmer & Jan, 1987; Schrader & Merritt, 2007; also see **Fig. 5**]. Two *dbd* neurons are located in the dorsal body wall of each

larval abdominal segment, between the muscle layer and the external cuticle. They are immediately distinguishable by their two, longitudinally-projecting dendrites, which extend from the cell body of the neuron along the long axis of the larva, into the underlying muscle. The axon of the *dbd* neuron projects perpendicularly to the CNS, giving the neuron a distinctive T-shape.

At the gross anatomical level, *dbd* neurons appear highly similar to SRO neurons, as well as crayfish stretch receptors and mammalian muscle spindles. All of these receptors exhibit similar shape and orientation, relative to striated muscle fibres, with which they interface [see, for example, Fitz-Ritson, 1982; Swerup & Rydqvist, 1996]. Additionally, studies in *Manduca* show evidence of a sensory-motor feedback loop, connecting SROs with associated motor neurons [Levine, 1984; Tamarkin & Levine, 1996]. These resemble the association of muscle spindles with gamma motor neuron fibres, innervating the intrafusal muscle [Boyd, 1986; Banks, 1988], and *dbd* neurons in *Drosophila* do appear to be similarly connected [Hughes & Thomas, 2007]. Overall, there is sufficient likelihood that these receptors may all share some homology.

As a result, it was hypothesized that an understanding of the underlying mechanisms of *dbd* neurons would provide insight into the molecular workings of these analogous stretch receptors. Thus, *Drosophila melanogaster* was proposed as a suitable model organism. It was put forward that the simplicity of the anatomy of *Drosophila* larvae would facilitate recordings of receptor potentials. The larval *dbd* neuron is readily identifiable and is easy to access for electrophysiological recording, as previously demonstrated [Nair *et al*., 2010][7], indicating that data acquisition should be realistic. Additionally, the genetic toolbox for *Drosophila* would be a great asset in probing for components of a mechanotransduction system.

3.2. Electrophysiology

3.2.1. Dissection set-up

Third instar larvae were pinned rostrally and caudally in a Sylgard-lined, 35mm dish, and filleted via a lateral, longitudinal incision and dorsal, transverse incisions, rostrally and caudally. The viscera were excised with forceps and the dorsal cuticle was folded out,

7 The work of this group is laid out in more detail below, establishing the basis of the technique development that occurred in this project.

longitudinally, and pinned, resulting in a cleaned pelt, presenting the internal aspect uppermost, with the outer cuticle proximal to the dish [see **Fig. 20**]. The dissection was carried out with the preparation bathed in HL3 solution [Stewart *et al.*, 1994] and using a dissecting microscope, between x10 and x40 magnification.

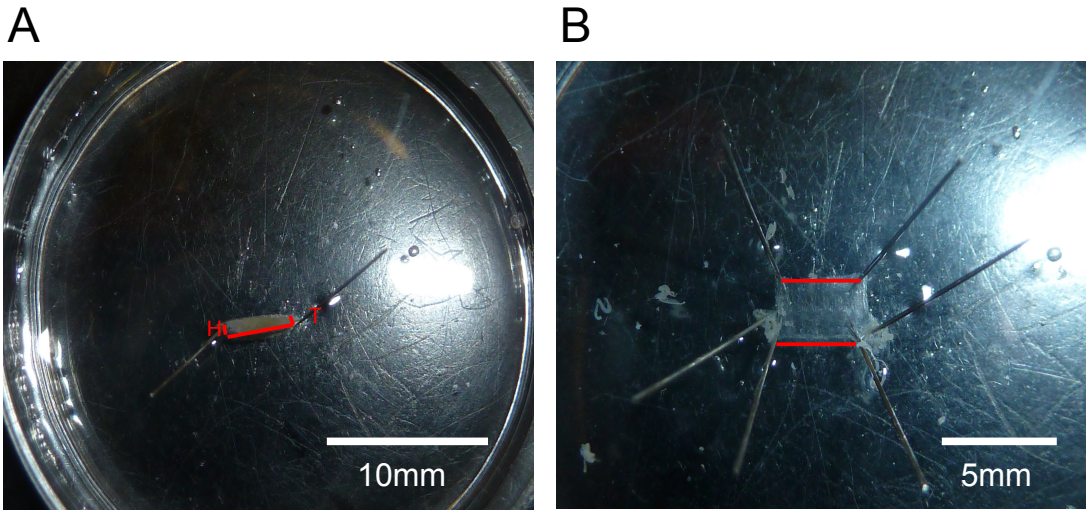

Figure 20: Larval dissection for electrophysiology. (A) A larva is pinned rostrally (H) and caudally (T) in a 35mm Sylgard-lined dish. A longitudinal lateral incision and two dorsal transverse incisions (red lines) are made. (B) The viscera are excised and the dorsal pelt is reflected, longitudinally, and pinned in each corner, exposing the internal musculature (red lines highlight cut edges).

As previously intimated, this technique is based upon that outlined in earlier works – predominantly that of Nair *et al.* [2010], but with some reference to earlier work by Baines & Bate [1998]. However, a number of considerations influenced the development of this technique, resulting in modifications to those used in these prior studies. Firstly, both previous electrophysiological studies of *dbd* neurons had used 1st instar larvae, demonstrating that it is possible to make recordings from early-stage larval neurons. However, it was proposed that using later-stage, 3rd instar larvae would facilitate dissections and recordings, due to their larger size. Indeed, dissections of 3rd instar larvae presented no discernible issues and were therefore utilised throughout.

Secondly, due to the position of *dbd* neurons within the larvae, a lateral, longitudinal incision was preferred to the more traditional longitudinal dorsal mid-line incision. Whilst a lateral incision jeopardises one of the bilateral pair of neurons, one neuron *per* segment is always preserved. A mid-line incision risks damaging or impairing access to both.

Thirdly, HL3 (70mM NaCl, 5mM KCl, 1.5mM $CaCl_2$, 20mM $MgCl_2$, 10mM $NaHCO_3$,

5mM Trehalose, 115mM Sucrose, 5mM HEPES) was preferred as an external saline solution to HL3.1 (as HL3, except 4mM $MgCl_2$). It had been observed that there are inconsistencies in neuronal excitability properties at NMJs when recordings were performed in HL3 as opposed to the modified HL3.1 [Feng *et al.*, 2004]. However, as these variations were only reported in NMJs, which were not the focus of this study, HL3 was considered sufficient. Additionally, Feng *et al.* [2004] reported that preparations in "standard saline" (128mM NaCl, 2mM KCl, 1.8mM $CaCl_2$, 4mM $MgCl_2$, 35.5mM Sucrose, 5mM HEPES) [solution A, Jan & Jan, 1976] suffer in terms of longevity, which became especially noticeable after 1-2 hours. This gave a further reason to prefer the use of HL3 over "standard saline".

3.2.2. Recording set-up

Prior to this study, recordings of stretch-evoked potentials in mechanosensory neurons in *Drosophila* had not been attempted. Recordings of mechanosensory potentials in mammalian neurons existed and previous studies had achieved recordings from *dbd* neurons. In order to achieve recordings of stretch-evoked potentials, the techniques used in earlier studies were used as a starting point for the development of a mechanoreceptor recording protocol in *dbd* neurons in *Drosophila* larvae.

Hunt *et al.* [1978] had recorded receptor potentials in mammalian muscle spindles by poisoning the afferent axon with TTX and then recording, via sharp electrode, from the axon. TTX blocked the initiation of action potentials so that changes in the receptor could be detected. A similar technique had also been employed in crustacean stretch receptor recordings [*e.g.* Brown *et al.*, 1978]. The neurons in *Drosophila*, however, are too small for this type of recording. Previous studies of *Drosophila* neurons, both of central neurons and primary sensory neurons, had successfully used whole-cell patch clamping to record from these cells [Baines & Bate, 1998; Nair *et al.*, 2010]. Therefore, this technique seemed a likely approach for recording mechanoreceptor potentials.

Both Baines & Bate [1998] and Nair *et al.* [2010] used a protease digest system, administered via a large-diameter patch electrode, to digest small portions of the muscle tissue above the target recording sites in the dissected larval preparation, exposing the cell bodies of the underlying neurons, to allow patching. They then successfully showed recordings from *Drosophila* neurons in whole-cell configuration.

Thus, dissected larvae [as described above] were viewed with a Nikon inverted microscope at 400x magnification. Magnification was achieved with a Wetzlar SPL 20/0.25 and either a

Nikon CFW 10x eyepiece or a WF 20x eyepiece. This enabled visualisation of *dbd* neurons by eye. In the dissected preparation, access to the *dbd* neuron is inhibited by the overlying muscle layer. The *dbd* neuron lies between the musculature and the outer cuticle. In order to access it with a patch electrode, it is necessary to partially digest the muscle layer. A small portion of muscle overlying the *dbd* neuron was digested with 1% Type-XIV protease [Sigma], administered via a large-diameter patch electrode, using a Narishige MC-35 micromanipulator. The muscle layer can be seen degrading as it peels away from the preparation. Debris was removed by suction into the protease pipette and the pipette was withdrawn.

A 1μm patch pipette (pipette resistance between 10MΩ and 20MΩ), containing internal saline [140mM KCH_3SO_3, 2mM $MgCl_2$, 2mM EGTA, 5mM KCl 20mM HEPES, pH7.4 – Nair *et al.*, 2010] was then introduced, and suction applied to form a seal and subsequent whole-cell configuration of the *dbd* neuron cell body, using a manual syringe. The electrode was held in an Axon Instruments CV201 headstage, connected to an Axopatch 200 patch amplifier. The amplifier interfaced with a PC, running Windows XP, via a Digidata 1200. Recordings were made in whole-cell configuration, recorded in real-time in WinEDR or WinWCP [© University of Strathclyde].

This protocol was initially taken entirely from the methods of Nair *et al.* [2010]. However, some adaptations were required in order to optimise the recording environment. Firstly, the longevity of the preparation in the recording configuration, which was already naturally limited, was further reduced by the harsh environment that exists post-protease application. This was a significant issue as the initial lifetime of the preparation, during which recordings could be made that were both reliable and representative of normal physiology, was only around two hours for a long-lived preparation. Protease digest could reduce this to 30 minutes, which significantly reduced the time available to successfully patch a neuron.

Secondly, achieving a successful, high-quality patch in these preparations is already a significant challenge. The necessary protease digest removes much of the anchoring tissue, resulting in the cell body of the neuron being able to acquire some degree of movement, due to fluid motion in the dish. This results in a high failure rate for patching attempts. The rate of successful patching was ~10%, on average wasting every second preparation entirely.

In order to overcome these issues, the Sylgard-lined dish that was initially used for pinning out the preparations was substituted for a custom-made Sylgard-lined flow chamber [see **Fig. 21**]. The advantage of the flow chamber over the dish set-up is that it permits the

removal of the protease after it has had the desired effect and allows washing with fresh saline, to give a more stable recording climate. Limiting the protease application time in this fashion greatly reduced extraneous structural damage to the tissue surrounding the *dbd* neuron, as well as limiting degradation of the neuron itself. This made the neuron less motile and, therefore, easier to patch successfully, increasing the success rate to ~20%. Reduced tissue damage also enabled patching of multiple *dbd* neurons within the same preparation, as longevity was less adversely affected. This availability of additional neurons helped compensate for the failure rate of patches. Thus, a well-dissected preparation, with four well-presented segments, containing a total of 8 *dbd* neurons, now yielded successful patches of 1-2 neurons per preparation, on average.

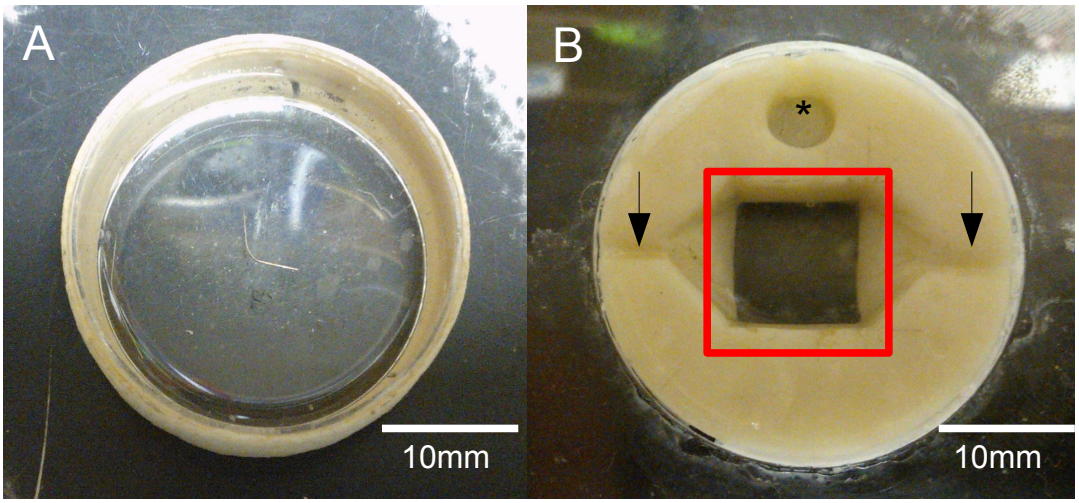

Figure 21: A custom-made Sylgard-lined flow-chamber was devised to replace the Sylgard-lined dish, previously used. Dissecting and recording from a larval preparation in a dish (A), whilst useful, prevented efficient removal of the protease solution from the preparation, post-digest, resulting in on-going degradation of the preparation, beyond the point of utility. This format also precluded washing drug solutions on and off. A shallow, Sylgard-lined, wax-mould flow chamber was substituted (B). The preparation was pinned, as before, in the centre of the chamber, comprised of a Sylgard-lined coverslip (outlined in red). For recordings, the dish was flooded with recording solution. The circular mould at the top of the dish provided a secure receptacle for the earth electrode (*). The bilateral channels (arrows) enabled the washing on and off of additional solutions, permitting the removal of proteases, post-digest, as well as the application of drug solutions.

3.2.3. Mechanical stimulation

Having established a protocol for recording receptor potentials from *dbd* neurons, the remaining challenge in setting up this system as a model for mechanotransduction recording was to incorporate a method for mechanically stimulating the receptor, within the established recording setup. Hitherto, mechanical stimulation of a *dbd* neuron preparation had not been reported in any published study. The main issue with this is providing sufficient stimulation to the cell in order to evoke physiological responses, whilst simultaneously avoiding rupture of the pipette seal and adverse damage to the electrode resistance. Delmas *et al.* [2011] summarise a number of methods currently available for mechanically stimulating a cell, which is being recorded from using patch-clamping. However, this review deals mostly with individual or cultured cells. Therefore, taking into account the preparation being studied, a number of methods were devised and trialled.

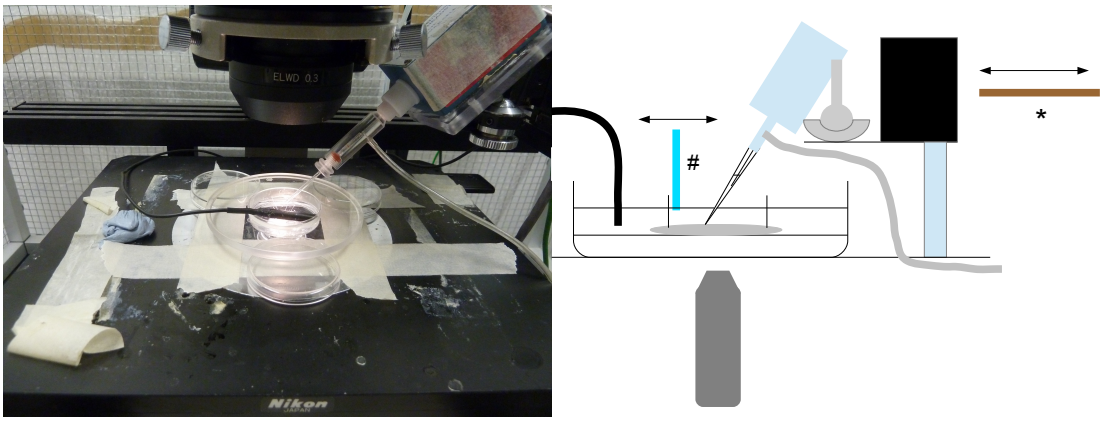

Figure 22: An insulated probe was used to mechanically move the electrode holder configuration, relative to the preparation, to provide mechanical stimulation. Left: the recording apparatus was set up as detailed in Section 3.2.2 (apparatus shown includes the dish, in place of the flow chamber). Right: a diagrammatic representation of the apparatus. Once whole-cell configuration had been acquired, a rigid, insulated probe, such as a wooden ruler, was used to tap the electrode holder, hold it briefly, and then release it, allowing it to recoil to its initial position (* in diagram, not visible in photograph). The automated technique (p.55ff) exchanges this probe for an electrically-driven piezoelectric wafer (# in diagram, not visible in photograph), which actuates the pin in the head of the larva [see **Fig.26**].

As a starting point, the method of puffing a fluid across the preparation, as outlined by Delmas *et al.* [2011], detailed in McCarter *et al.* [1999], was considered. It was thought that this method would provide the necessary stimulation to the neuron. However, within the

confines of the experimental configuration, this approach proved ineffective as insufficient force resulted.

The second method that was considered, although cruder in practice, proved more effective. It consisted of manually displacing the cell-electrode configuration, after successful patch acquisition, via an 'elongated tap' approach. The electrode holder was manually displaced, using an insulated probe (such as a wooden rod or ruler, or some similar, rigid object), by a push, a brief hold, and, finally, releasing the holder again [see **Fig. 22**]. This somewhat 'low-tech' approach successfully evoked what will later be shown to be maximal responses from the neuron, which could be recorded without damaging the patch seal. Thus, this technique was suitable for both quantifying receptor potentials and for testing pharmacological and genetic manipulations of the *dbd* neuron system.

Figure 23 [opposite]: Mechanically stimulating *dbd* neurons evoked stimulus-dependent responses, displaying variation proportional to the range of stimuli. Following mechanical stimulation, using the manual method [see **Fig. 22**], electrical adaptation was recorded in each stimulated neuron. Generally, neurons exhibited 'classical' stretch-evoked responses (A, B, C, E, F, H, I, K, L). However, significant variations on this theme were noticeable, due to an inability of this technique to produce reliably repeatable stimuli. Thus, a range of hold lengths are apparent (*cf.* A, C & H). Some hold phases are interrupted by movement (as in B, D & I) causing disruption of the stable hold potential. A minority of recordings appear to show spike-like events (G & J). These are mechanoresponses, however the stimuli lack a defined hold period. Thus, these may be the static stretch depolarisation responses, as recorded in stretch-and-hold protocols (*cf.* A, B, E). Alternatively, the initial depolarisation may be considered to be a spiking event. Mechanically stimulating non-neuronal cells, in contrast to stimulating *dbd* neurons, evokes square depolarisation responses, in place of the adapting mechanoresponse of the receptors (M & N). Traces shown taken from recordings from four neurons (1: A-C, 2: D-G, 3: H & I, 4: J-L). All traces shown with 0mv line (horizontal line) and stimulus protocol (below each trace).

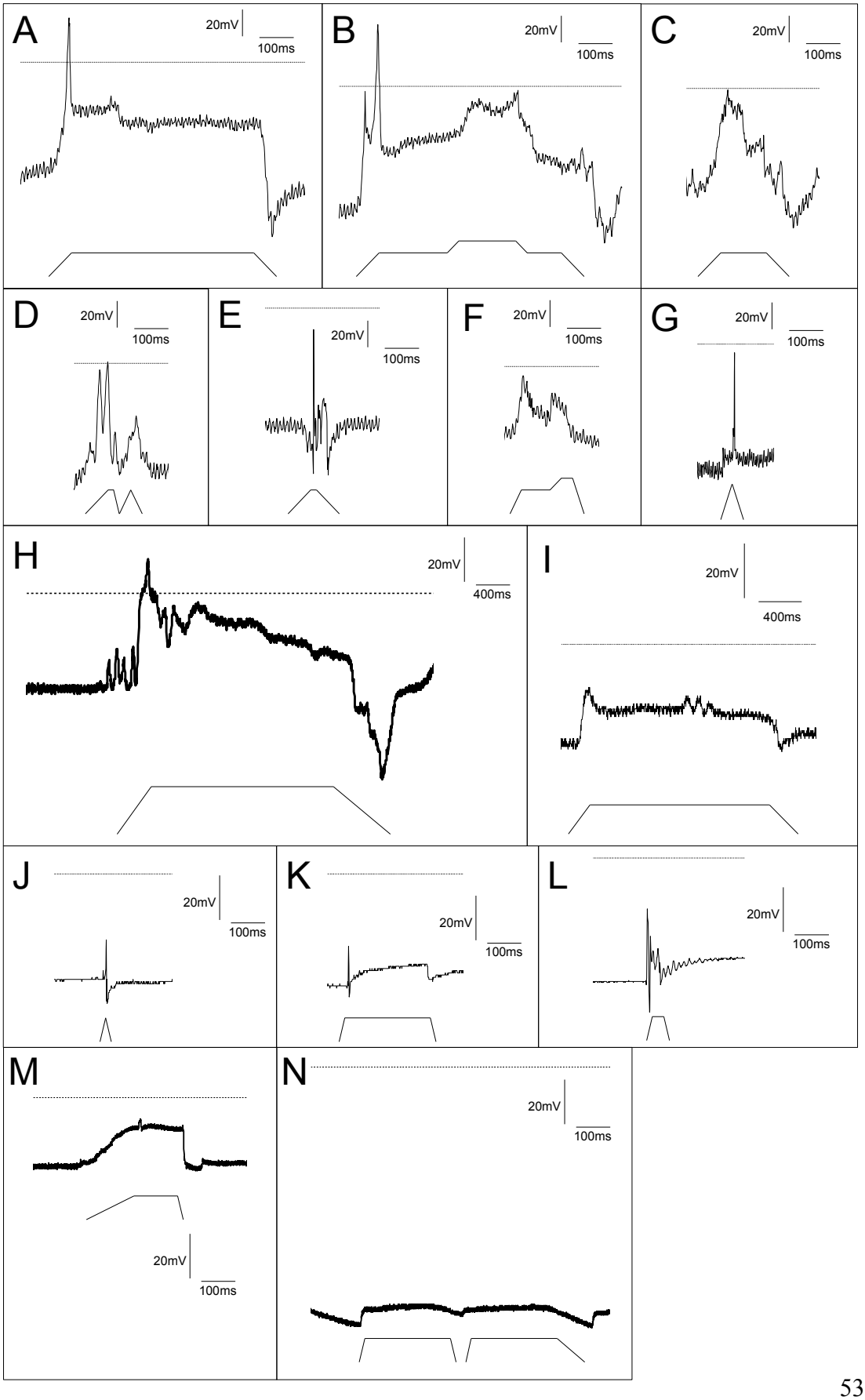
A
20mV
100ms
B
20mV
100ms
C
20mV
100ms
D
20mV
100ms
E
20mV
100ms
F
20mV
100ms
G
20mV
100ms
H
20mV
400ms
I
20mV
400ms
J
20mV
100ms
K
20mV
100ms
L
20mV
100ms
M
20mV
100ms
N
20mV
100ms

Examples of data, recorded from a number of *dbd* neurons, in control (w^{1118}) flies, are shown [see **Fig. 23**]. These data illustrate the effectiveness of this technique in evoking stretch-dependent responses from a number of *dbd* neurons. The classic response to stretch-and-hold stimuli can clearly be seen in the responses of neurons 1, 2 and 3 [**Fig. 23 A, E, H & I**]. In these examples, dynamic stretch evoked a large, initial depolarisation, which partially repolarised to a 'hold' potential upon transition to static stretch. Release of stimulus resulted in hyperpolarisation, before a return to resting membrane potential. Other responses, whilst not as clearly conforming to this classic pattern, still clearly show phases of response that correspond to these recognised distinctions [**Fig. 23B, C, D, F, K & L**].

In some recording trials, the electrode missed the target cell and instead patched onto the underlying cuticle. In contrast to the responses of *dbd* neurons, attempting to mechanically stimulate epithelial cells did not produce the mechanoresponsive profile seen in *dbd* neurons. Instead, stretching these cells produced square, depolarisation pulses [**Fig. 23M & N**]. Such pulses would perhaps be consistent with the presence of an MNaC, such as a mechanosensitive epithelial sodium channel. Clearly, though, these cells lack the adaptive machinery that enables the multivariate, adaptive response of the mechanosensory *dbd* neurons.

A significant factor in this variability is likely that this technique was also highly unstable, showing poor repeatability, due to the inability to accurately quantify stimuli, beyond a large margin of error. Consecutive stimulations of a single neuron [see **Fig. 23A, B &C**], whilst attempted similarly, could not be performed identically, resulting in non-identical responses; between preparations this is even more apparent [*cf.* **Fig. 23A & H**]. However, it will later be shown that this is, to some extent, discountable, provided the evoked response is maximal. Thus, data obtained in this manner are still useful and representative.

Secondly, the manual control of stimulation was prone to shakiness, introducing an element of instability to the stimuli themselves. Thus, the hold phase of stimuli were inconsistent and liable to interruption [see **Fig. 23A, D & F**]. In such cases, the latter (post-interruption) portions of the responses have low reliability and are unsuitable for quantitative analysis.[8]

Thirdly, in a small fraction of responses, typically those that occurred when no discernible hold phase was used, 'spike-like' responses were observed [**Fig. 23G & J**]. It is important to once again stress that these responses are still due to mechanical stimulation, not current injection. This is important as, whilst they appear to resemble action potential, they are also equivalent to the initial depolarisations of the stretch response. It may be that this initial

8 Responses with unstable stimuli are not used for subsequent analysis in the following sections.

depolarisation is in fact a spike (this has been suggested to be the case in the muscle spindle [RW. Banks, personal communication]), but at this stage no definitive conclusion can be made. In none of the mechanoresponses was a series of action potentials observed.

At this point, it should be noted that, when electrically stimulating *dbd* neurons, Nair *et al* [2010] did record trains of spikes in response to 6pA current pulses. It could be considered curious, therefore, that these were not observed here. Perhaps this is due to the nature of the stimuli – the hold potential, established during static stretch, may prevent further depolarisation events. Indeed it can be seen that when additional stretch is applied, whilst the neuron is already extensively stretched, the depolarisation response appears somewhat abortive [see **Fig. 23B & F**]. This may indicate that the *dbd* normally communicates to the CNS via a single action potential to signal dynamic stretch onset, acting to limit movement by preventing over-extension.

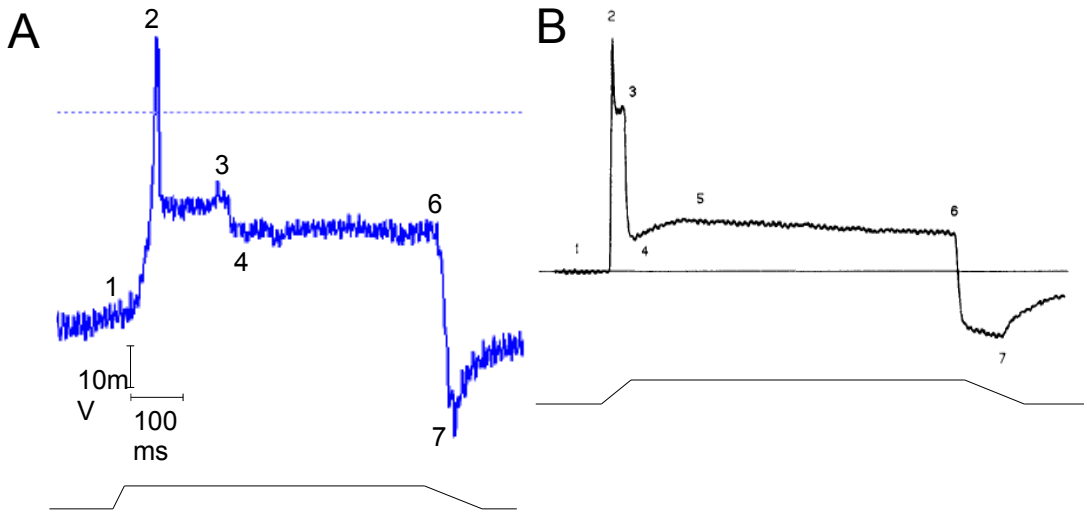

Figure 24: Electrophysiological responses of *dbd* neurons appear similar to those previously recorded in muscle spindles. (A) In response to a dynamic stretch, the *dbd* neuron exhibits a receptor potential, composed of an initial depolarisation (1-2), followed by a partial repolarisation (3). As the stimulus transitions to a static stretch, the neuron partially repolarises to a hold potential (4), which is maintained throughout the static stretch (4-6). Upon release, the neuron hyperpolarises (7), before returning to rest. (B) This stereotypical response was also previously observed in muscle spindle receptor potentials [*cf.* **Fig. 3**]. Lower traces show stimuli.

It should also be noted, though, that cell capacitance has not been noted for the cells that were recorded from in this study. It has been assumed that all *dbd* neurons are identical in this regard, as cell capacitance is a function of the thickness of the lipid bilayer, and thus can

generally be considered constant [Niebur, 2008]. However, capacitance is a factor in determining conductance velocity of, for example, action potentials. This information would, therefore, be useful in addressing this question of *dbd* action potential generation and communication to the CNS.

Nonetheless, by mechanically stimulating the cell, while recording in whole-cell configuration, it was possible to obtain a fairly consistent recordings of the *dbd* neuron receptor potential, generated in response to a stretch stimulus [see **Fig. 24**]. The overall profile of the receptor potential is complex, with several distinguishable features, most notably the initial depolarisation in response to dynamic stretch (E_p – 2 in **Fig. 24A**), the static stretch hold potential (E_{hold} – 4-6 in **Fig. 24A**) and the post-release hyperpolarisation (E_h – 7 in **Fig. 24A**). Strikingly, these same features were previously observed for mammalian muscle spindle cells [Hunt *et al.*, 1978].

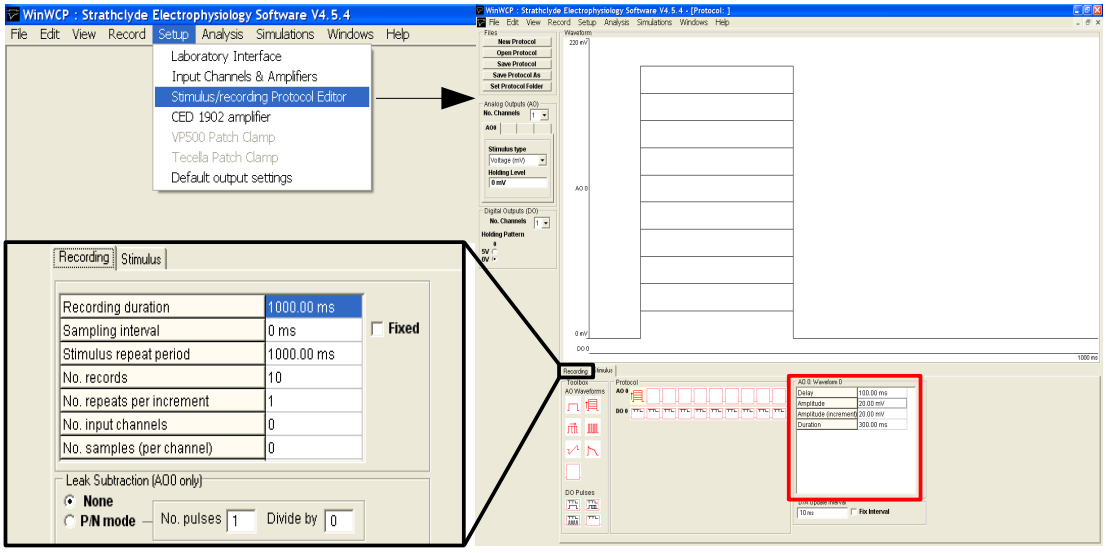

Figure 25: Mechanical stimuli were generated using the Protocol Editor in WinWCP. In order to mechanically stimulate the neuron, a stimulus protocol was designed in WinWCP. This programme contains a Stimulus/recording Protocol Editor, which enables specific, electrical stimuli to be designed. Stimulus amplitude and duration, amplitude increase increments and inter-stimuli delay duration can be set (red box), as well as recording duration, number of increments and number of protocol loops (black box). A current-clamp protocol was used to generate stimuli, which were output to a piezoelectric wafer. The wafer deflected in proportion to the current passed across it, providing a stretch stimulus to the larval preparation via the movement of the pin in the head of the preparation.

Despite the success of the above approach, its limitations with regard to being able to

produce graded and repeatable stimuli necessitated further refinement. Accordingly, and due to the assistance and materials made available through a collaboration with the Bewick laboratory [University of Aberdeen], a modification to the above technique was devised, utilising a piezoelectric wafer [PZT507, Morgan Electro Ceramics, UK] and WinWCP. Stimulus protocols could be created in WinWCP, in the manner of a current-clamp protocol, but instead of directly stimulating the cell, these stimuli could be used to drive a piezoelectric wafer [see **Fig. 25**].

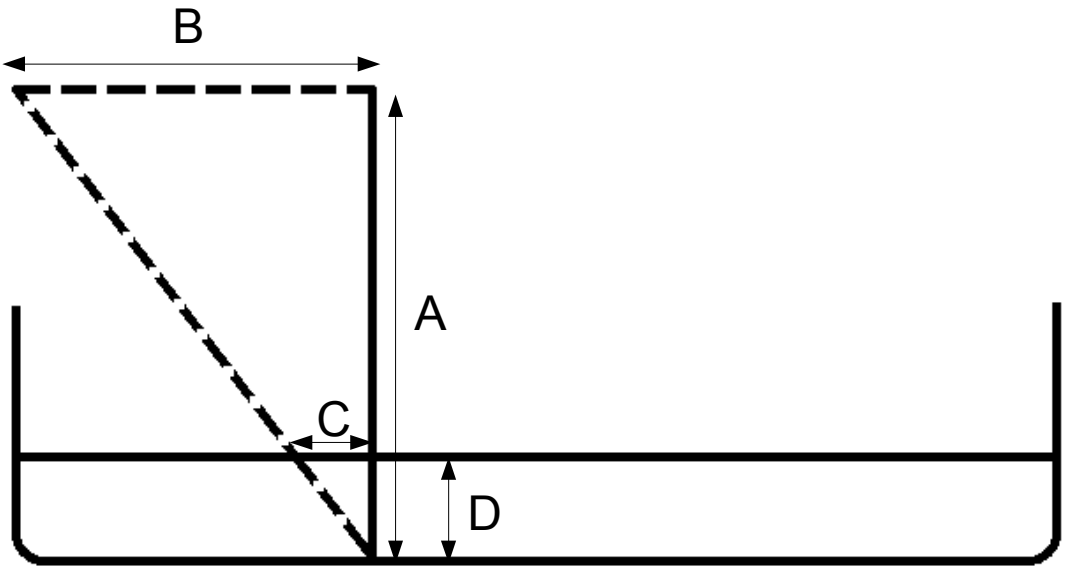

Figure 26: Calculating the stretch applied to the pinned larval preparation. For recording, a filleted larva is pinned on a Sylgard-lined dish with pins of length, *A*. The fire-polished probe, driven by a stimulus from WinWCP, deflects the top of the head pin by a calibrated displacement, *B*. Assuming a rigid pin, the displacement at the height of the pinned preparation, *C*, can be calculated as a ratio of the length of pin below the preparation, *D*, to the total pin length, *A*.

Ramp-and-hold stretch protocols of 0.5nA, 1nA and 2nA current pulses were generated in WinWCP, to drive the wafer. These corresponded to 795μm, 840μm and 962μm wafer deflections. A fire-polished, glass probe was affixed to the wafer to mechanically stimulate the cell, *in vivo*. This was achieved via positioning of the probe to, when activated, deflect the pin positioned in the head of the larva. The deflection of the pin stretched the pinned preparation, from the head end, thus stretching the dendrites of the *dbd* neuron, via elongation of the attached muscle. Using trigonometric calculations, the actual magnitude of stretches experienced by the preparation were calculated to be 76μm, 80μm and 92μm [see

Figure 27 [opposite]: Consistent stimuli produce reliable, stretch-dependent responses from *dbd* neurons. (A) Using WinWCP, 795μm, 840μm and 962μm wafer displacements, corresponding to stretches of 76μm, 80μm and 92μm (lower traces) were applied to larval preparations. Recordings from *dbd* neurons showed stretch responses that were equivalent between preparations (n=11, p>0.5). (B) Stretch-evoked initial depolarisation amplitude is proportional to stretch-impulse. 'Twitching' (instantaneous stretching) evokes a maximal initial depolarisation (data not shown). This is consistent between both manual and calibrated stimulus techniques (n=5, p>0.05[n.s.]). Ramp-and-hold stimuli evoke lower peak depolarisations, which are proportional to the stimulus amplitude (n=11, p<0.0001[*]).

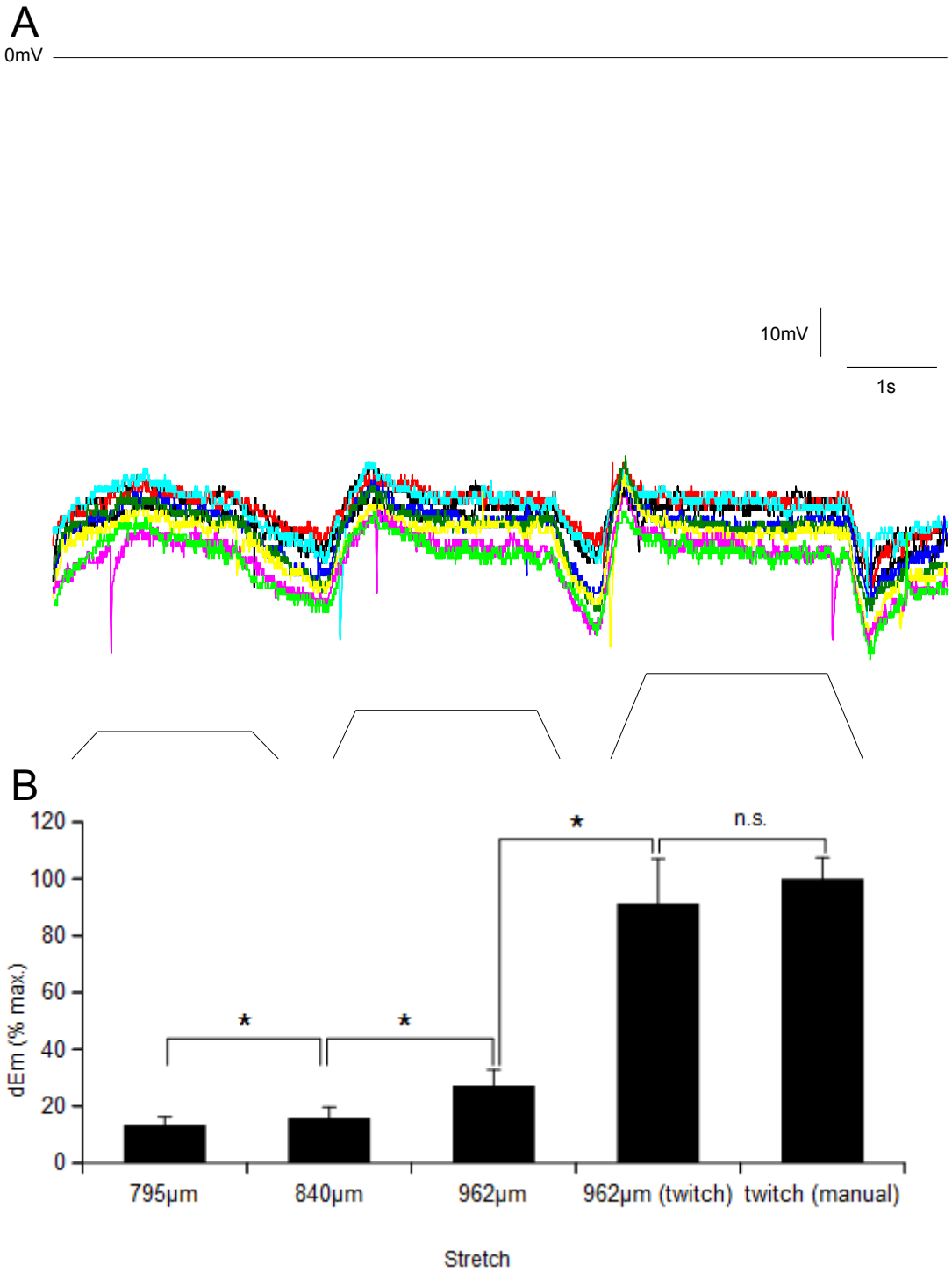
A
0mV
10mV
1s
B
120
100
80
60
40
20
0
dEm (% max.)
*
*
*
n.s.
795µm
840µm
962µm
962µm (twitch)
twitch (manual)
Stretch

Fig. 26], or 38%, 40% and 46% extensions, respectively, relative to the average length of a *dbd* neuron, measured as the distance between the tips of the two dendrites [see **Fig. 5B**].

The use of WinWCP as a stimulus generator enabled graded and repeatable stimuli to be presented. The automation of the stimulus process also greatly increased maximum recording duration, reducing breakages and patch disruptions. Furthermore, the quantifiable stimuli allow for a direct comparison of stimulus amplitude and response amplitude. Recordings from multiple neurons, under identical stimulation protocols could now be achieved. These showed that the stretch-evoked potentials, observed in *dbd* neurons are stereotyped events that are stimulus-dependent [see **Fig. 27A**]. Consistent receptor potentials are produced in response to identical stimuli, across several animals.

It was observed that the amplitude of E_p was proportional to the mechanical impulse applied to the ending. Thus, the larger the deflection of the ending, the greater the evoked E_p. Additionally, however, a rapid twitch deflection evoked a greater E_p than a slow ramp stretch of equivalent length, hence E_p is proportional to impulse, rather than force [see **Fig. 27B**]. This finding is interesting, in that it suggests that a role for these receptors may be to detect change in length over time, rather than specific length change - stretch and tonicity - which might implicate them in regulation of co-ordination and movement speed, for example.

Unfortunately, the equipment required for the use of this technique was locally unavailable. Consequently, this technique could only be used for a limited number of experiments and the majority of data acquired necessarily relied upon its precursor technique. However, a comparison of the 'twitch' data from the calibrated technique with data from the unrefined precursor method showed that the evoked receptor potentials in each case were equivalent [see **Fig. 28**]. This indicated that the manual stimulation method may have produced a maximum evoked response, meaning that data gathered with that technique could be considered to all have equivalent, maximal stimuli. Thus, due to relationship between both sets of data – those derived from manual and calibrated stimuli – they could each be used in quantitative analyses of *dbd* neuron stretch-evoked responses. Additionally, both sets of data are inter-relatable, allowing comparisons between the two types to be performed, as required.

3.3 Observed responses of *dbd* neurons correlate to previous muscle spindle data

One particularly interesting feature of the stretch responses of *dbd* neurons appeared to be their similarity to those of mammalian muscle spindles. As previously shown by Hunt *et al.*

[1978], muscle spindles exhibit stereotypical responses to ramp-and-hold stretch stimuli [see **Fig. 3**]. A qualitative assessment of traces of the voltage responses of *dbd* neurons to ramp-and-hold stimuli, via a simple side-by-side visual comparison, strongly suggested that there were links between the two data [see **Fig. 24**]. Both types of stretch responses display large depolarisation responses to dynamic stretching, followed by rapid adaptation to a 'hold' potential, maintained throughout static stretch, before hyperpolarising as tension is released and returning to rest.

Quantitative analyses were therefore performed on the *dbd* data by investigating the relationship between the pre-stretch membrane potential [E_{mrest}: point 1 in **Fig. 24A & B**] and the effect of stretch manipulations on the three most distinctive repeatable features of stretch-evoked receptor potentials [see **Fig. 24**]: the initial depolarisation (E_p: 2-1), the hold potential during static stretch (E_{hold}: 6-1) and the post-release hyperpolarisation (E_h: 7-1). Larval preparations were stimulated with ramp-and-hold stretch protocols, modified to give incomplete release of the stimuli. Thus, subsequent stimulations occurred from increasing basal lengths. The three features, E_p, E_{hold} and E_h, showed consistent correlation with pre-stretch membrane potential [see **Fig. 28**].

When the data from all neurons were collated it seemed that E_p and E_{hold} varied in proportion to E_{mrest}, whilst E_h remained comparatively constant. Additionally, it was observed that, regardless of E_{mrest}, the change in membrane potential to reach E_p ($dEm = E_p - E_{mrest}$) remained relatively constant, being, on average, only weakly correlated with E_{mrest} (average Pearson=0.3). These relationships are very similar to those described previously in mammalian muscle spindles [Hunt *et al.*, 1978].

Additionally, muscle spindles were reported to show stimulus-dependency of E_p [Hunt *et al.*, 1978], and it was found that *dbd* neurons exhibit a similar trait. Receptor potential recordings were made for *dbd* neurons that were sequentially stimulated by applying increasing mechanical displacements of 76µm, 80µm and 92µm to the pin. The amplitudes of the initial depolarisation responses were proportional to the amplitudes of the stretch stimuli [see **Fig. 27**]. In conclusion, these data demonstrate that *dbd* neurons are stretch receptors and that they have properties similar to those of vertebrate muscle spindles.

3.4 Summary

This novel examination of the larval *Drosophila* system has produced a successful working protocol for studying the effects of physiologically relevant mechanical stimuli on stretch-

evoked potentials of stretch-sensitive endings. The technique, detailed here, allows for accurate stimulation of the *dbd* neuron, *in vivo*, using carefully calibrated stimuli. Consequently, detailed measurements can be made of the stimulus-evoked responses of *dbd* neurons and these responses can be accurately characterised in terms of their stimulus-dependence.

Furthermore, these data suggest that *dbd* neurons may indeed function as muscle stretch receptors, having been shown to response to mechanical, stretching stimuli. Additionally, *dbd* neurons and muscle spindles both respond to stretch stimuli in similar ways and may possibly utilise similar mechanisms to do so, indicating that the fly model is a suitable system for exploring mechanisms of mechanotransduction, which may be useful in understanding mammalian stretch transduction. Consequently, this means that both mechanotransduction in muscle spindles and *dbd* neurons are described by the *in silico* model, detailed in **Ch.2**. Thus, the fly system can be utilised to test the predictions of the *in silico* model, in order to identify mechanotransduction ion channels involved in stretch responses.

Figure 28 [opposite]: Key *dbd* receptor potential relationships resemble those of mammalian muscle spindles. (A-D, left) Sample recordings from 4 *dbd* neurons, each in a different larva (upper traces), in response to ramp-and-hold stretch stimuli (lower traces). Consecutive stimuli originate from sequentially increased initial lengths, achieved through incomplete release of the prior stimulus. (A-D, right) The average amplitude of the three, common features of the receptor potential responses, from each preparation, are highly correlated with the initial length of the receptors (Pearson correlation results shown for each feature). Overall, E_p shows the highest correlation to initial length (average Pearson=0.95), E_{hold} is less, but still strongly, correlated (average Pearson=0.88), whilst E_h is the least correlated (average Pearson=0.6).

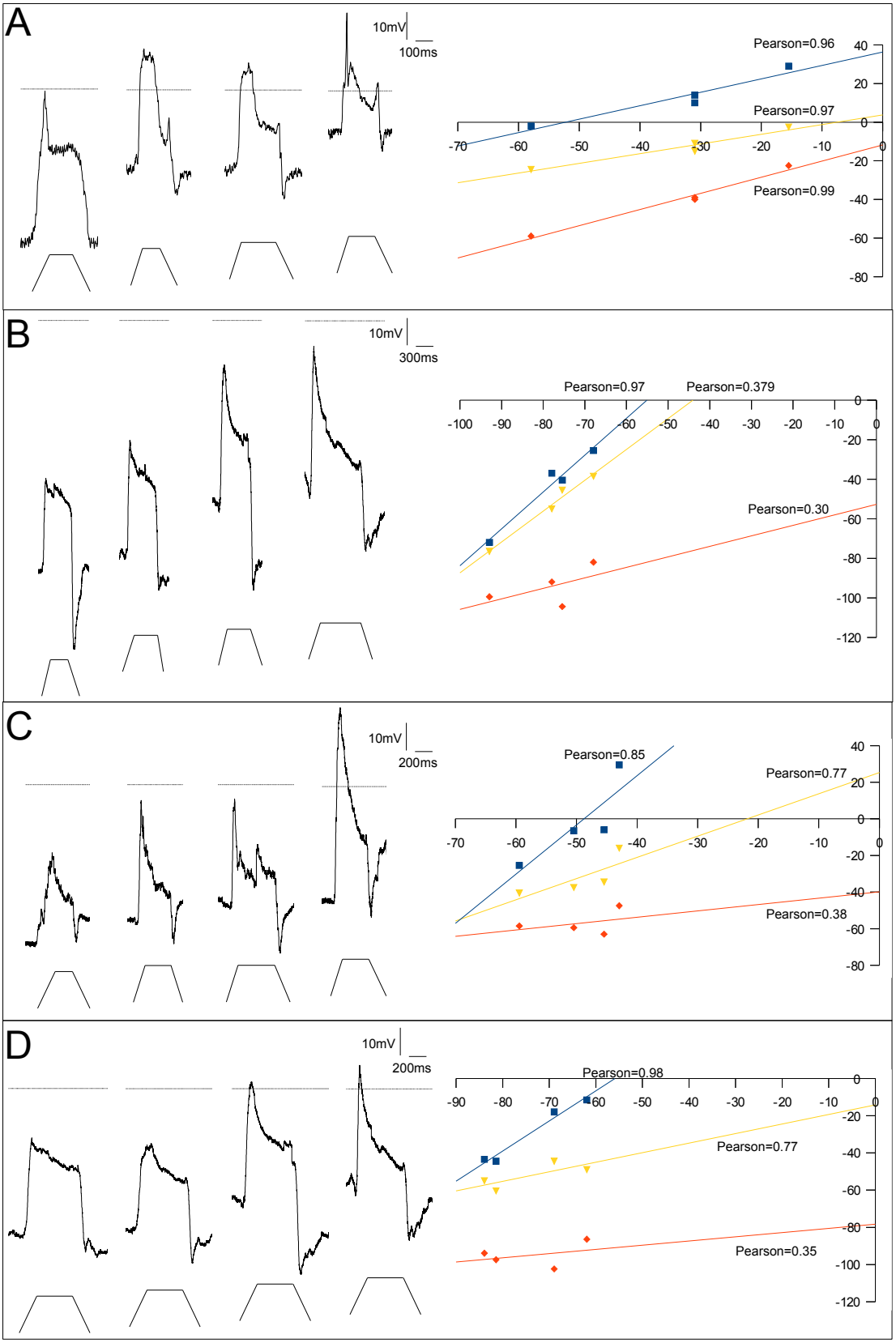
A
10mV
100ms
Pearson=0.96
Pearson=0.97
Pearson=0.99
B
10mV
300ms
Pearson=0.97
Pearson=0.379
Pearson=0.30
C
10mV
200ms
Pearson=0.85
Pearson=0.77
Pearson=0.38
D
10mV
200ms
Pearson=0.98
Pearson=0.77
Pearson=0.35

4. Molecules of mechanotransduction in *dbd* neurons

Thus far, a general model of mechanotransduction has been constructed, based upon presumed components of a stretch-activated neuron. These assumptions were based upon prior experimental data. This has been shown to be a good representation of stretch-activated electrical behaviour in various stretch-sensitive endings, including *dbd* neurons, as was subsequently shown by the development of a technique to enable recording of *dbd* receptor potentials. Using a combination of the predictions of the mathematical model and data collected from the *in vivo* model system, targeted experiments could be conducted to directly verify and show functional roles for candidate mechanotransduction molecules.

4.1. Candidate channels

As highlighted previously, mechanotransduction appears to be mediated by a number of molecular components. The *in silico* model [detailed in **Ch.2**] provides a framework for predicting the roles of certain, necessary components of the biophysical machinery of stretch transduction. Using the *in vivo* model [as outlined in **Ch.3**], candidates for these components can be assayed, with reference to the *in silico* model, to attempt to identify what roles particular entities might play within the overall apparatus of the receptor system.

As no part of any mechanism has hitherto been established within the *dbd* mechanotransduction system, identifying the hypothesized primary MNaC within this receptor would be of particular interest. According to the specifications of the *in silico* model, such a channel would be a mechanically-gated cation channel, probably permeable to sodium (although not necessarily sodium-selective)[9]. As stated in chapter one, a number of such channels have been identified. Currently, two potential candidates have been shown to be expressed in *dbd* neurons – TRPA1 and DmPiezo [Shen *et al.*, 2011; Kim *et al.*, 2012]. Although these channels have been identified in these neurons, no evidence has been forthcoming to indicate whether or not these channels are involved in stretch detection in this system, as their identification in *dbd* neurons was reported as an incidental finding of the above studies. Using the *in silico* model, the contributions of a primary MNaC to the receptor potential can be isolated, predicting the effect of inhibition of the MNaC on the

9 The reversal potential of the primary MSC current in the model corresponds to that of sodium.

receptor potential. Thus, an effective screen for MNaC candidates can be performed by investigating the effect of inhibiting these candidate channels, *in vivo*, and making comparisons to the theoretical model.

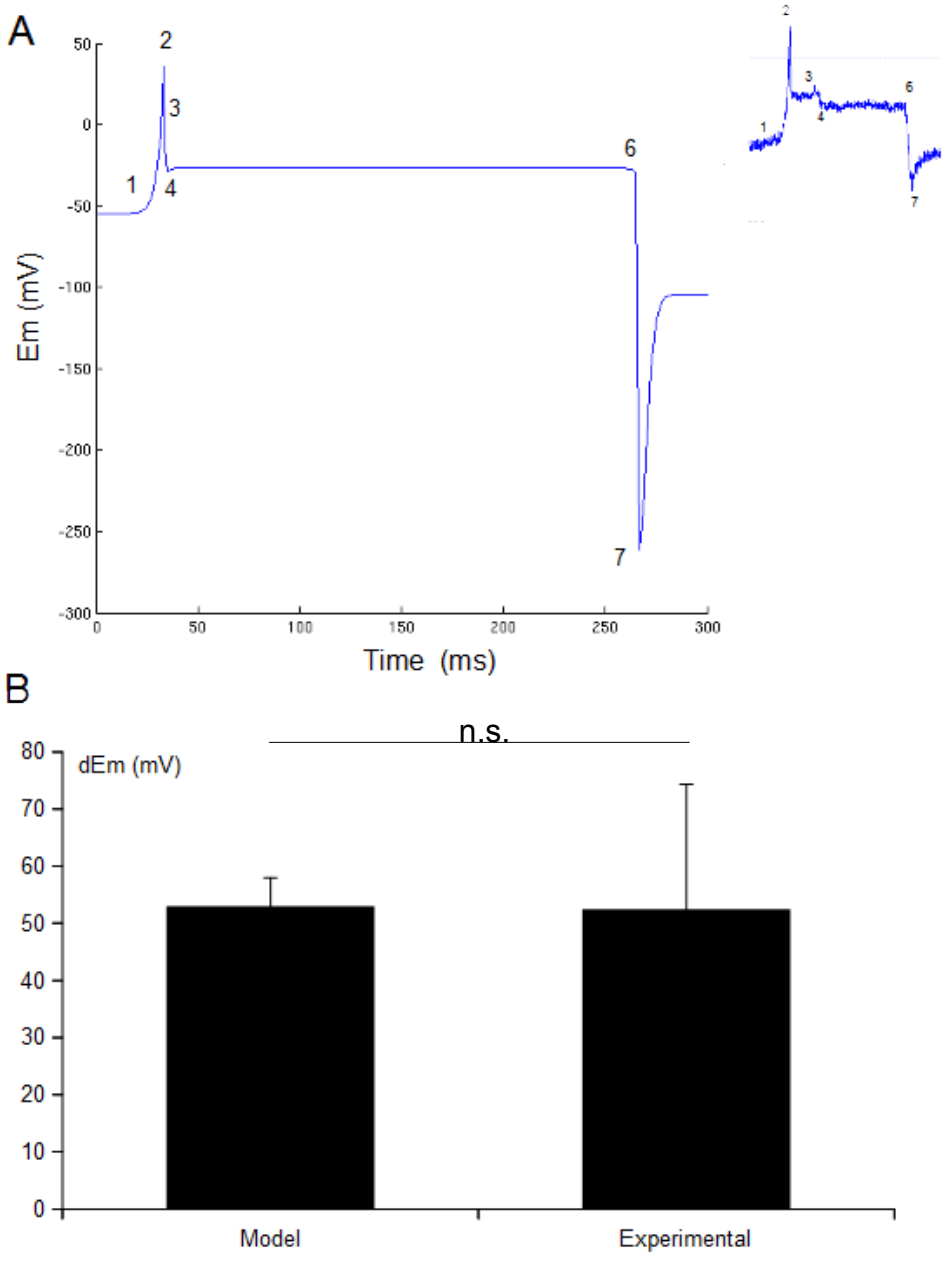

Figure 29 [opposite]: An *in silico* biophysical model of the receptor potential of stretch-activated neurons accurately reproduces experimentally-observed data. (A) The *in silico* model accurately reproduces the most striking features of the dynamic and static stretch responses seen in *dbd* neurons (inset). It is noted that the model does not currently accurately describe the response to the post-release phase of the stimulus protocol, but this aspect is under development. (B) In the *in silico* model, the values of *dEm* ($dEm=E_p-E_{mrest}$) accurately reflect the mean observed values of *dEm* in *dbd* neurons [see **Fig. 28D**] although the experimental data show more variability (n=10, p=0.5 [ANOVA]). All data are mean ±SD.

4.1.1. Predictions from the theoretical model

Having developed a mathematical model that could faithfully reproduce the experimentally-observed electrophysiology of stretch receptors, this model could be utilised to attempt to predict the role of putative system components. In this model, it is proposed that a combination of mechanically-gated and voltage-gated channels are concertedly activated by a stretch stimulus to recapitulate the responses recorded in stretch-activated *dbd* neurons, to both dynamic and static stretches [see **Fig. 19**].

The model was initially based upon data obtained from crayfish stretch receptors, but was also able to reproduce mammalian receptor potential from muscle spindles [see **Fig. 17C**]. Here, it is shown that the receptor potentials recorded from *dbd* neurons also display the same characteristics. A comparison of the modelled and recorded values for *dEm* revealed that the model accurately reflected the *in vivo* results [see **Fig. 29**]. Thus, the *in silico* model is a reliable reporter of *dbd* stretch-evoked electrical adaptation. Therefore, the *in silico* model can be used to predict the role of an MNaC in our *in vivo* model system.

As previously shown, by using this model, the effect of modulating the activation of the MNaC, which forms the basis of this model, was investigated as activity was incrementally reduced via serial reduction of the MNaC activation term. As the activity of this channel was reduced, a corresponding reduction in stretch-activated depolarisation was observed in the modelled receptor potential [see **Fig. 18**]. Additionally, a corresponding, step-wise inhibition of the remaining phases of the modelled response was also seen, *i.e.*, the amplitudes of the after-depolarisation and hold potential were equally reduced, in proportion to the reduction in the peak depolarisation.

Due to the extant discrepancies in the post-release phase of the stimulus protocol, no predictions could be made regarding effects in this phase and thus this phase was omitted from the modelling predictions. However, as the model would appear to suggest that hyperpolarisation is MNaC-independent [see **Ch.2.2.1**], the predictions made can still be considered applicable.

Interpreting these results, this model suggests that inhibition of the MNaC, modelled as a reduction in the activation term, inhibits depolarisation of the afferent ending in response to a stretch stimulus and, furthermore, inhibits generation of the receptor potential, as a whole. This suggests that all stages of the mechanotransduction response in stretch-activated endings are dependent upon a functional MNaC. This modelling predicts that inhibition of the channel *in vivo* would similarly progressively reduce then abolish the response in a

neuron.

One consideration that must be accounted for is the alternative possibility that reducing stimulation, as opposed to inhibiting the MNaC directly, would, in theory, have the same effect. This effect was shown when the *in vivo* system was characterised [see **Fig. 28**]. In order to test the effect on stretch-evoked depolarisation of *dbd* neurons of the various conditions outlined below, consistent, maximal stimuli [see **Ch.3.2.4]** were used for all control and test scenarios. Thus, any effects seen in these experiments can confidently be attributed to the specific experimental condition of interest in each case.

4.1.2. Pharmacology of *dbd* neurons

The mathematical model of mechanotransduction assumes that the primary MSC in stretch-activated neurons should be a mechanosensory sodium channel. Therefore, the effect of replacing Na^+ in the extracellular saline with NMDG, to block sodium conductance, was tested. Stretch-evoked recordings were made from *dbd* neurons in HL3 saline containing 80mM Na^+. HL3 with NMDG-Cl substituted for Na^+ was then washed on. Stretch-evoked depolarisation was greatly reduced, but not abolished, in the presence of NMDG [see **Fig. 30A & E**].

Secondly, previous studies of mammalian muscle spindles have shown that the response of this type of ending is sensitive to amiloride and its analogues, which block MSCs [Bewick *et al.*, 2005; Simon *et al.*, 2010]. As muscle spindles are anatomically and electrophysiologically similar to *dbd* neurons, and given their similar physiological roles, *dbd* neurons were examined for amiloride sensitivity.

Stretch-evoked receptor potential recordings were made with increasing concentrations of 0μM, 10μM, 20μM and 30μM amiloride. The receptor potential *dEm* was inhibited in a dose-dependent manner by amiloride, being inhibited by ~80% by 30μM amiloride [see **Fig. 30B & F**]. This is consistent with previous results in muscle spindles, which indicated that amiloride blocked responses by 50% at around 10μM and by 75% at around 100μM [Simon *et al.*, 2010].

The two candidate MNaC channels that are known to be expressed in *dbd* neurons are DmPiezo and TRPA1. Both TRPA1 and DmPiezo are blocked by ruthenium red [Coste *et al.*, 2010]. Therefore, as an initial, non-selective screen to see whether one of these two channels may be actively contributing to stretch adaptation, the effect of ruthenium red on the

electrical responses of *dbd* neurons was tested. A concentration of 30μM ruthenium red is known to block around 80% of Piezo-mediated cation currents in *Piezo*-transfected HEK239T cells [Coste *et al.*, 2012]. Therefore, the effects of both 15μM and 30μM were tested. It was observed that stretch-evoked depolarisation in *dbd* neurons was inhibited in a dose-dependent manner [see **Fig. 30 C & G**]. These initial results suggested that our candidates could indeed be involved in this system. Therefore, I moved on to test this hypothesis by a more targeted, genetic approach.

4.2. Candidate channels – DmPiezo

The first candidate channel to be specifically screened was DmPiezo. The identification of *Piezo* proteins as pore-forming ion channels is fairly recent [Coste *et al.*, 2010]. Since then, this family of ion channels has had their mechanosensitivity demonstrated in cell culture [Coste *et al.*, 2012] and they have been implicated in mechanosensitive behaviours [Kim *et al.*, 2012]. Kim *et al.* [2012] also showed that *dbd* neurons express DmPiezo - the only Piezo family member in *Drosophila*. Together, all of this information seemed to suggest a likely role for DmPiezo in *dbd* neuron mechanotransduction. However, this had never been directly tested, nor did this evidence show whether DmPiezo could be a primary MNaC in these endings.

Figure 30 [opposite]: Receptor depolarisation in *dbd* neurons is inhibited by blocking a sodium-dependent MSC. (A) Replacing Na^+ in the extracellular medium with NMDG resulted in a significant reduction in *dEm* in stretch-evoked responses by 79.8% (±2.7%, $p<0.0001$, $n=3$). (B) Stretch-evoked depolarisation of the receptor ending in *dbd* neurons was inhibited by amiloride. The change in membrane potential (*dEm*) is normalised to the pre-drug control. Depolarisation was reduced in a dose-dependent manner ($n=5$, $p<0.001$). (C) Ruthenium red application also reduces stretch-evoked depolarisation dose-dependently ($n=7$, $p<0.0001$). (D-G) Representative traces for control (D), NMDG (E), amiloride (F) and ruthenium red (G). Dashed lines on traces = 0mV; stimuli indicated by solid bars beneath each trace.

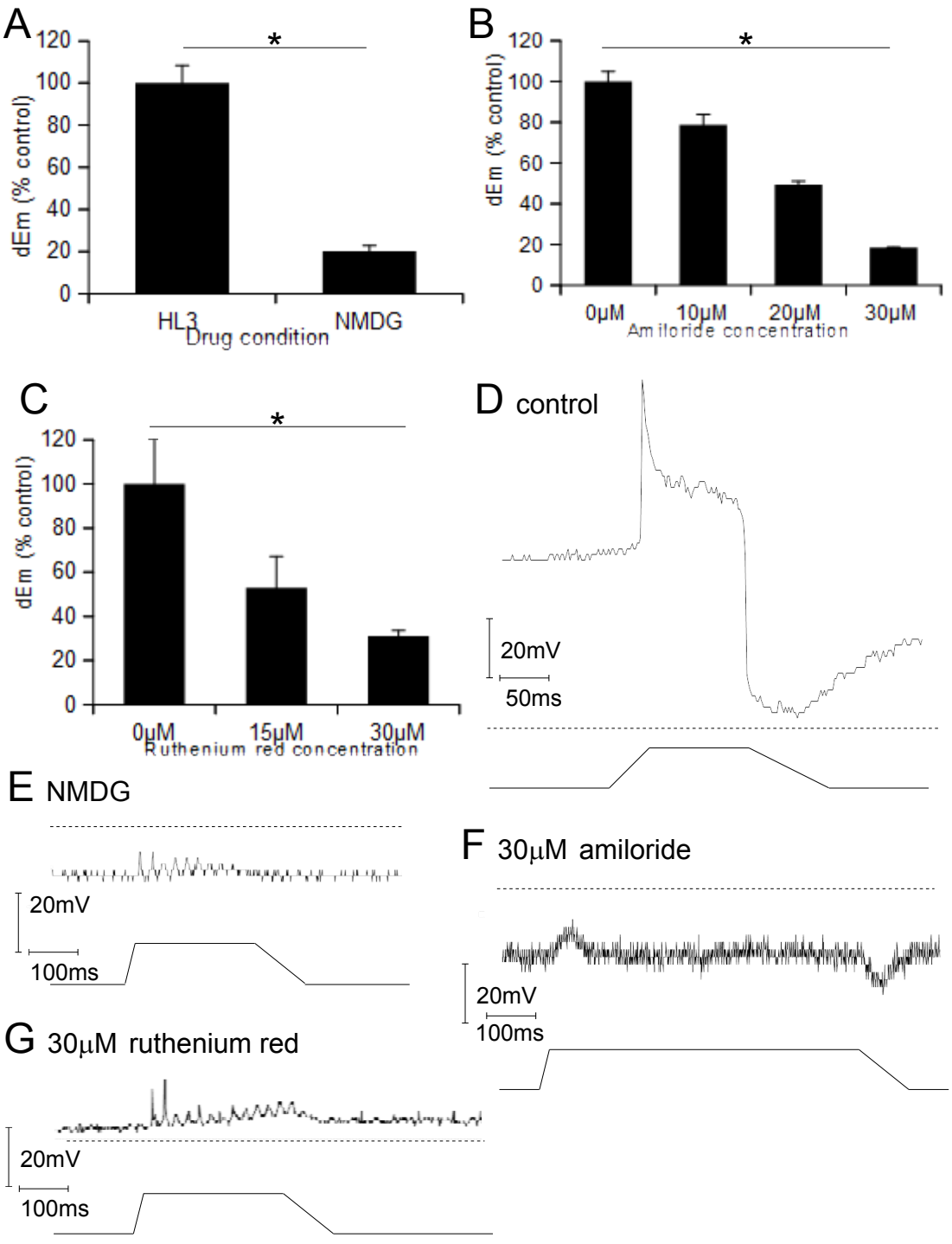
A
B
C
D control
E NMDG
F 30μM amiloride
G 30μM ruthenium red
dEm (% control)
HL3
NMDG
Drug condition
0μM
10μM
20μM
30μM
Amiloride concentration
15μM
Ruthenium red concentration
20mV
50ms
100ms
*

Thus, experiments were conducted to investigate whether DmPiezo could fulfil the role of primary MNaC. The pharmacology that had already been carried out in order to characterise *dbd* neurons showed a ruthenium red sensitivity in the neural responses to stretch stimuli [see **Fig. 30C & G**]. This finding was consistent with the earlier results of Coste *et al.* [2012], which showed an effect of ruthenium red on Piezo conductance in cell cultures. It was shown that 30μmolL^{-1} ruthenium red blocked ~80% of the response to mechanical stimuli in both cases. These data seemed to indicate a role for DmPiezo in *dbd* neuron mechanotransduction. Therefore, this hypothesis was tested directly, using the electrophysiological recording protocol [see **Ch.3**] in conjunction with genetic manipulation of *dmpiezo*.

4.2.1. Genetic targeting of DmPiezo

To investigate the hypothesis that DmPiezo is the gating channel for stretch-activated receptor potential generation, the effect of RNAi knock-down of DmPiezo was examined. RNAi knock-down was tested for two different *Piezo*-RNAi knock-down lines, driven by *piezo-Gal4* (*piezo-Gal4*, *UAS-piezo* larvae). This technique enables the specific disruption of the target gene of interest [Dietzl *et al.*, 2007], whilst avoiding alteration to any other part of the transduction apparatus, enabling a detailed examination of the role of this gene in *dbd* neuron stretch transduction.

Figure 31 [opposite]: Loss of TRPA1 and DmPiezo function have small and large effects respectively on response to stretch. (A) Stretch-evoked depolarisation was recorded in response to maximal stretch stimuli in *dbd* neurons of control (w^{1118} – other control data not shown), $TrpA1^{1}$ mutants or RNAi knockdown larvae. Data were compared to the previously-measured effect on w^{1118} treated with 30μM ruthenium red [see **Fig. 30C**]. Loss of TRPA1 inhibited stretch-evoked depolarisation <40% (n=3, p<0.0001), whereas the inhibition by ruthenium red is at least 3x more profound (n=7, p<0.0001). RNAi knock-down of TRPA1 similarly partially abolishes stretch-evoked depolarisation (*dEm*=68% control, n=3, p<0.0001). When *dmpiezo* expression is reduced via RNAi knock-down, the receptor potential is almost completely abolished (E_p<5mV) compared to corresponding controls (GD993 – *dEm*=1.3% controls, n=3, KK101815 – *dEm*=14.9% controls, n=4, p<0.0001). (B-E) Representative traces for control (B), *dmpiezo* knock-down line GD993 ©, *dmpiezo* knock-down line KK101815 (D) and $TrpA1^{1}$ mutant (E). Dashed lines on traces = 0mV; stimuli indicated by solid bars beneath each trace.

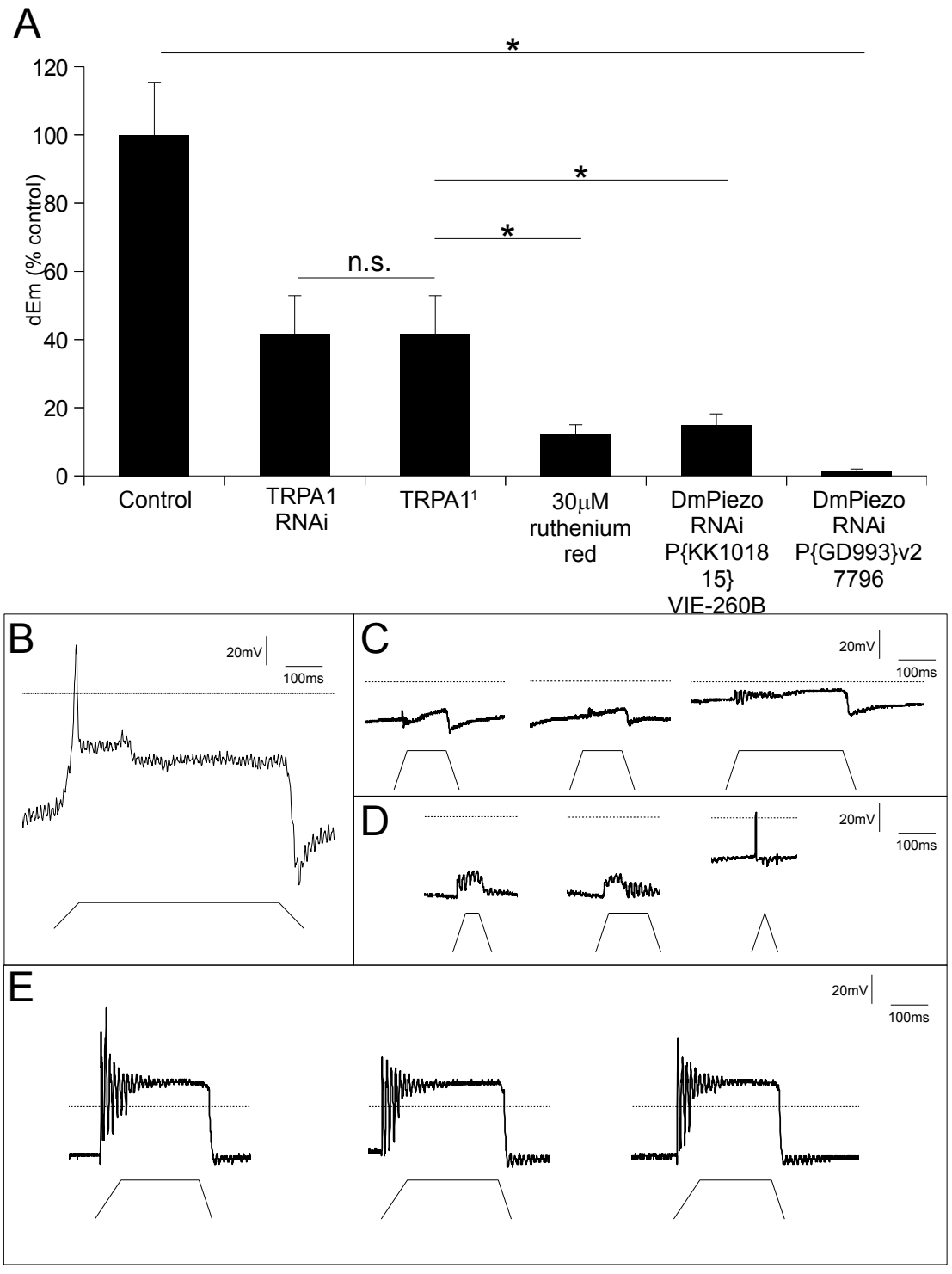
A
dEm (% control)
120
100
80
60
40
20
0
*
*
*
n.s.
Control
TRPA1 RNAi
TRPA1[1]
30μM ruthenium red
DmPiezo RNAi P{KK101815} VIE-260B
DmPiezo RNAi P{GD993}v27796
B
20mV
100ms
C
20mV
100ms
D
20mV
100ms
E
20mV
100ms

When DmPiezo expression is reduced via RNAi knock-down, *dbd* neuron depolarisation was almost completely abolished [see **Fig. 31A, D & C**]. This abolition of the receptor potential was consistent in both knock-down lines [see **Fig. 31A**], with *dEm* being consistently below 5mV for maximal stimuli (compared to an average amplitude of 56mV for control neurons). This suggests that DmPiezo may be the primary MNaC responsible for the stretch-evoked response in *dbd* neurons. This response of the *dmpiezo*-RNAi *dbd* neurons is consistent with the results obtained in the ruthenium red, amiloride and NMDG experiments.

Interestingly, with very short stimuli it was occasionally possible to see small, spike-like events. However, these only occurred in neurons with comparatively high resting potentials [see end trace in **Fig. 31D**]. This suggests that some spontaneous activation of VNaCs can still occur in these lines.

Errors, however, are an inherent risk of the RNAi system. The RNAi may be achieving incomplete knock-down, with residual expression remaining sufficient to produce a normal phenotype. Knock-down efficacy could be determined via the use of, *e.g.*, immunohistochemistry, to detect any remaining protein. Alternatively, a genetic approach, such as PCR, could be used to identify any extant expression in the knock-down lines. Use of a confirmed null-mutant line would have been ideal for overcoming these issues, however one was unavailable nor was the time required to generate and confirm one. Subsequent work could examine suitable confirmation of this approach.

Nonetheless, two separate RNAi lines (*P{KK101815}VIE-260B* and w^{1118}*; P{GD993}v2796* [Vienna *Drosophila* RNAi Center]) were used to control against off-target effects or background effects of the RNAi itself. In addition to these lines, appropriate control experiments were performed with the uncrossed RNAi background strains, the uncrossed *piezo-Gal4* driver strain and a w^{1118} background line. The results achieved indicate that both lines exhibited comparable phenotypes, both demonstrating the predicted inhibition of the stretch response. This would indicate that appropriate, although not necessarily complete, knock-downs of the desired gene had been achieved in each case.

4.3. Candidate channels – TRPA1

From the results of the pharmacological characterisation of *dbd* neurons, it was apparent that primary mechanotransduction in these endings is mediated by an MSC that is sensitive

to both ruthenium red and amiloride. In addition to DmPiezo, the only other ion channel known to be expressed in *dbd* neurons that could fit these parameters is TRPA1 [Shen *et al.*, 2011]. Ruthenium red is known to block TRP channels [*e.g.*, Farris *et al.*, 2004], and evidence has been put forward to show that TRPA1 can exhibit amiloride sensitivity [Banke, 2011]. Therefore, the putative role of TRPA1 as a primary MNaC in *dbd* neurons was examined.

To examine the role of TRPA1, *dbd* neurons of larvae carrying the $TrpA1^{1}$ mutation were tested, electrophysiologically. This mutation had previously been shown to be a genetic null [Kim *et al.*, 2012]. When compared to control, *dbd* neurons in $TrpA1^{1}$ larval pelts exhibited slightly inhibited receptor potential generation ($dEm \approx -40\%$, $p<0.0001$). This indicates that TRPA1 may be active in the stretch-response of these neurons, but is insufficient to explain the effect of ruthenium red, accounting for <30% of the effect of ruthenium red blockade [see **Fig. 31A & E**].

In addition to this, $TrpA1^{1}$ mutant larvae also displayed apparent loss of post-release hyperpolarisation amplitude in their *dbd* stretch-evoked responses. The initial depolarisation also appeared less stable, occurring as a series of oscillations, unlike the clear, single depolarisations in w^{1118} *dbd* neurons. The loss of post-release adaptation would perhaps be consistent with this being a Ca^{2+}-mediated process [see **Ch. 2.4**], if TRPA1 is responsible for a stretch-dependent Ca^{2+} current in these neurons. The 'wobbly' initial depolarisation may be due to the stimulus. These data were collected using the manual stimulation method [see **Ch. 3.2.3**], which carries the risk of inherent instability in the stimulus. However, perhaps these data suggest a possible role for TRPA1 in stabilising the initial depolarisation resonse to dynamic stretches.

Overall, these results would seem to suggest that both DmPiezo and TRPA1 play distinct roles in the mechanotransduction apparatus of *dbd* neurons. DmPiezo appears to be responsible for mediating initial stretch-activated depolarisation, whilst TRPA1 is employed in some supporting capacity, which contributes to the initial depolarisation but only in an auxiliary fashion.

4.4. Candidate channels – PPK family

Thus far, only channels known to be expressed in *dbd* neurons have been examined. However, ion channel expression in *dbd* neurons is not an area that is comprehensively

covered by the literature. The two channels that were studied, above, are the only two mechanosensory channels that are known to be expressed in these neurons. However, many other channels possess similar pharmacological profiles to the two channels that have been examined, and, despite the completeness of receptor inhibition that is elicited by DmPiezo knock-down, it cannot be definitively concluded that the pharmacological results are purely Piezo mediated.

Therefore, a screen of other mechanosensory channels was conducted, to examine whether another channel could account for the pharmacology that had been observed. Ruthenium red and amiloride are both broad-spectrum MSC blockers, known to have inhibitory effects on many channel-types. However, data from mammalian stretch receptors has indicated a role for a DEG/ENaC channel in stretch responses [Simon *et al.*, 2010]. As has already been illustrated, these receptors are analogous to *dbd* neurons. As no evidence for DEG/ENaC expression in *dbd* neurons had yet been shown, priority was given to examining whether *Drosophila* DEG/ENaC orthologues - the *pickpocket* (*ppk*) gene family - were expressed in *dbd* neurons, as these data would provide additional information on likely homology, at the molecular level, between the mechanisms in these two receptor types.

There are 31 members of the *ppk* family, including *rpk* (*ppk2*) and *Nach* (*ppk4*). A systematic, *in situ* hybridisation screen [Tautz & Pfeifle, 1989] of these genes was carried out to visually examine whether these were expressed in *dbd* neurons of late w^{1118} embryos. The results of this screen are summarise in **Table 1**.[10] Given the available time and resources, this was considered to be the most suitable and effective way to provide basic data on the likelihood of the involvement of any of these genes in receptor behaviour. Some expression data for a minority of these genes already existed, therefore it would be possible to assess the validity of any results of this screen by comparison with known expression data for the few genes this was available for, thus improving confidence in novel data for genes whose expression in *dbd* neurons was previously uncharacterised.

As there are so many members of the *ppk* family, specific data on any one gene is sparse. The expression of many *ppk* genes is uncharacterised. Some studies have visually identified expression of a small subset of *ppk* genes by *in situ* hybridisation: *ppk1*, *ppk2* (*rpk*), *ppk10*, *ppk11*, *ppk19*, *ppk23*, *ppk28* and *ppk29* [Adams *et al.*, 1998; Liu *et al.*, 2003; Jinushi-Nakao *et al.*, 2007; Cameron *et al.*, 2010; Thistle *et al.*, 2012]. Only *ppk1*, *rpk*, *ppk23*, *ppk28* and *ppk29* have been seen outside of the trachea, with some expression in gustatory receptors,

10 Supplementary data may be found in **Appendix ii.**

Gene	Previously-published expression data[11]	Results of *in situ* screen[12]
ppk1	PNS expression in da neurons†	Strong expression in trachea and PNS
ppk3	Very low expression in late embryos^	Some punctate colouration seen, potentially in anterior sensory cells
Nach	No known embryonic expression[13]	No staining seen
ppk5	No known embryonic expression	No staining seen
ppk6	No known embryonic expression	Some expression in a rostral sense organ complex/dorsal sense organs in initial segments.
ppk7	Very low expression in embryos^^	Some non-PNS expression in late-stage
ppk8	No known embryonic expression	Tracheal staining in late embryos
ppk9	Expression only seen in adults^^	High anterior expression in early embryo, but indiscernible in late stages
ppk10	Trachea*	No staining seen
ppk11	Trachea*	No staining seen
ppk12	Pupae only^, ^^	Staining throughout late embryonic trachea
ppk13	No known embryonic expression	No staining seen
ppk14	No known embryonic expression	Tracheal staining
ppk15	Pupae and adult only^, ^^	No staining seen
ppk16	No known embryonic expression	Light tracheal staining
ppk17	Very low expression detected in late embryo onwards^, ^^	Tracheal staining observed in late embryo
ppk18	Pupae only^^	Tracheal staining
ppk19	Trachea* in early embryo^, ^^	Extensive tracheal staining
ppk20	Early embryo only^^	Tracheal staining
ppk21	Pupae only^, ^^	Extensive tracheal staining
ppk22	Some expression in pupae and early adult^^	No staining seen
ppk23	Gustatory receptor neurons (adult)‡‡. Low expression also detected in late embryo^, ^^	Slight expression seen in ventral basiconical or campaniform sensilla

11 Data obtained from FlyBase or specific articles, where indicated. Details of embryonic expression are provided, where available.

12 For expression location identifications, micrographs of *in situ* hybridisation labelling compared to cell locations given in Hartenstein, 1993.

13 Indicates either that previous studies [see Table legend] have not seen expression or no data has previously been presented concerning this gene.

Gene	Previously-published expression data	Results of *in situ* screen
ppk24	No known embryonic expression	No staining seen
ppk25	No known embryonic expression	Extensive tracheal staining
ppk26	Late embryonic & larval expression, comparable to ppk1 expression levels[^^]	Strong expression in the head. May also be expressed in lateral basiconical sensillum
ppk27	No known embryonic expression	No staining seen
ppk28	Trachea[*] and gustatory receptor neurons (adult)[++]	Trachea
ppk29	Gustatory receptor neurons (adult)[‡‡]	No staining seen
ppk30	Very low expression in mid-late embryos[^, ^^]	No staining seen
ppk31	No known embryonic expression	Extensive tracheal staining

Table 1: Summary of *in situ* hybridisation screen results for MNaC candidate expression in *dbd* neurons. Larval expression of all *pickpocket* genes was visualised via *in situ* hybridisation of each gene. Expression in late (stages 15-17) embryos was examined to determine whether any *ppk*s were expressed in *dbd* neurons. A literature search was performed to identify any extant expression data. Where data existed, results were compared to validate the screening protocol and increase confidence in novel data, where no prior data existed. [[+]Zhou *et al.*, 1999; [*]Liu *et al.*, 2003; [†]Jinushi-Nakao *et al.*, 2007; [‡]Hamada *et al.*, 2008; [++]Cameron *et al.*, 2010; [^]modENCODE data from Graveley *et al.*, 2011; [**]Jepson *et al.*, 2012; [‡‡]Thistle *et al.*, 2012; [^^]Zelle *et al.*, 2013]

however there is no indication that any of these are present in the PNS of the abdomen or thorax of late embryos, except *ppk1* and *rpk*.

The expression pattern of *ppk1* is an important marker. Staining for *ppk1*, in addition to extensive tracheal staining, elicits punctate staining of a single cell of the dorsal *da* neuron cluster [see **Fig. 32A & B**]. This pattern, especially the presence of distinct puncta in the dorsal *da* region, is what would be expected in *in situ* preparations that positively label the *dbd* neuron. However, *ppk1* is known to be expressed in *md* neurons, but not in *dbd* neurons [Kim *et al.*, 2012]. Adams *et al.* [1998] noted similar punctate staining in their examination of *rpk*. However, they also reported that it is not expressed in *dbd* neurons.

As *md* and *dbd* neurons are adjacent, it could be difficult to ascertain whether staining in an *in situ* preparation is of *dbd*, *md*, or both. Thus, any staining that produces a pattern similar to *ppk1* labelling could be considered a potential positive candidate. Staining of *ppk1* was repeated here as a positive control for dorsal *da* cluster labelling. Any labelling that was

negative in this region can be excluded as possibly being expressed in *dbd*. A repeat of *rpk* staining was not conducted as *ppk1* staining provides sufficient positive control and *rpk* expression in *dbd* neurons has already been sufficiently discounted [Adams *et al.*, 1998].

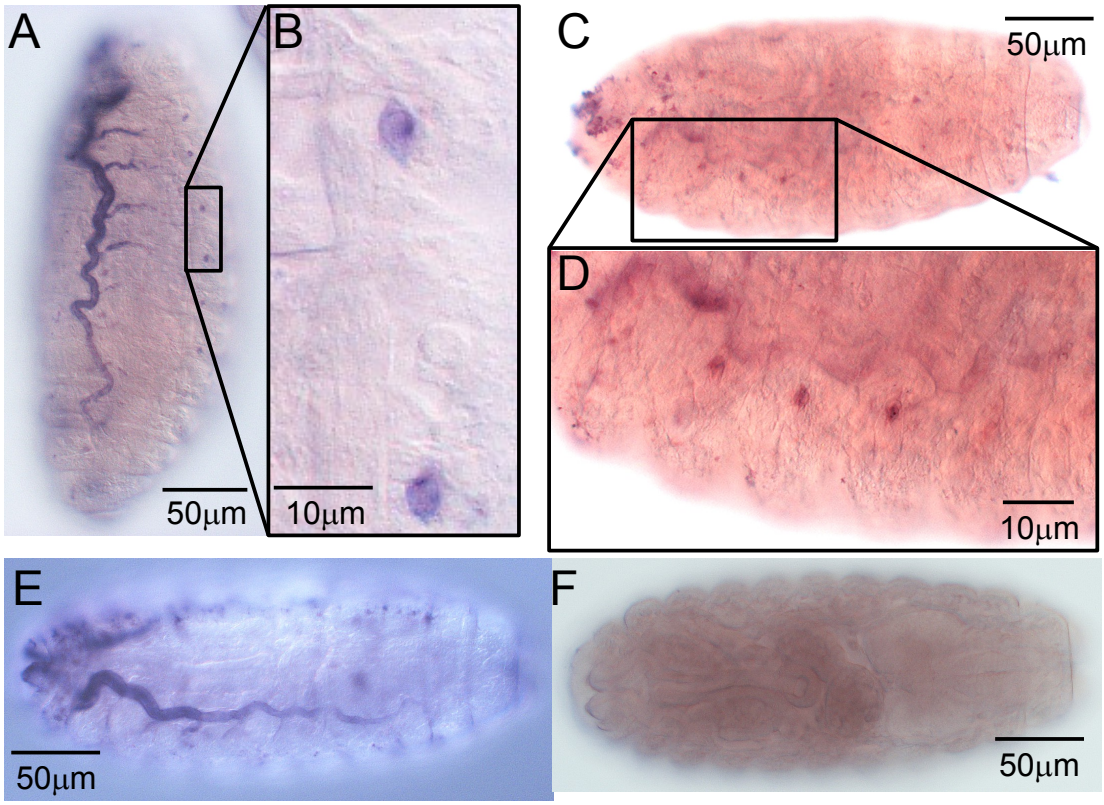

Figure 32: Sample results of the *in situ hybridisation* screen of *ppk* genes in embryonic *Drosophila*. (A) *In situ* labelling of *ppk1* produces a distinctive pattern of tracheal and peripheral punctate labelling (B). (C) Labelling of *ppk26* confirmed previous reports of low expression in late embryo, producing slight anterior tracheal labelling, as well as labelling in 3, distinct anterior puncta, possibly lateral basiconical sensillae (D). Labelling of *ppk31* produced previously unreported tracheal staining (E), reminiscent of that seen by Liu *et al.* [2003] for other *ppk* genes, although this could be artefactual. (F) The majority of assays, however, produced no visible embryonic staining (example figure: *ppk13*). All panels are representative sample images.

Aside from visualisation data, the other significant source of information on *ppk* expression in embryos is the modENCODE Temporal Expression Data mRNA-Seq dataset [Graveley *et al.*, 2011]. These data indicate embryonic expression, in the later stages of embryogenesis, of *ppk1*, *ppk2*, *ppk17*, *ppk20*, *ppk23*, *ppk26*, *ppk29* and *ppk30*. Although there is some overlap with the previous *in situ* data, above, this dataset indicates embryonic expression of

additional *ppk* genes, whilst simultaneously failing to recapitulate the evidence for embryonic expression of *ppk10*, *ppk11*, *ppk23* and *ppk28*.

Furthermore, a subsequent expression analysis of *ppk* genes was carried out by Zelle *et al.* in 2013. This study indicated additional embryonic expression of *ppk7*, *ppk19*, *ppk23*, *ppk26* and *ppk30*, once again indicating some disparity with the data highlighted above. Thus, the utility of whole-animal expression data appears to be of only limited use in identifying genes that may only be expressed in a small subset of PNS neurons, thereby having tiny overall expression when the rest of the animal is considered.

Staining comparable to that seen in earlier visualisation studies [Adams *et al.*, 1998; Liu *et al.*, 2003; Jinushi-Nakao *et al.*, 2007] was seen for *ppk1*, *ppk19* and *ppk28*. Expression that is in agreement with available expression data [Graveley *et al.*, 2011; Zelle *et al.*, 2013] was recorded for *ppk3*, *ppk7*, *ppk15*, *ppk17*, *ppk22*, *ppk23* and *ppk26* [**Fig. 32C & D**]. Novel expression of *ppk6*, *ppk8*, *ppk9*, *ppk12*, *ppk14*, *ppk16*, *ppk18*, *ppk20*, *ppk21*, *ppk25* and *ppk31* [**Fig. 32E**] were seen, where no previous data existed for expression of these genes in embryos. These were predominantly visualised in the trachea, as seen for other genes by Liu *et al.* [2003]. Whether or not these are true stains or artefacts is uncertain, however, as tracheal staining can be considered 'false' staining [Liu *et al.*, 2003]. Some punctate staining was seen in anterior segments of the thorax and head for *ppk3*, *ppk6*, *ppk23* and *ppk26*. These may correspond to rostral sense organ complex/dorsal sense organs in initial segments (*ppk3* and *ppk6*), ventral basiconical or campaniform sensilla (*ppk26*), or lateral basiconical sensilla (*ppk23*). However, these locations are unconfirmed and would require further corroboration, which is outwith the focus of this investigation. No staining was seen for *ppk10*, *ppk11* and *ppk30* where previously it had been reported in embryos. Expression of the remaining genes was not observed at all in late embryos [*e.g.* **Fig. 32F**]. No previous data existed for comparison, possibly for this reason.

Overall, in this *in situ* screen, no evidence was found for expression of any *ppk* genes in *dbd* neurons in late embryos. The only members of this gene family known to be expressed in the abdominal PNS remain *ppk1* and *rpk*, as had been previously found [Adams *et al.*, 1998; Jinushi-Nakao *et al.*, 2007]. It may be that other *ppk* genes are expressed in larval *dbd* neurons, with transcription commencing at the 1st instar stage. This would not be picked up by the *in situ* hybridisation screen. However, there are no data, to date, that can confirm or deny this. Nonetheless, it is difficult to see why genes expressed in 1st instar larvae would not

be detectable in very late (stage 16 [Abrams *et al.*, 1993]) embryos. This is supported by the findings of Adams *et al.* [1998], Ainsley *et al.* [2003] and Liu *et al.* [2003], whose larval immunostaining corresponds with the localisation of *ppk* genes they report in their accompanying *in situ* work. In the absence of any other known *Drosophila* DEG/ENaC homologues, it would appear that this ion channel family are uninvolved in *dbd* neuron stretch transduction.

Whilst no positive control staining for the location of *dbd* has been carried, The stereotypical anatomy of *Drosophila* allow a reliable knowledge of its location in each embryo, particularly as it relates to the position of *md*. Thus, positive staining for *dbd*-expressed genes should have produced a pattern of staining comparable to that of *ppk1* in the peripheral neurons. As this was absent from all of the genes assayed, it can fairly confidently be stated that the absence of positive labelling of *dbd* for any of these genes is reliable. However, if desired, this could be further confirmed via electrophysiological analysis (*per* **Ch. 4.2.1** & **4.3**) or immunohistochemical imaging. The latter could also be used to check for the presence of protein, as opposed to the mRNA, which was the target of the *in situ* probes.

4.5 Summary

This analysis of *dbd* neurons has examined the potential molecular mechanotransduction machinery of these endings in an attempt to dissect some of the protein mediators of their stretch-sensitive apparatus. Starting with the predictions of the effect of MNaC inhibition from the theoretical model, examination via two broad-spectrum MSC blockers identified a strong MNaC-dependency for *dbd* stretch activation. This was further shown to be heavily sodium-dependent, in accordance with a key assumption regarding this system.

Subsequent assays involving two ion channels, known to be expressed in *dbd* neurons – TRPA1 and DmPiezo – revealed that both of these proteins play distinct roles in *dbd* stretch transduction, although initial receptor potential depolarisation shows significantly more DmPiezo-dependence than involvement of TRPA1. However, a visual examination failed to show any likelihood of DEG/ENaC expression in *dbd* neurons, contrary to expectation, given the evidence of a DEG/ENaC-mediated system operating in muscle spindles. This indicates that these two systems, whilst highly similar at the behavioural level, show distinct molecular mechanisms.

5. Discussion

5.1. Summary

Mechanotransduction is a complex aspect of physiology. Its involvement in many, diverse roles makes it especially difficult to understand. Furthermore, the processes that occur between stimulus and afferent firing of a mechanosensitive neuron, to say nothing of non-neuronal mechanotransduction, appear intricate and remain, as yet, largely unknown. This study has examined stretch-dependent mechanosensation – the initial conversion of a mechanical stimulus to electrical activity within a sensory neuron – to promote understanding of the molecular components that may comprise such a transduction system. Whilst mediators of initial stretch transduction were identified in an *in vivo* system, the identities of downstream effectors of these molecules remain speculative. Furthermore, the hypothesis that the *dbd* neuron system, investigated here, could be a model stretch transduction system has been shown to be valid, but limited with regard to the specification of the molecules identified as mechanotransducers within other endings. Nonetheless, the mathematical model that has been presented here, built upon electrophysiological data from stretch receptors of various species, has indicated that despite the disparity in the molecular mediators of mechanotransduction expressed in stretch receptors of various species, such receptors may still share a common mechanism of activation, as evidenced by their electrophysiological similarities.

5.2. Modelling mechanotransduction

5.2.1. Understanding receptor potentials

One of the outstanding problems in decoding receptor potentials was the apparent complexity of receptor potential profiles. Hunt *et al.* [1978] had demonstrated that the receptor potential of a muscle spindle was comprised of various ionic currents, including sodium, potassium and calcium. Similarly, the receptor potential of crayfish stretch receptors had also been shown to require these ionic components [Ottoson & Swerup, 1985a; 1985b]. The multivariate forms of stretch-evoked receptor potentials predisposed the supposition that many mediating molecular components underpinned them. Indeed, the first attempt at

modelling a stretch-evoked response limited itself to only addressing the contribution of an MNaC to primary mechanotransduction in the crayfish stretch receptor [Swerup & Rydqvist, 1996].

The mathematical model presented here indicates that the receptor potential profile of stretch-activated afferent endings can be simply recreated with minimal components. It indicates that much of the apparent complexity of the receptor potential, in a number of stretch-sensitive endings, can be accounted for by a small number of ionic currents, activated in combination. By building up a recreation of the receptor potential via a bottom-up approach, an uncomplicated solution results.

The model began with the characterisation of an MNaC as the underpinning gating mechanism of the modelled receptor – a crayfish stretch receptor – as proposed by Swerup & Rydqvist [1996]. However, this early model disregarded TTX-, 4-AP- and TEA-sensitive components of the receptor potential, not only known in crayfish stretch receptors, but also in muscle spindles [Hunt *et al.*, 1978]. Adding these to the MNaC-only model recapitulated untreated *in vivo* recordings [Suslak *et al.*, 2011]. Interestingly, Hunt *et al.* [1978] and Ottoson & Swerup [1985b] had shown a TEA-sensitive K^+ component in their respective studies, and it appeared that this model of the crayfish receptor potential might also describe the mammalian muscle spindle [Suslak *et al.*, 2011].

Indeed, further extension of the model to account for a novel MKC component, potentially gated by Ca^{2+}, was sufficient to adequately describe the full receptor potential profile of these stretch receptors. Such a component has recently been postulated to be part of the mechanotransduction apparatus of the muscle spindle, in a recent, qualitative model of stretch-mediating components of the spindle ending [Bewick & Banks, 2014]. In their review, Bewick and Banks postulate a role for both the calcium-activated SK2 and BK potassium channels, as part of feedback control mechanisms involved in receptor potential generation. Their analysis, derived independently, would seem to stand as good corroboration of the hypothesized Ca^{2+}-dependent MKC of my model. They postulated candidate channels in the muscle spindle system, which can be experimentally tested using the predictions of my model.

Some calcium flux was already known to play a role in both crayfish stretch receptor and muscle spindle receptor potentials [Hunt *et al.*, 1978; Ottoson & Swerup, 1985a]. My model now indicates that this may be involved in gating an MKC – a K_{Ca} channel. However, the calcium current provided by the model Ca_v is only a small fraction (<1%) of the total inward

current – much less than the 20% estimated by Hunt *et al.* [1978]. Transient Ca^{2+} influx via Ca_v channels is also insufficient to activate K_{Ca} channels [Vergara *et al.*, 1998; Fettiplace & Fuchs, 1999]. Overall, these suggest that an additional Ca^{2+} component is missing from the current model, possibly an intracellular calcium store release mechanism. This model also describes the adaptation in *dbd* neurons of *Drosophila* larvae, in which TTX- and TEA-sensitive currents had also been recorded, and whose ionic dependence had also been shown to be comprised of Na^+, K^+ and Ca^{2+} currents [Nair *et al.*, 2010]. Recordings of receptor potentials from *dbd* neurons are qualitatively very similar to the mathematical model voltage trace outputs. Furthermore, this study has shown that there is strong quantitative parity between these two datasets, and thus between receptor potentials in stretch-sensitive endings of a number of species.

However, in addition to these similar features, *dbd* stretch responses show some apparent distinctions from muscle spindle responses. Most obvious from a casual observation is that the ratio of the amplitude of E_{hold} to E_p in the *dbd* response seems to be approximately half that reported in muscle spindles [see **Fig. 33**]. These are, however, preliminary data and further investigation of this phenomenon is required, to confirm whether this is a significant observation. If verified, this would appear to suggest that, although the *dbd* and muscle spindle systems are highly similar in terms of their stretch response machinery, they do possess some subtle distinctions. This is not unexpected, due to the not insignificant differences between flies and mammals. Thus, whilst the fly model is undeniably useful in understanding the mammalian system, it is important to recognise the inevitable limitations.

However, it is also worth noting one key drawback of this 'universal' approach to modelling the biophysics of stretch transduction: the approximations required. Subtle variances are apparent between the behaviours of muscle spindles, crayfish stretch receptors and *dbd* neurons, which are missed by the mathematical model. Whilst all three display the same, overall waveforms, certain specifications are apparent. The after-depolarisation that occurs in both muscle spindles and *dbd* neurons appears absent in crayfish stretch receptors, and even in those endings that do express this feature, the amplitudes are distinct, appearing larger in muscle spindles than *dbd* neurons. The shape of the post-release hyperpolarisations also varies. Both arthropod receptors exhibit a rapid hyperpolarisation that slowly recovers. However, muscle spindles appear to have a dual-component hyperpolarisation that has a rapid onset, followed by a further, gradual hyperpolarising component, before slow recovery

commences. As my mathematical model has attempted to model a generalised stretch response, it necessarily misses some of the specialised physiological attributes of individual receptor types. A more specialised approach may modify the generalisations of this model to reveal more regarding the specifics of other endings.

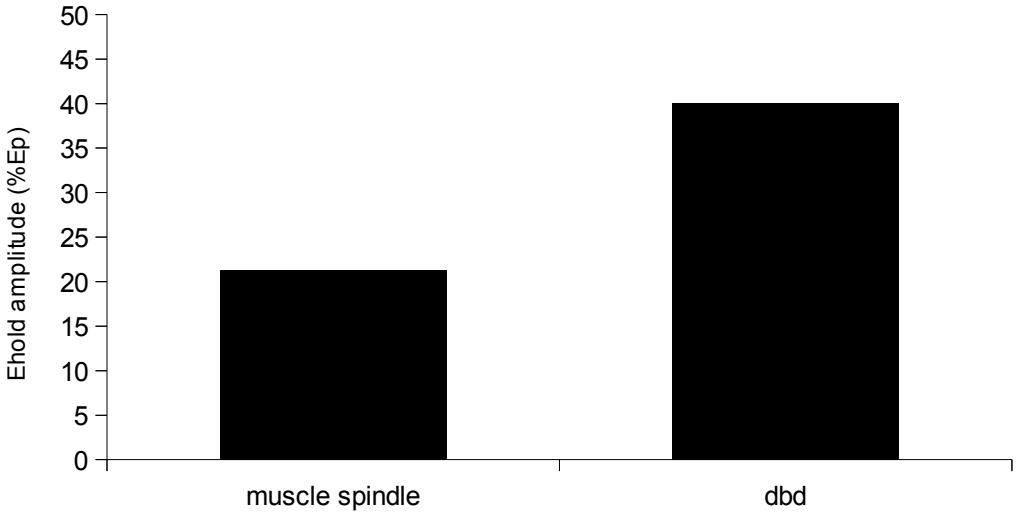

Figure 33: Muscle spindles display higher static repolarisation than *dbd* neurons. Muscle spindles and *dbd* neurons both display partial repolarisation upon the transition from dynamic stretch stimulus to static stretch. However, whilst muscle spindles appear to repolarise to 20% ±0.65% E_p [data inferred from analysis of Hunt *et al.*, 1978], *dbd* neurons only repolarise to 40% ±4.3% E_p.

Furthermore, the limitations of this model, as a whole, should be recognised. As pointed out in **Ch. 2.4**, this model is not spatially constrained. Whilst, as previously stated, this does not significantly impact the ability of the model to make meaningful inferences regarding receptor potential generation, it does prohibit its ability to address the key question of downstream signalling. One key issue that remains to be addressed is how a stretch receptor utilises its mechanically-gated stretch response to generate afferent signals.

5.2.2. From stretch to signal

In 2005, Bewick *et al.* proposed a partial, qualitative model for molecular mechanotransduction in muscle spindles. Although that model focused on the afferent discharge of the spindle, as opposed to its receptor potential, the proposed mechanism

underlying the modulation of discharge rates was tied in to events within the sensory terminal, allying that model with the one described here. There are a number of distinctive similarities between the model of Bewick *et al.* and this model, as well as a number of differences, which are of interest. Whilst the older model is purely speculative and does not attempt to quantify any data, the assumptions that underlie it and their relation to the quantitative *in silico* model, that has been presented here, are notable.

Firstly, it is apparent that both models rely upon the presence of an MNaC to initiate any downstream stretch-mediated processes. The hypothetical model [Bewick *et al.*, 2005] proposed the necessity of cation influxes in order to depolarise the ending, commencing the sequence of events that would regulate afferent discharge. My current *in silico* model mirrors this hypothesis and, combined with *in vivo* data from *dbd* neurons, strongly supports the prior hypothesis of both sodium and calcium currents in the early stages of stretch responses.

However, beyond this point, there is clear divergence in the aspects of stretch responses that are considered by each model: the latter model focuses on the ionic adaptation of a stretch sensitive ending, including the role of potassium, whilst the earlier model is more concerned with downstream effectors of afferent firing regulation. From the point of view of this study, it would be interesting to consider what role such downstream components may have in locally regulating the ionic fluxes within the sensory terminal.

Investigating the overlap of these models may provide insight into the complex mechanisms that occur within mechanosensory terminals. The afferent firing properties of *dbd* neurons are still unknown. Action potentials can be evoked in *dbd* neurons under current-clamp conditions [Nair *et al.*, 2010], but the relationship between these recordings and stretch-evoked responses has not been investigated. It is also not known whether stretch stimuli initiate firing, or merely alter baseline firing rates, as is the case in muscle spindles [Bewick *et al.*, 2005].

Of particular interest is the comparative rarity of action potentials in my recordings from *dbd* neurons. Nair *et al.*, [2010] managed to evoke spike trains in response to a 6pA current pulse, yet in my recordings, whilst single spike (or spike-like) events were seen, these were infrequent, and were never observed as a train of action potentials. It would be useful to re-examine and re-implement the current-clamp experiments of Nair *et al.* [2010], in conjunction with stretch stimulation, in order to perform a side-by side comparison of the responses of *dbd* to the two stimulation methods.

In addition, it would be interesting to address the means by which afferent signalling occ-

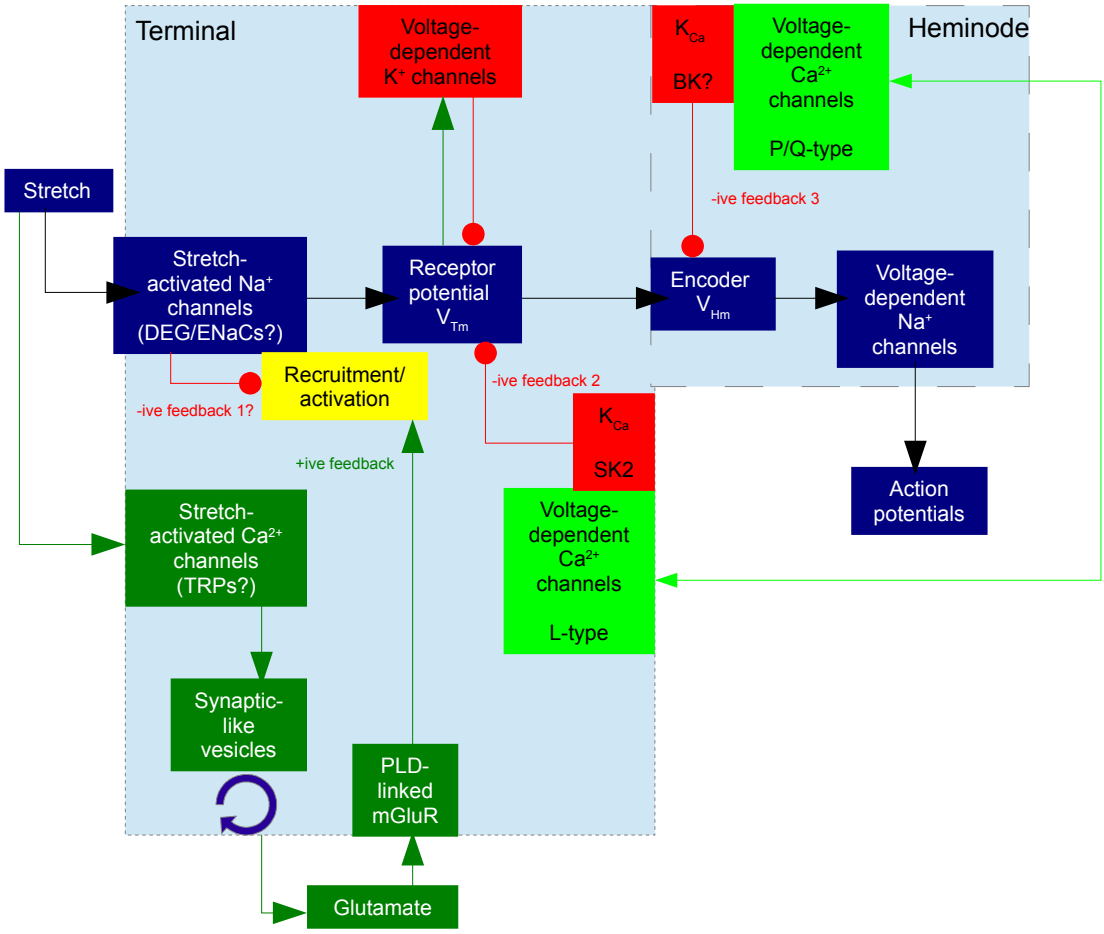

Figure 34: Flow chart to illustrate the main events of mechanosensory transduction. The principal feed-forward pathway from stimulus (stretch) to output (action potentials) is shown by the black arrows. The overall gain of this pathway may be controlled by several feedback pathways: negative feedback 1 is at present hypothetical and is included to account for the reversible silencing of the primary ending by PCCG-13 inhibition of the PLD-linked mGluR; the positive feedback pathway is the well-established SLV/glutamatergic loop; negative feedbacks 2 and 3 involve different kinds of K_{Ca}, one located in the terminal, the other in the heminode and both perhaps triggered by action potentials opening voltage-gated Ca^{2+} channels. Green lines and arrowheads indicate enhancing/excitatory actions; red lines and circles indicate reducing/inhibitory actions; V_{Tm} – terminal potential, V_{Hm} – heminode potential [adapted from Bewick & Banks, 2014].

-urs from *dbd*, which is all the more peculiar if spikes are, indeed, rare events for these neurons. Little remains known about sensory neurons, as much attention has been instead devoted to the study of the CNS. Thus, the workings and mechanisms of PNS function leave a lot to the imagination. It may be that single spikes signal the onset of stretch and

polarisation the termination of same, indicating duration. However, it may also be that action potentials are generated but not back-propagated in these neurons. Additional studies of the properties of *dbd* are required.

Another interesting question to ask is whether or not *dbd* neurons utilise an intra-terminal vesicular mechanism to modulate their activity. This study has supported the earlier hypothesis of stretch-evoked sodium and calcium currents within the afferent terminal of stretch-sensitive endings, which were proposed to be required to initiate the glutamate-mediated modulation of afferent firing in muscle spindles [Bewick *et al.*, 2005]. However, there is currently no evidence to indicate that a similar system may be employed in *dbd* neurons, although such systems have also been shown in other mechanosensory systems, like lanceolate endings in rat hair follicles [Banks *et al.*, 2013].

In their more recent summary of the current understanding of muscle spindle stretch activation and regulation, Bewick and Banks [2014] have made an initial effort to tie the twin aspects of receptor potential generation and afferent firing together. Their model [see **Fig. 34**] proposes a concerted activation of both stretch-activated Na^+ and Ca^{2+} channels, as well as distinct roles for BK and SK K_{Ca} channels in firing and receptor potential generation, respectively. That model is in some agreement with the model that is presented here. Certainly, in my model, additional calcium is required from somewhere in order to enable the MKC to function. Conceivably, this could come from an independent stretch-activated channel, or via a non-selective MSC. However, my model also purports that the most likely MKC activator is calcium, as opposed to direct stretch activation, which is the mechanism that appears to be the preferred candidate of Bewick and Banks [2014].

5.3. Candidate mechanotransducers

5.3.1. Roles of Piezo and TrpA1

Although expression data from previous studies had shown that both Piezo and TRPA1 were present in *dbd* neurons [Kim *et al.*, 2010; Shen *et al.*,2011], this study represents the first data that directly implicates these two ion channels in the electrophysiological responses of *dbd* neurons to stretch. Not only that, but it was also observed that loss of Piezo in these neurons produced a noticeable effect on stretch-evoked depolarisation, consistent with the predictions of the *in silico* model for the effect of a loss of the primary MNaC in a stretch-

activated ending. The essential role of Piezo in *dbd* stretch responses is strong evidence for Piezo as the primary MNaC in these receptors.

Furthermore, it was also observed that TRPA1 makes a small but significant contribution to stretch-evoked depolarisation in these endings. This contribution appears to be dependent upon activation of functional Piezo channels, although it is not necessarily dependent upon any charge conductance by Piezo. Whilst the exact interaction between Piezo and TRPA1 is uncertain, it is interesting to note that the relative proportion of the TRPA1 contribution to stretch evoked depolarisation (~40% stretch-evoked depolarisation) is quantitatively similar to the depolarisation that can still be evoked when Na^+ was completely replaced with NMDG. Together, these suggest TRPA1 may be contributing to a Ca^{2+} current, which is consistent with evidence that Ca^{2+} is the major permeant ion of TRPA1 channels [Bobkov *et al.*, 2011]. This observation is also well correlated with the quantitative contribution by Ca^{2+} ions to the stretch-activated receptor potential in mammalian muscle spindles [Hunt *et al.*, 1978]. In that study, the residual potential change was due to a stretch-activated Ca^{2+} current, the source of which was not identified.

The mathematical model also appears to indicate a role for a K_{Ca} channel. A TRPA1-mediated Ca^{2+} current may provide a mechanism for introducing calcium into this system, initiating the activation of a K_{Ca}. This would accord well with the mathematical model, in which there is a voltage-activated Ca^{2+} current evoked by the stretch-dependent initial depolarisation. This would be insufficient to activate a K_{Ca}, but it may trigger some mechanism of release of intracellular calcium. However, no mechanism for this latter process is proposed in the mathematical model, nor is it clear what mechanism might exist in *dbd* neurons to facilitate this. It could be, though, that this omission may account for some discrepancies between the model and *in vivo* data, but it is currently unclear as to how such terms might be included.

Together, then, these results may indicate a mechanism within *dbd* neurons, that is initiated by the stretch-activation of Piezo channels, permitting cation influx, subsequently activating downstream TRPA1 channels. This would appear to involve some physical interaction, rather than a voltage-gated mechanism, although, as suggested in the *in silico* model, the latter mechanism is permissible. Both the *in silico* model parameters and the *in vivo* data could indicate that Piezo communicates a sodium current, whereas TRPA1 is conducting calcium into the receptor terminal, although Piezo has been shown to be calcium-permeable and non-selective [Coste *et al.*, 2010]. It is hypothesized that this calcium influx may then activate a K_{Ca} to repolarise the ending, while TRPA1 rapidly inactivates. Reduction of tension would

inactivate Piezo, leading to hyperpolarisation, before the K_{Ca} also inactivates, returning the receptor to a resting state [see **Fig. 35**].

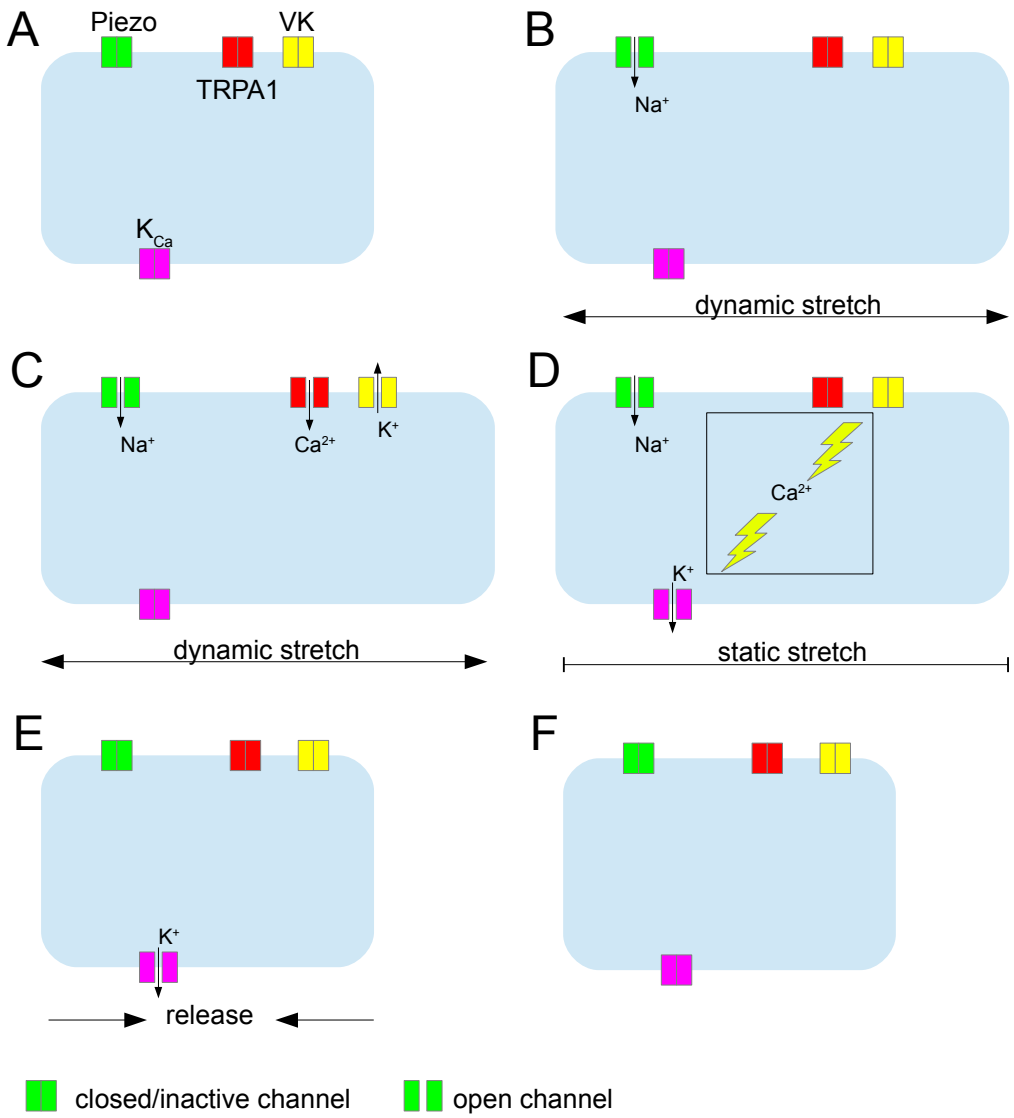

Figure 35: Proposed model of molecular mechanotransducers in *dbd* neurons. Based on the results of this investigation, Piezo and TRPA1 are known ion channels within the transducing apparatus of *dbd* (A). These most likely mediate Na^+ and Ca^{2+} entry into the endings, respectively, upon application of a stretch stimulus (B). VKC (as yet unidentified) are activated by this initial depolarisation (C) and K_{Ca} (also putative) are activated by an unidentified intracellular calcium-mediated process (D). Relaxation acts as a termination signal for all the mechanosensory entities, with some persistent Ca^{2+} delaying inactivation of the K_{Ca} (E), which eventually inactivates, returning the ending to rest (F) [*cf.* **Fig. 19**].

Further experimental examination of the role of TRPA1, which may potentially have a bimodal sensory role in this receptor [Shen *et al.*, 2011], as well as further investigation of how it may interact with Piezo may provide very useful insight into primary sensory transduction pathways. For example, Ca^{2+} influx through TRPA1 has been recently shown as having a strong role in activating TRPV1 channels in nociceptive neurons [Staruschenko *et al.*, 2010], while a similar Ca^{2+} influx in mechanosensory terminals may be responsible for the Ca^{2+}-mediated activation of synaptic-like vesicle recycling in these endings [Bewick *et al.*, 2005].

5.3.2. ~~*E pluribus unum*~~ *Ex uno plures*

It is apparent, at this point, that a solution to the problem of understanding mechanotransduction may not be straightforward, as indicated at the beginning of this study. Two main strands of evidence now indicate that, at the molecular level, different organisms utilise distinct components to construct their stretch tranduction apparatus. Firstly, electrophysiological data from various stretch receptors, whilst strikingly similar, do display subtle variations in form, perhaps indicative of slight distinctions in the transduction processes that occur in each one.

Secondly, and perhaps more convincingly, experimental assays of various stretch-activated ending types have hitherto identified several different candidate channels in such receptors. It has been shown, here, that both DmPiezo and TRPA1 play important roles in the stretch-transducing capabilities of *dbd* neurons in larval *Drosophila*. However, attempts to detect expression of Piezo in mammalian muscle spindles have failed to indicate the expression of either mammalian homologue – Piezo1 and Piezo2 – in spindle terminals [GSB unpublished observations]. Similarly, muscle spindles express ENaC proteins, which could potentially form MSCs [Simon *et al.*, 2010]. However, it has been shown, here, that no known *Drosophila* ENaC homologues (*ppk* family members) are present in *dbd* neurons. Thus, it appears likely that muscle spindles may use ENaCs as MNaCs, whilst *dbd* neurons use a Piezo-dependent system.

However, whilst there appears to be significant disparity in the molecular mediators of mechanotransduction, there may be an underlying commonality after all. Despite the subtle variations in the electrophysiology of these endings, they all share very similar properties. The mathematical model, presented here, while partially incomplete, is a very good

approximation of the electrical behaviour of all the receptor types that were examined, being based on data from a crayfish system, qualitatively resembling mammalian data and quantitatively describing data from *Drosophila*.

Furthermore, when considered at the level of ionic currents, as opposed to specifically considering ion channels, from both the mathematical model and existing experimental data, there appears to be a high degree of similarity between the ionic requirements for receptor potential generation in various endings. Crayfish stretch receptors and muscle spindles both exhibit similar ionic dependencies, with respect to sodium, potassium and calcium [Hunt *et al.*, 1978; Ottoson & Swerup, 1985a]. The data presented here are also consistent with the relative Na^{+}/Ca^{2+} dependencies of these two receptors.

That one model of stretch receptor adaptation can describe the behaviour, at a biophysical level, of three, distinct receptor types, in three different species, may support, somewhat interestingly, the hypotheses that some degree of common mechanism is shared by these mechanosensitive endings [Benos, 2004; Kung, 2005]. This *in silico* model provides an electrophysiological mechanism to describe stretch receptor behaviour, but does not stipulate that this must be achieved by a shared molecular mechanism. Indeed, despite their similar anatomy and identical stretch-evoked receptor potentials, the molecular mechanisms of *dbd* neurons and muscle spindles appear to be distinct.

Thus, contrary to Benos' hypothesis [Benos, 2004], there are at least two, and possibly many more, mechanisms of generating the similar complex receptor responses associated with stretch across phyla. Nonetheless, the mechanism of activation, at the biophysical level, appears to be consistent, perhaps, with Kung's hypothesis [Kung, 2005] that different ion channels may mediate the same processes, due to their evolutionary commonalities. Thus, it may be that stretch transduction has an evolutionarily ancient origin that has diversified, in terms of its mediators, over the ages, reflecting the complexity and diversity of the situations in which it is employed by various organisms. This raises the interesting question of what physiological drive demands that stretch responses take the specific, complex electrophysiological form observed in these different receptors. Analysis of additional mechanoreceptor types may yield further diversity of molecular mechanisms, both within and between species.

Furthermore, the role of *dbd* neurons, and thus DmPiezo, within the context of the whole organism remains to be considered. As *dbd* neurons are associated with larval striated muscle

[Schrader & Merritt, 2007], it can be hypothesized that any perturbation of *dbd* function would produce a phenotype in larval locomotion, specifically that larvae lacking Piezo would exhibit reduced movement, compared to control larvae, over an equivalent period of time. Here, a preliminary assay has been performed to examine this. Larvae with the *dmpiezo*-RNAi construct [see **Ch.4.2.1**] were examined in a larval crawling assay.

Compared to background controls, it was observed that *dmpiezo*-RNAi larvae were significantly less active. On average they crawled less than ⅓ the distance of control larvae [see **Fig. 36**]. Additionally, casual observations indicated that, not only were control larvae more active in terms of exploration and crawling, but that, even when not crawling, control larvae exhibited much more motile behaviour, *e.g.*, rearing, writhing, burrowing and rolling. *dmpiezo*-RNAi larvae, in contrast, tended to remain static and immobile on the dish.

However, when interpreting these results, it is important to note that Piezo is expressed in a number of cells and cell types, other than *dbd*, principally in other *md* neurons, but also in other non-neuronal tissues [Kim *et al.*,2012]. Thus, any effect on larval locomotion in this assay cannot be solely attributed to the loss of *dbd* function. However, *md* neurons have heretofore not been associated with defects in free movement, being rather more implicated in nociception [Kim *et al.*, 2012].

The above notwithstanding, the results of earlier electrophysiological assays [above] indicate that loss of Piezo is sufficient to abolish *dbd* activity and this correlates with reduced larval motility. Additionally, these results show strong agreement with earlier results that observed similar motor defects in larvae with inhibited *dbd* firing [Suster & Bate, 2002; Hughes & Thomas, 2007].

These preliminary data suggest a role for *dbd* neurons in a sensory-motor feedback loop in the larval *Drosophila* thoraco-abdominal segment, and further point to the significant role of DmPiezo within that system. Understanding of the circuitry of the stretch-mediated motor control of larval peristaltic movement may be a powerful tool for contextualising stretch receptors of more complex organisms.

In light of this work, however, there remain questions to be addressed on the functionality of *dbd* neurons: their relation to stretch receptors in other organisms and the question of how they convert mechanical stimuli into an afferent signal. Principally, the behavioural work begun here could be developed to investigate the roles of *dbd* and Piezo in locomotion in more detail. A *dbd*-specific driver for the RNAi knock-down would be invaluable, in order to investigate whether observed crawling deficits are due to loss of *dbd* function, and not the

involvement of other neurons or non-neuronal cells. For example, the only cross-over of Piezo and TRPA1 expression in neurons is in *dbd* [*cf.* Shen *et al.*, 2011 & Kim *et al.*, 2012]. Another alternative might be to use an *amos* driver. This proneural gene, which regulated *atonal* in *Drosophila* embryogenesis, drives differentiation of the Ch neurons, but also *dbd*, which distinguishes it from other *da* neurons [Goulding, zur Lage & Jarman, 2000].

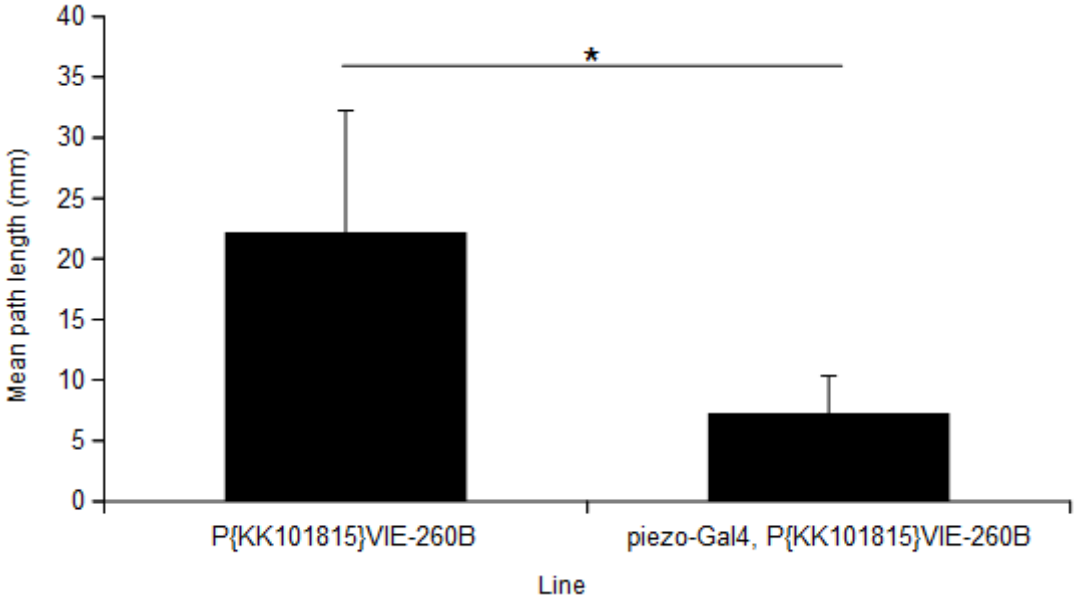

Figure 36: Loss of *dmpiezo* in *dbd* neurons inhibits larval locomotion. Over a period of five minutes, control larvae were recorded moving an average distance of 22mm (±10mm), whereas *dmPiezo*-RNAi larvae only moved an average of 7mm (±3mm) over the same time period, 32.8% control (n=28, p<0.0001).

Similarly, such an approach could be used to examine the molecular apparatus of *dbd* neurons in more detail. *Use of a suitable driver strain, crossed to a line expressing a GCaMP construct [Akerboom et al., 2012], e.g.* GCaMP5, could be used to examine calcium events in these neurons. Such events would be predicted to occur in the event of the putative vesicular recycling system [see **Ch. 5.2.2**], providing a useful initial screen for such a mechanism. Additionally, the temporal resolution of this technique makes it suitable for examining the timing of any stretch-induced calcium events that have been suggested to be a part of this system [see **Ch. 5.3.1**].

Thirdly, as mentioned above [see **Ch. 3.2.3**], follow-up experiments should be carried out to assess, in depth, the relation of these results to those obtained by Nair *et al.* [2010]. Given the apparent disparity between the outputs recorded from *dbd* neurons in the two studies, the

mechanisms that are involved in generating responses to current and mechanical stimulation of these neurons should be analysed and compared. Clearly some disparity exists between these studies in terms of their characterisation of *dbd* neurons. Why this should exist and to what extent it is stimulus-dependent will be of interest to future experimental design.

As a follow-up to this, the distinctions between voltage-activated and stretch-activated components of *dbd* neurons could be assessed, including their localisation. This would likely be a lengthy process, requiring the identification of the full transduction apparatus of *dbd* neurons, from stretch detection to output generation, followed by individual interrogation of these components, by genetic and pharmacological means. However, additional means, such as fluorescence-tagging of known proteins could be accomplished to identify subcellular organisation of the components of the transduction apparatus. Additionally, ablation of the dendrites or axon at various distances from the cell body and comparison of current-clamped and stretch-activated responses, alongside comparisons to the theoretical model, could be used to distinguish voltage- and stretch-activated components.

Finally, the wider question of the general homology of stretch receptors across species, while is has been touched on here, remains largely unaddressed. It has been shown that *dbd* neurons utilise a Piezo- and TRPA1-dependent mechanism, and that this is not likely to be conserved in mammals. However, the pharmacology of *Drosophila* and mammalian stretch receptors are distinctly similar. Further pharmacological testing of *dbd* neurons, as well as those of other arthropods, will surely indicate how far this similarity goes, as only a limited range of compounds have been examined here.

6. Standard materials and methods

This section contains descriptions of all standard techniques and reagents used in the work described above. Any specialised techniques and protocols that were developed as part of this project are described within the body of the text, at the appropriate point, as these form part of this research. All protocols and reagents referred to in the main text are as below, unless otherwise specified.

6.1 Solutions

10% bovine serum albumin (BSA):

10% b/w BSA powder [Roche, Ltd] in 1x phosphate-buffered saline (PBS)

Blocking buffer:

30% b/w normal goat serum in PAT3 [Iyer, 2010]

Electrophoresis gel:

0.8% agarose was dissolved in TAE, with heating. When slightly cooled, 7μL/100mL GelRed [Biotium] was added and the gel mixture was poured into a mould to solidify.

Gel loading buffer:

50% w/v glycerol, 0.25% w/v bromophenol blue, in 1x TBE [Sambrook & Russell, 2001]

HL (hæmolymph-like) 3:

70mM NaCl, 5mM KCl, 1.5mM $CaCl_2$, 20mM $MgCl_2$, 10 $NaHCO_3$, 5mM Trehalose, 115mM sucrose, 5mM HEPES, in deionised water, pH to 7.2 [Stewart *et al.*, 1994].

HL3.1:

70mM NaCl, 5mM KCl, 10mM $NaHCO_3$, 5mM Trehalose, 4mM $MgCl_2$, 1.5mM $CaCl_2$, 115mM sucrose, 5mM HEPES, in deionised water pH to 7.2 [Feng *et al.*, 2004].

Hybridisation buffer (Hyb):

25mL 50% deionised formamide, 12.5mL 5x sodium citrate, 500μL 10mg/mL tRNA, 50μL

50mg/mL heparin, 50µL 0.1% tween20, 12mL H_2O, pH to 6.5 [Sambrook & Russell, 2001]

Lysis buffer:

100mM Tris-HCl pH9, 100mM EDTA, 1% b/w sodium dodecyl sulphate (SDS), in deionised water [Sambrook & Russell, 2001]

PAT3:

0.5% b/w Triton X-100, 5% b/v 10% BSA in 1x PBS [Iyer, 2010].

Patch pipette internal solution:

140mM KCH_3SO_3, 2mM $MgCl_2$, 2mM EGTA, 5mM KCl, 20mM HEPES, in deionised water, pH to 7.4 [Nair *et al.*, 2010].

PBS:

1x PBS tablet [Sigma] in 200mL deionised H_2O.

PBS Tween (PBTw):

0.1% w/v tween20 in PBS

Reaction solution (for *in situ* hybridisation colour reaction):

100mM Tris pH 9.5, 100mM NaCl, in deionised water [Sambrook & Russell, 2001]

Tris/acetic acid/EDTA (TAE):

40mM Tris base, 19mM glacial acetic acid, 1mM EDTA, in deionised water [Sambrook & Russell, 2001]

20x Tris/Borate/EDTA (TBE):

1g NaOH, 216g Tris base, 110g boric acid, 14.8g EDTA, in 1L deionised H_2O [Sambrook & Russell, 2001]

Tris/EDTA (TE):

10mM Tris pH 8.0, 1mM EDTA, in deionised water [Sambrook & Russell, 2001]

6.2 Techniques

Fly lines: Experiments were carried out using the following fly lines: w^{1118}, a *Piezo-Gal4* driver strain [kindly donated by S.E. Kim], two *Piezo-RNAi* strains - *P{KK101815}VIE-260B* and w^{1118}*; P{GD993}v2796* [Vienna *Drosophila* RNAi Center], a TrpA1 RNAi line - w^{1118}*; P{GD2375}v37249* [Vienna *Drosophila* RNAi Center] – and w^{1118}*; TrpA1*^{1} [Bloomington *Drosophila* Stock Center], a TrpA1 mutant.

Fly husbandry: Fly stocks were kept in bottles containing food substrate, stored at 18°C and tipped into fresh food every 2-4 weeks. Lines required for experiments were stored at 21°C and tipped into fresh food every week. Crosses were performed in phials containing food, stored at 25°C. To produce embryos for collection, flies were transferred to a cage, surmounting a red wine agar plate, supplied with a small mass of food substrate, changed daily, and incubated at 25°C.

Fly dissection: Third instar larvae were pinned rostrally and caudally in a 35mm Sylgard-lined dish containing HL3. One longitudinal lateral incision was made followed by rostral and caudal transverse incisions of the superior pelt and evisceration. The dissected pelt was opened to expose the innermost aspect and pinned four-square.

Fly immunohistochemistry: Dissected pelts were fixed overnight at 4°C in 1% w/v formaldehyde, made up in HL3. Fixed pelts were washed 3 times, at room temperature, in PAT3, for one hour each, then in blocking buffer for 2 hours at room temperature. Primary antibody (1/1000 rabbit α-GFP [Invitrogen]) was applied at room temperature for 2 hours, then moved to 4°C overnight. The preparation was again washed 3 times, for one hour each time, with PAT3, followed by incubation with secondary antibody (1/400 GFP goat α-rabbit) for 2 hours at room temperature, then 5 days at 4°C. Three final PAT3 washes were performed, as before, followed by 1 PBS wash. Preparations were slide-mounted in Vectashield [Vector, Inc.] [protocol adapted from Iyer, 2010].

Fly electrophysiology: As the development and performance of this protocol formed a significant part of the body of work represented in this thesis, the relevant details of this technique are specified in **Ch.3**.

Modelling: Modelling, *in silico*, was done in Matlab[14]. Full source code for the model can be found in **Appendix i**.

Analysis: Statistical tests, appropriate to each data comparison, were carried out using tools available in OpenOffice Calc. Where ANOVA has been performed, a dedicated, open-

14 "I put the numbers into this magic box and out came my thesis!" [PhD comics, 3.7.2012]

source ANOVA tool was used, which is freely available at: http://www.physics.csbsju.edu/stats/anova.html.

Gel electrophoresis: Electrophoresis was used to test yields of DNA, PCR product and probe labelling [see below]. In each case, a gel was prepared [as above] and placed in a bath of TAE. 8μL of each required sample was mixed with 2μL of loading buffer and loaded into separate wells. A marker well was loaded with 2μL Hyperladder IV™ [Bioline]. Samples were run for 30-45 minutes and viewed under UV, for visual confirmation. All gel images were generated as Polaroid™ stills, which were subsequently digitised.

DNA collection: Approximately 50 control (w^{1118}) flies were immobilised with CO_2 and collected in a 2mL Eppendorf tube. 200μL of lysis buffer was added and the tube was frozen at -20°C. Once the mixture was frozen solid, the tube was removed from the freezer and the the contents were thawed and homogenized. A further 600μL lysis buffer was added and the mixture was incubated for 30 minutes at 70°C. 150μL CH_3CO_2K was incubated on ice and then added to the fly-lysis buffer mixture, which was then incubated on ice for a further 20 minutes. This mixture was then centrifuged at 14000rpm for 20 minutes at 4°C. The resulting supernatant was drawn off and split equally between two tubes, with the volume in each tube being noted. 0.9 volumes of isopropanol was added to each tube (*e.g.* 0.375mL isopropanol for 0.5 mL supernatant) and the contents of each tube were well mixed and centrifuged for a further 10 minutes. The supernatant was removed and discarded, and the pellets were washed in 70% EtOH and allowed to air-dry. Each pellet was re-suspended in 50μL TE and the two tubes were pooled together. 100mL phenol-chloroform was added. The mixture was vigorously mixed and centrifuged for another 10 minutes, after which the upper, aqueous layer was removed to a clean tube. 5μL 3M CH_3CO_2Na was added and mixed in, followed by further addition of 250μL cold 100% EtOH. This was mixed again and then stored at -20°C overnight. After storage, the mixture was centrifuged again, with the supernatant being discarded, leaving a pellet. This was washed and dried, as above, before being re-suspended in 100μL TE. Yield was checked by gel electrophoresis.

Primer design: FlyBase [flybase.org] was queried for the gene of interest and the coding sequence for that gene was acquired from the relevant web page. The sequence for a large exon [usually the largest, ideally >500bp] was copied into the online primer design tool, Primer3 [http://bioinfo.ut.ee/primer3-0.4.0/]. This tool automatically outputted primers

for the selected gene. A T7 recognition sequence (GTAATACGACTCACTATAGGGC) was appended to the 3' primer and the required nucleotide sequences were ordered from Sigma-Aldrich Ltd., UK. Primers arrived as dry pellets, which were re-suspended, in TE, to 100μM.

Polymerase chain reaction (PCR): The following reaction mix was prepared (with components added in this order): 31.5μL deionised H_2O, 5μL buffer stock solution [Roche, Ltd.], 1μL dNTP solution [Roche, Ltd.], 5μL 10μM of each primer, 2μL DNA [from "DNA collection"] and 0.5μL Taq polymerase [Roche, Ltd.]. The components were mixed thoroughly and briefly centrifuged to collect all components at the base of the tube. PCR was then performed in a Techne TC-512 machine, running the following heat cycle: (A) 2 minute ramp to 94°C, (B) 30s hold at 94°C, (C) 30s ramp to 55°C, (D) 2 minute ramp-and-hold at 72°C , repeat steps B-D 29 times for a 30-cycle PCR, (E) 10 minute hold at 72°C, and (F) a final ramp to 4°C. The product was then stored at -20°C until needed. Each test reaction was run in parallel to a positive control (known sample) and a negative control (containing no DNA). 8μL of each PCR product was run on a gel to test for reaction success.

PCR product purification: PCR products were purified using the Thermo Fisher Scientific Inc. GeneJet™ Gel Extraction Kit, according to the instructions therewith supplied.

RNA probe labelling: The following reaction was carried out with reagents in the DIG RNA labelling kit [Roche, Ltd.]. To a sterile, RNase-free tube, kept on ice, the following reagents were added: 6.5μL purified PCR product [as above], 1μL dNTP labelling mixture, 1μL transcription buffer, 0.5μL RNase inhibitor and 1μL T7 RNA polymerase. The mixture was then incubated for at least 2 hours at 37°C. The reaction was then stopped by adding 2μL 0.2M EDTA. The product was then tested by gel electrophoresis.

Probe purification: RNA Probes were purified using the Thermo Fisher Scientific Inc. GeneJet™ RNA Purification Kit, according to the instructions therewith supplied.

Embryo fixation: Embryos were collected on red wine agar plates [see Fly Husbandry] and then removed to a sieve by rinsing with water and gentle brushing. The embryos were then washed in 50% w/v bleach in water for 4 minutes to dechorionate them, and then rinsed thoroughly in water, to remove the bleach. The dechorionated embryos were then transferred to a scintillation phial, to which were added 3.75mL 1x PBS, 1.25mL formaldehyde and 5mL n-heptane. The phial and its contents were then shaken vigorously

for 20 minutes. After shaking, the lower phase of liquid was removed and 10mL MeOH was added. The phial and its contents were immediately given another vigorous shake for 2 minutes to devitellinate the embryos. Devitellinated embryos then sink to the bottom of the phial and these were then removed to a 2mL Eppendorf tube, washed twice with MeOH and then stored, in MeOH, at -20°C.

***In situ* hybridisation:** Fixed embryos were sequentially washed in 70% MeOH (w/v in PBTw), 50% MeOH, 30 % MeOH and finally in PBTw for 5 minutes each. Following these, embryos were post-fixed in 10% w/v formaldehyde in PBTw for 20 minutes, followed by another 5x 5 minute washes in PBTw, and then a 10 minute wash in 50:50 PBTw-Hyb. After washing, the embryos were incubated in Hyb at 70°C for 2 hours. The purified RNA probe [see above] was diluted to an appropriate concentration (between 1:100 and 1:500, depending upon efficacy) in Hyb, heat-shocked at 94°C for two minutes, and then rapidly chilled on ice. After the embryos have incubated in the Hyb for two hours, the buffer was removed and the diluted probe was added and left at 70°C overnight[15]. After incubation with the probe, the probe was removed and stored. The embryos were washed, sequentially, at 70°C, once in Hyb, then in 50:50 Hyb-PBTw and then 4x in PBTw, all for 30 minutes and with all solutions pre-heated to 70°C. Then the embryos received one final 10 minute wash with PBTw at room temperature. After this wash, the embryos were incubated with 1:2000 α-DIG alkaline phosphatase [Roche, Ltd.] w/v PBTw overnight at 4°C. After antibody incubation, the antibody was removed and the embryos were washed 3x for 20 minutes in PBTw, before being transferred to a microtitre plate and being rinsed a further 3x with reaction solution. After rinsing 1mL reaction solution was added to each batch of embryos, along with 20μL NBT/BCIP (nitro-blue tetrazolium chloride/5-bromo-4-chloro-3'-indolyphosphate p-toluidine salt) [Roche, Ltd.] and incubated for several hours, until a colour reaction developed. This was determined, visually, via microscopy. Once a reaction was observed, the reaction was halted by washing with PBTw. Embryos were then slide-mounted in 70% glycerol w/v PBTw.

Larval crawling assay: Four genetically identical larvae were placed on a Sylgard-lined dish, free from impediments. The dish was then covered with a colourless overlay and left, to allow the larvae to acclimatise. The position of each larva in the dish was then marked by inscribing a coloured point on the overlay, directly above the position of the head of each larva. Each larva was distinguished by a different colour. The larvae were

15 "I went to have a few beers with my friends" [PhD comics, 3.7.2012]

then observed for five minutes, moving freely within the dish, with no external stimuli presented. The position of the each larva was marked every minute, as above, and the displacement vector for each larva over each minute was also inscribed in the appropriate colour. After five minutes, the overlays were removed. For each larva, the length of the five, one-minute displacement vectors were summed to give a measure of the total distance covered by each larva over the five-minute observation period. Control and test experiments were conducted simultaneously

7. References

Abrams, JM., White, K., Fessler, LI. & Steller, H., 1993. Programmed cell death during *Drosophila* embryogenesis. *Development*, **117**, pp.29-43.

Adams, CM., Anderson, MG., Motto, DG., Price, MP., Johnson, WA. & Welsh, MJ., 1998. Ripped Pocket and Pickpocket, novel *Drosophila* DEG/ENaC subunits expressed in early development and in mechanosensory neurons. *J. Cell Biol.*, **140**, pp.143-52.

Ainsley, JA., Pettus, JM., Bosenko, D., Gerstein, CE., Zinkevich, N., Anderson, MG., Adams, CM., Welsh, MJ. & Johnson, WA., 2003. Enhanced locomotion caused by loss of the *Drosophila* DEG/ENaC protein Pickpocket1. *Curr. Biol.*, **13**, pp.1557-63.

Akerboom, J., Chen, T-W., Wardill1, TJ., Tian, L., Marvin, JS., Mutlu, S., Calderón, NC., Esposti, F., Borghuis, BG., Sun, RS., Gordus, A., Orger, MB., Portugues, R., Engert, F., Macklin, JJ., Filosa, A., Aggarwal, A., Kerr, RA., Takagi, R., Kracun, S., Shigetomi, E., Khakh, BS., Baier, H., Lagnado, L., Wang, SS-H., Bargmann, CI., Kimmel, BE., Jayaraman, V., Svoboda, K., Kim, DS.,Schreiter, ER. & Looger, LL., 2012. Optimization of a GCaMP calcium indicator for neural activity imaging. *J. Neurosci.*, **32**(40), pp.13819-40.

Aristotle, n.d. *Physics*. Translated from Ancient Greek by R. P. Hardie and R. K. Gaye. Adelaide: University of Adelaide.

Baines, RA. & Bate, M., 1998. Electrophysiological development of central neurons in the *Drosophila* embryo. *J. Neurosci.*, 18(12), pp.4673–83.

Bang, H., Kim, Y. & Kim, D., 2000. TREK-2, a new member of the mechanosensitive tandem-pore K^+ channel family. *J. Biol. Chem.*, 275(23), pp.17412-9.

Banke, TG., 2011. The dilated TRPA1 channel pore state is blocked by amiloride and analogues. *Brain Res.*, **1381**, pp.21-30.

Banks, RW., 1988. Studies on the motor innervation of tenuissimus muscle spindles in the anaesthetized cat. *J. Physiol. Lond.*, **406**, pp.70.

Banks, RW., Cahusac, PM., Graca, A., Kain, N., Shenton, F., Singh, P., Nja, A., Simon, A., Watson, S., Slater, CR. & Bewick, GS. 2013. Glutamatergic modulation of synaptic-like vesicle recycling in mechanosensory lanceolate nerve terminals of mammalian hair follicles. *J. Physiol.*, **591**(10), pp.2523-40.

Bennet-Clark, HC., 1971. Acoustics of insect song. *Nature*, **234**, pp.255-9

Benos, DJ., 2004. Sensing tension – recognising ENaC as a stretch sensor. *Hypertension*, **44**, pp.616-7.

Berkefeld, H., Fakler, B. & Schulte, U., 2010., Ca^{2+}-activated K^+ channels: from protein

complexes to function. *Physiol. Rev.*, **90**(4), 1437-59.

Berntson, A. K. & Walmsley, B., 2008. Characterization of a potassium-based leak conductance in the medial nucleus of the trapezoid body. *Hearing Res.*, **244**(1-2), pp.98-106.

Bewick, GS. & Banks, RW., 2014. Mechanotransduction in the muscle spindle. *Pflugers Arch. - Eur. J. Physiol.* [Online], DOI 10.1007/s00424-014-1536-9.

Bewick, GS., Reid, B., Richardson, C. & Banks, RW., 2005. Autogenic modulation of mechanoreceptor excitability by glutamate release from synaptic-like vesicles: evidence from the rat muscle spindle primary sensory ending. *J. Physiol.*, **562**:381–94.

Bianchi, L. & Driscoll, M., 2002. Protons at the date: DEG/ENaC ion channels help us feel and remember. *Neuron*, **34**, pp.337-40.

Bobkov, YV., Corey, EA. & Ache BW., 2011. The pore properties of human nociceptor channel TRPA1 evaluated in single channel recordings. *Biochem. Biophys. Acta.*, **1808**(4), pp.1120-8.

Bodmer, R. & Jan, YN., 1987. Morphological differentiation of the embryonic peripheral neurons in *Drosophila*. *Roux's Arch. Dev. Biol.*, **196**, pp.69-77.

Boyd, IA., 1986. Two types of static γ-axon in cat muscle spindles. *Q. J. Exp. Physiol.*, **71**, pp.307-27.

Brink, F., Jr., Bronk, DW. & Larrabee, MG., 1946. Chemical excitation of nerve. *Ann. NY. Acad. Sci.*, **47**, pp.457-85.

Brown, HM., Ottoson, D. & Rydqvist, B., 1978. Crayfish stretch receptor: an investigation with voltage-clamp and ion-sensitive electrodes. *J. Physiol.*, **284**, pp.155-79.

Cameron, P., Hiroi, M., Ngai, N. & Scott, K., 2010. The molecular basis for water taste in *Drosophila*. *Nature*, **465**(6), pp.91-6.

Campbell, DL., Giles, WR., Hume, JR., Noble, D. & Shibata, EF., 1988. Reversal potential of the calcium current in bull-frog atrial myocytes. *J. Physiol.*, **403**, pp.267-86.

Carlson, SD., Hilgers, SL. & Juang, J-L., 1997. First developmental signs of the scolopale (glial) cell and neuron comprising the chordotonal organ in the *Drosophila* embryo. *Glia*, **19**, pp.269-74.

Caterina, MJ., Schumacher, MA., Tominaga, M., Rosen, TA., Levine, JD. & Julius, D., 1997. The capsaicin receptor: a heat-activated ion channel in the pain pathway. *Nature*, **389**, pp.816-24.

Chatterjee, S., Chapman, KE. & Fisher, AB., 2008. Lung ischemia: a model for endothelial mechanotransduction. *Cell Biochem. Biophys.*, 52, pp.125–138.

Colbert, HA., Smith, TL. & Bargmann, CI., 1997. OSM-9, A novel protein with structural similarity to channels, is required for olfaction, mechanosensation, and olfactory adaptation in *Caenorhabditis elegans*. *J. Neurosci.*, **17**(21), pp.8259-69.

Conti, F., Hille, B., Neumcke, B., Nonner, W. & Stampfli, R., 1976. Measurement of the conductance of the sodium channel from current fluctuations at the node of Ranvier. *J. Physiol.*, **262**(3), pp.699-727.

Corey, DP., García-Añoveros, J., Holt, JR., Kwan, KY., Lin, S-Y., Vollrath, MA., Amalfitano, A., Cheung, E. L-M., Derfler, BH., Duggan, A., Géléoc, GSG., Gray, PA., Hoffman, MP. Rehm, HL., Tamasauskas, D. & Zhang, D-S., 2004. TRPA1 is a candidate for the mechanosensitive transduction channel of vertebrate hair cells. *Nature*, **432**, pp.723-30.

Coste, B., Mathur, J., Schmidt, M., Earley, TJ., Ranade, S., Petrus, MJ., Dubin, AE. & Patapoutian, A., 2010. Piezo1 and Piezo2 are essential components of distinct mechanically activated cation channels. *Science*, **330**, pp.55-60.

Coste, B., Xiao, B., Santos, JS., Syeda, R., Grandl, J., Spencer, KS., Kim, SE., Schmidt, M., Mathur, J., Dubin, AE., Montal, M. & Patapoutian, A., 2012. Piezo proteins are pore-forming subunits of mechanically activated channels. *Nature*, **483**, pp.176-83.

Damann, N., Voets, T. & Nilius, B., 2008. TRPs in our senses. *Curr. Biol.*, **18**, pp.R880-9.

De, R., Zemel, A. & Safran, SA., 2010. Theoretical concepts and models of cellular mechanosensing. *Methods Cell Biol.*, **98**, pp.143-75.

Delmas, P., Hao, J. & Rodat-Despoix, L., 2011.Molecular mechanisms of mechanotransduction in mammalian sensory neurons. *Nat. Rev. Neurosci.*, **140** (12), pp.139-53.

Del Valle, ME., Cobo, T., Cobo, JL. & Vega, JA., 2012. Mechanosensory neurons, cutaneous mechanoreceptors, and putative mechanoproteins. *Microsc. Res. Tech.*, **75**(8), pp.1033-43.

Dietzl, G., Chen, D., Schnorrer, F., Su, K-C., Barinova, Y., Fellner, M., Gasser, B., Kinsey, K., Oppel, S., Scheiblauer, S., Couto, A., Marra, V., Keleman, K. & Dickson, BJ., 2007 A genome-wide transgenic RNAi library for conditional gene inactivation in *Drosophila*. *Nature*, **488**, pp.151-7.

Driscoll, M. & Chalfie, M., 1991. The *mec-4* gene is a member of a family of *Caenorhabditis elegans* genes that can mutate to induce neuronal degeneration. *Nature*, **349**, pp.588-93.

Drummond, HA., Grifoni, SC. & Jernigan, NL., 2008. A new trick for an old dogma: ENaC proteins as mechanotransducers in vascular smooth muscle. *Physiol.*, **23**, pp.23-31.

Drummond, HA., Welsh, MJ. & Abboud, FM., 2001. ENaC subunits are molecular

components of the arterial baroreceptor complex. *Ann. N. Y. Acad. Sci.*, **940**, pp.42-7.

Eberl, DF., Hardy, RW. & Kernan, MJ., 2000. Genetically similar transduction mechanisms for touch and hearing in *Drosophila*. *J. Neurosci.*, **20**(16), pp.5981-88.

Edwards, C., Ottoson, D., Rydqvist, B & Swerup, C., 1981. The permeability of the transducer membrane of the crayfish stretch receptor to calcium and other divalent cations. *Neurosci.*, **8**(7), pp.1455-60.

Farris, HE., LeBlanc, CL., Goswami, J. & Ricci AJ., 2004. Probing the pore of the auditory hair cell mechanotransducer channel in turtle. *J. Physiol.*, **558**(3), pp.769-92.

Faucherre, A., Nargeot, J., Mangoni, ME. & Jopling. C., 2013. *piezo2b* regulates vertebrate light touch response. *J. Neurosci.*, **33**(43), pp.17089-94

Feng, Y., Ueda, A. & Wu, CF., 2004. A modified minimal hemolymph-like solution, HL3.1, for physiological recordings at the neuromuscular junction of normal and mutant *Drosophila* larvae. *J. Neurogenetics*, **18**, pp.377-402.

Fettiplace, R. & Fuchs, PA., 1999. Mechanisms of hair cell tuning. *Annu. Rev. Physiol.*, **61**, pp.809-34.

Finlayson, LH. & Lowenstein, O., 1958. The structure and function of abdominal stretch receptors in insects. *Proc. R Soc Lond. B Biol. Sci.*, **148**(933), pp.433-49.

Fitz-Ritson, D., 1982. The anatomy and physiology of the muscle spindle, and its role in posture and movement: a review. *J. Can. Chiropr. Assoc.*, **26**(4), pp.144-50.

Franco Jr., A. & Lansman, JB., 1990. Calcium entry through stretch-inactivated ion channels in *mdx* myotubes. *Nature,* **334**, pp.670-3.

Furness, DM., Hackney, CM. & Evans, MG., 2010. Localisation of the mechanotransducer channels in mammalian cochlear hair cells provides clues to their gating. *J. Physiol.*, **588**(Pt 5), pp.765-72.

García-Añoveros, J., Samad, TA., Žuvela-Jelaska, L., Woolf, CJ. & Corey, DP., 2001. Transport and localization of the DEG/ENaC ion channel BNaC1a to peripheral mechanosensory terminals of dorsal root ganglia neurons. *J. Neurosci.*, **21**(8), pp.2678-86.

Gautam, M., Gojova, A. & Barakat, AI., 2006. Flow-activated ion channels in vascular endothelium. *Cell Biochem. Biophys.*, **46**(3), pp.277-84.

Girardi-Schappo, M., Tragtenberg, MHR. & Kinouchi, O., 2013. A brief history of excitable map-based neurons and neural networks. *J. Neurosci. Meth.*, **220**(2), pp.116-30.

Goodman, MB., Ernstrom, GG., Chelur, DS., O'Hagan, R., Yao, CA. & Chalfie, M., 2002. MEC-2 regulates *C. elegans* DEG/ENaC channels needed for mechanosensation. *Nature*, **415**, pp.1039-43.

Goodman, MB., Lumpkin, EA., Ricci, A., Tracey, WD., Kernan, M. & Nicolson, T., 2004. Molecules and mechanisms of mechanotransduction. *J. Neurosci.*, **24**(42), pp.9220-2.

Goodman, MB. & Schwarz, EM., 2003. Transducing touch in *Caenorhabditis elegans*. *Ann. Rev. Physiol.*, **65**, pp.429-52.

Goulding, SE., zur Lage, P. & Jarman, AP., 2000. *amos*, a proneural gene for *Drosophila* olfactory sense organs that is regulated by *lozenge*. *Neuron*, **25**, pp.69-78.

Graveley, BR., Brooks, AN., Carlson, JW., Duff, MO., Landolin, JM., Yang, L., Artieri, CG., van Baren, MJ., Boley, N., Booth, BW., Brown, JB., Cherbas, L., Davis, CA., Dobin, A., Li, R., Lin, W., Malone, JH., Mattiuzzo, NR., Miller, D., Sturgill, D., Tuch, BB., Zaleski, C., Zhang, D., Blanchette, M., Dudoit, S., Eads, B., Green, RE., Hammonds, A., Jiang, L., Kapranov, P., Langton, L., Perrimon, N., Sandler, JE., Wan, KH., Willingham, A., Zhang, Y., Zou, Y., Andrews, J., Bickel, PJ., Brenner, SE., Brent, MR., Cherbas, P., Gingeras, TR., Hoskins, RA., Kaufman, TC., Oliver, B. & Celniker, SE., 2011. The developmental transcriptome of *Drosophila melanogaster*. *Nature*, **471**, pp.473-9.

Hamada, FN., Rosenzweig, M., Kang, K., Pulver, SR., Ghezzi, A., Jegla, TJ. & Garrity, PA., 2008. An internal thermal sensor controlling temperature preference in *Drosophila*. *Nature*, **454**(10), pp.217-22.

Hamill, OP., 2006. Twenty odd years of stretch-sensitive channels. *Pflugers Arch. - Eur. J. Physiol.*, **453**, pp.333-51.

Hamill, OP. & Martinac, B., 2001. Molecular basis of mechanotransduction in living cells. *Physiol. Rev.*, **81**(2), pp.685-740.

Hamill, OP. & McBride, DW., Jr., 1995. Mechanoreceptive membrane ion channels. *Am. Sci.*, **83**, pp. 30–7.

Hammami, S., Willumsen, NJ., Olsen, HL., Morera, FJ., Latorre, R. & Klaerke, DA., 2009. Cell volume and membrane stretch independently control K+ channel activity. *J. Physiol.*, **587**(10), pp.2225-31.

Hartenstein, V., 1993. *The Atlas of Drosophila Development*. Cold Spring Harbor Laboratory Press.

Hicks, GA. & Marrion, NV., 1998. Ca^{2+}-dependent inactivation of large conductance Ca^{2+}-activated K^+ (BK) channels in rat hippocampal neurones produced by pore block from an associated particle. *J. Physiol.*, **508**(3), pp.721-34.

Hoffman, BD. & Crocker, JC., 2009. Cell mechanics: dissecting the physical responses of cells to force. *Annu. Rev. Biomed. Eng.*, **11**, pp.259-88.

Hughes, CL. & Thomas, JB., 2007. A sensory feedback circuit coordinates muscle activity in

Drosophila. *Mol. Cell. Neurosci.*, **35**, pp.383-96.

Hullinger, M., Matthews, PBC. & Noth, J., 1977. Static and dynamic fusimotor action on the response of Ia fibres to low frequency sinusoidal stretching of wide ranging amplitude. *J. Physiol. Lond.*, **267**, pp.811-38.

Hunt, CC., 1990. Mammalian muscle spindle: peripheral mechanisms. *Physiol. Rev.*, **70**(3), pp.643-63.

Hunt, CC. & Wilkinson, RS., 1980. An analysis of receptor potential and tension of isolated cat muscle spindles in response to sinusoidal stretch. *J. Physiol. Lond.*, **302**, pp.241-62.

Hunt, CC., Wilkinson, RS. & Fukami, Y., 1978. Ionic basis of the receptor potential in primary endings of mammalian muscle spindles. *J. Gen. Physiol.*, **71**, pp.683–98.

Ishiko, N. & Loewenstein, WR., 1959. Electrical output of a receptor membrane. *Science*, **130**, pp.1405-6.

Iyer, N., 2010. *Fly Light Project: Immunohistochemistry protocol for GAL 4 and Lex A Lines*. [Protocol] November 29th, 2010. Ashburn, VA: HHMI Janelia Farm Research Campus.

Jan, LY. & Jan, YN., 1976. Properties of the larval neuromuscular junction in *Drosophila melanogaster*. *J. Physiol.*, **262**(1), pp.189-214.

Jepson, JEC., Shahidullah, M., Lamaze, A., Peterson, D., Pan, H. & Koh, K., 2012. *dyschronic*, a *Drosophila h*omolog of a deaf-blindness gene, regulates circadian output and Slowpoke channels. *PLoS. Genetics*, **8**(4), pp.e1002671.

Jinushi-Nakao, S., Arvind, R., Amikura, R., Kinameri, E., Liu, AW. & Moore, AW., 2007. Knot/Collier and Cut control different aspects of dendrite cytoskeleton and synergize to define final arbor shape. *Neuron*, **56**, pp.963-78.

Josipovic, Z., 2014. Neural correlates of nondual awareness in meditation. *Ann. NY. Acad. Sci.*, **1307**, pp.9-18.

Kaila, K., Rydqvist, B., Pasternack, M. & Voipio, J., 1992. Inward current caused by sodium-dependent uptake of GABA in the crayfish stretch receptor neurone. *J. Physiol.*, **453**, pp.627-45.

Kaila, K., Rydqvist, B., Swerup, C. & Voipio, J., 1987. Stimulation-induced changes in the intracellular sodium activity of the crayfish stretch receptor. *Neurosci. Letters*, **74**, pp.53-7.

Kaplan, R., 2014. BN102: Principles of Neurobiology - Ion Channel Function [Online] (Updated 28th Jan. 2014) Available at: https://wiki.brown.edu/confluence/display/Spring07BN0102S01/Ion+Channel+Function [Accessed 3rd Mar. 2014].

Katz, B., 1949. The efferent regulation of the muscle spindle in the frog. *J. Exp. Biol.*, **26**, pp.201-17.

Kellenberger, S. & Schild, L., 2002. Epithelial sodium channel/degenerin family of ion channels: a variety of functions for a shared structure. *Physiol. Rev.*, **82**, pp.735-67.

Kepecs, A. & Fishell, G., 2014. Interneuron cell types are fit to function. *Nature*, **505**, pp.318-26.

Kernan, MJ., 2007. Mechanotransduction and auditory transduction in *Drosophila*. *Pflugers Arch. - Eur. J. Physiol.*, **454**, pp.703-20.

Kim, SE., Coste, B., Chadha, A., Cook, B. & Patapoutian, A., 2012. The role of *Drosophila* Piezo in mechanical nociception. *Nature*, **483**, pp.209-13.

Kloda, A. & Martinac, B. 2001. Mechanosensitive channel of *Thermoplasma*, the cell wall-less Archaea: cloning and molecular characterization. *Cell Biochem. Biophys.*, **34**(3), pp.321-47.

Kung, C., 2005. A possible unifying principle for mechanosensation. *Nature*, **436**, pp.647-54.

Lennartson, B., 1980. Number and distribution of muscle spindles in the masticatory muscles of the rat. *J. Anat.*, **130**(2), pp.279-88.

Levina, N., Tötemeyer, S., Stokes, NR., Louis, P., Jones, MA. & Booth, IR., 1999. Protection of *Escherichia coli* cells against extreme turgor by activation of MscS and MscL mechanosensitive channels: identification of genes required for MscS activity. *EMBO J.*, **18**, pp.1730-7.

Levine, RB., 1984. Changes in neuronal circuits during insect metamorphosis. *J. Exp. Biol.*, **112**, pp.27-44.

Li, C., Edwards, MD., Jeong, H., Roth, J. & Booth, IR., 2007. Identification of mutations that alter the gating of the *Escherichia coli* mechanosensitive channel protein, MscK. *Mol. Microbiol.*, **64**(2), pp.560–74.

Libby, JL., 1961. The nervous system of certain abdominal segments and the innervation of the male reproductive system and genitalia of *Hyalophora cecropia* (*Lepidoptera*: *Saturnidae*). *Ann. Entomol. Sot. Am.*, **54**, pp.887-96.

Liu, L., Johnson, WA. & Welsh, MJ., 2003. *Drosophila* DEG/ENaC pickpocket genes are expressed in the tracheal system, where they may be involved in liquid clearance. *PNAS.*, **100**(4), pp.2128-33.

Loewenstein, WR., 1958. Generator processes of repetitive activity in a Pacinian corpuscle. *J. Gen. Physiol.*, **41**(4), pp.825-45.

Loewenstein, WR., 1958. Facilitation by previous activity in a Pacinian corpuscle. *J. Gen.*

Physiol., **41**(4), pp.847-56.

Lumpkin, EA., Marshall, KL. & Nelson, AM., 2010. The cell biology of touch. *J. Cell Biol.*, **191**(2), pp.237-48.

Maingret, F., Fosset, M., Lesage, F., Lazdunski, M. & Honore, E., 1999. TRAAK is a mammalian neuronal mechano-gated K^+ channel. *J. Biol. Chem.*, **274**(3), pp.1381-7.

Marcotti, W., 2012. Functional assembly of mammalian cochlear hair cells. *Exp. Physiol.*, **97**(4), pp.438-51.

Matthews, BHC., 1931. The response of a single end organ. *J. Physiol.*, **71**, pp.64-110.

Matthews, BHC., 1931. The response of a muscle spindle during active contraction of a muscle. *J. Physiol.*, **72**(2), pp.153-74.

Matthews, PBC., 1964. Muscle spindles and their motor control. *Physiol. Rev.*, **44**, pp.219-88.

McCarter, GC., Reichling, DB. & Levine, JD., 1999. Mechanical transduction by rat dorsal root ganglion neurons *in vitro*. *Neurosci. Lett.*, **273**(3), pp.179-82.

Members of the Sicilian Gambit, 2001. New approaches to antiarrhythmic therapy: emerging therapeutic applications of the cell biology of cardiac arrhythmias. *Cardiovasc. Res.*, **52**, pp.345-60.

Mendelson, M. & Loewenstein, WR., 1964. Mechanisms of receptor adaptation. *Science*, **144**(3618), pp.554-5.

Montell, C., 2001. Physiology, phylogeny, and functions of the TRP superfamily of cation channels. *Sci. STKE.*, **90**, re1.

Montell, C., 2005. *Drosophila* TRP channels. *Pflugers Arch. - Eur. J. Physiol.*, **451**, pp.19-28.

Moore, GP., Perkel, DH. & Segundo, JP., 1966. Statistical analysis and functional interpretation of neuronal spike data. *Ann. Rev. Physiol.*, **28**, pp.493-522.

Nair, A., Bate, M. & Pulver, SR., 2010. Characterization of voltage-gated ionic currents in a peripheral sensory neuron in larval *Drosophila*. *BMC Res. Notes*, **3**, pp.154-61.

Niebur, E., 2008. Electrical properties of cell membranes. *Scholarpedia*, **3**(6), pp.7166.

Ottoson, D. & Swerup, C., 1982. Studies on the role of calcium in adaptation of the crustacean stretch receptor. Effects of intracellular injection of calcium, EGTA and TEA. *Brain Res.*, **244**, pp.337-41.

Ottoson, D. & Swerup, C., 1985. Ionic dependence of early adaptation in the crustacean stretch receptor. *Brain Res.*, **336**, pp.1–8.

Ottoson, D. & Swerup, C., 1985. Effects of intracellular TEA injection on early adaptation of

crustacean stretch receptor. *Brain Res.*, **336**, pp.9–17.

Passmore, GM., Reilly, JM., Thakur, M., Keasberry, VN., Marsh, SJ., Dickenson, AH. & Brown, DA., 2012. Functional significance of M-type potassium channels in nociceptive cutaneous sensory endings. *Frontiers Mol. Neurosci.*, **5**(63), pp.1-12.

Patel, AJ., Lazdunski, M. & Honore, E., 2001. Lipid and mechano-gated 2P domain K^+ channels. *Curr. Opin. Cell Biol.*, **13**(4), pp.422-8.

Phillips, JK. & Arnolda, LF., 2002. BK channels, baroreflex sensitivity and genetic markers. *J. Hypertension*, **20**, pp.825–7.

Phillips, KR., Biswas, A. & Cyr, JL., 2008. How hair cells hear: the molecular basis of hair-cell mechanotransduction. *Curr. Opin. Otolaryngol. Head Neck Surg.*, **16**, pp.445-51.

Prescott, SA., Ma, Q. & De Koninck, Y., 2014. Normal and abnormal coding of somatosensory stimuli causing pain. *Nat. Neurosci.*, **17**, pp.183-91.

Qi, J., Peters, KW., Liu, C., Wang, JM., Edinger, RS., Johnson, JP., Watkins, SC. & Frizzell, RA., 1999. Regulation of the amiloride-sensitive epithelial sodium channel by syntaxin 1A. *J. Biol. Chem.*, **274**, pp. 30345–8.

Rydqvist, B., Lin, J-H., Sand, P. & Swerup, C., 2007. Mechanotransduction and the crayfish stretch receptor. *Physiol. Behav.*, **92**, pp.21–8.

Rydqvist, B. & Purali, N., 1993. Transducer properties of the rapidly adapting stretch receptor neurone in the crayfish (*Pacifastacus leniusculus*). *J. Physiol. Lond.*, **469**, pp.193-211.

Rydqvist, B. & Swerup, C., 1991. Stimulus-response properties of the slowly adapting stretch receptor neuron of the crayfish. *Acta Physiol. Scand.*, **143**, pp.11-9.

Rydqvist, B., Swerup, C. & Lännergren, J., 1990. Viscoelastic properties of the slowly adapting stretch receptor muscle of the crayfish. *Acta Physiol. Scand.*, **139**, pp.519-527.

Rydqvist, B. & Zhou, JY., 1989. Potential-dependent potassium currents in the slowly adapting stretch receptor neuron of the crayfish. *Acta Physiol. Scand.*, **137**(3), pp.409-19.

Sackin, H., 1995. Stretch-activated ion channels. *Kidney Int.*, **48**(4), pp1134-47.

Sambrook, J. & Russell, DW., 2001. *Moleuclar Cloning, a laboratory manual*. 3rd ed. New York: Cold Spring Harbor Laboratory Press.

Schrader, S. & Merritt, DJ., 2007. Dorsal longitudinal stretch receptor of *Drosophila melanogaster* larvae - fine structure and maturation. *Arthropod Struct. Dev.*, **36**, pp.157-69.

Shen, WL., Kwon, Y., Adegbola, AA., Luo, J., Chess, A. & Montell, C., 2011. Function of rhodopsin in temperature discrimination in *Drosophila*. *Science*, **331**, pp.1333-6.

Simon, A., Shenton, F., Hunter, I., Banks, RW. & Bewick, GS., 2010. Amiloride-sensitive

channels are a major contributor to mechanotransduction in mammalian muscle spindles. *J. Physiol.*, **588**(1), pp.171-85.

Simon, MA & Trimmer, BA, 2009. Movement encoding by a stretch receptor in the soft-bodied caterpillar, *Manduca sexta*. *J. Exp. Biol.*, **212**, pp.1021-31.

Staruschenko, A., Jeske, NA. & Akopian, AN., 2010. Contribution of TRPV1-TRPA1 interaction to the single channel properties of the TRPA1 channel. *J. Biol. Chem.*, **285**(20), pp.15167-77.

Stewart, BA., Atwood, HL., Renger, JJ., Wang, J. & Wu, CE., 1994. Improved stability of *Drosophila* larval neuromuscular preparations in haemolymph-like physiological solutions. *J. Comp. Physiol. A*, **175**, pp.179-91.

Suslak, TJ., 2011. *A mathematical model of electrical transduction events in crayfish stretch receptors.* MSc. University of Edinburgh.

Suslak, TJ., Armstrong, JD. & Jarman, AP., 2011. A general mathematical model of transduction events in mechano-sensory stretch receptors. *Network*, **22**(1-4), pp.133-42.

Suslak, TJ., Watson, S., Thompson, KJ, Bewick, GS., Armstrong, JD & Jarman, AP., 2014. Amiloride-sensitive *Piezo* is essential for stretch-activated mechanotransduction in larval *Drosophila dbd* neurons. xxxxxxx., **xxxx**, pp.xxxxxx.

Suster, ML. & Bate, M., 2002. Embryonic assembly of a central pattern generator without sensory input. *Nature*, **416**, pp.174-8.

Swerup, C. & Rydqvist, B., 1996. A mathematical model of the crustacean stretch receptor neuron. Biomechanics of the receptor muscle, mechanosensitive ion channels, and macrotransducer properties. *J. Neurophysiol.*, **76**(4), pp.2211-20.

Tamarkin, DA. & Levine, RB., 1996. Synaptic interactions between a muscle-associated proprioceptor and body wall muscle motor neurons in larval and adult *Manduca sexta*. *J. Neurophysiol.*, **76**(3), pp.1597-610.

Tautz, D. & Pfeifle, C., 1989. A non-radioactive in situ hybridization method for the localization of specific RNAs in *Drosophila* embryos reveals translational control of the segmentation gene *hunchback*. *Chromosoma*, **98**, pp.81-5.

Thistle, R., Cameron, P., Ghorayshi, A., Dennison, L., & Scott, K., 2012. Contact chemoreceptors mediate male-male repulsion and male-female attraction during *Drosophila* courtship. *Cell*, **149**, pp.1140-51.

Tobin, DM. & Bargmann, CI., 2004. Invertebrate nociception: behaviors, neurons and molecules. *J. Neurobiol.*, **61**(1), pp.161-74.

Vergara, C., Latorre, R., Marrion, NV. & Adelman, JP., 1998. Calcium-activatedpotassium

channels. *Curr. Opin. Neurobiol.*, **8**, pp321-9.

Waldmann, R., Champigny, G., Bassilana, F., Voilley, N. & Lazdunski, M., 1995. Molecular cloning and functional expression of a novel amiloride-sensitive Na^+ channel. *J. Biol. Chem.*, **270**(46), pp.27411-4.

Walker, RG., Willingham, AT. & Zuker, CS., 2000. A *Drosophila* mechanosensory transduction channel. *Science*, **287**, pp.2229-34.

Weddell, G. & Miller, S., 1962. Cutaneous sensibility. *Annu. Rev. Physiol.*, **24**, pp.199-222.

White, JG., Southgate, E., Thomson, JN. & Brenner, S., 1986. The structure of the nervous system of the nematode *C. elegans*. *Philos. Trans. R. Soc. London Ser. B*, **314**, pp.1–340.

Woo, SH., Ranade, S., Weyer, AD., Dubin, AE., Baba, Y., Qiu, Z., Petrus, M., Miyamoto, T., Reddy, K., Lumpkin, EA., Stucky, CL. & Patapoutian, A., 2014. Piezo2 is required for Merkel-cell mechanotransduction. *Nature*, **509**, pp.622-6.

Zelle, KM., Lu, B., Pyfrom, SC. & Ben-Shahar, Y., 2013. The genetic architecture of degenerin/epithelial sodium channels in *Drosophila*. *G3.*, **3**, pp.441-50.

Zhou, Y., Schopperle, WM., Murrey, H., Jaramillo, A., Dagan, D., Griffith, LC. & Levitan, IB., 1999. A dynamically regulated 14-3-3, Slob, and Slowpoke potassium channel complex in *Drosophila* presynaptic nerve terminals. *Neuron*, **22**, pp.809-18.

Appendix i. - Script of full receptor potential model

Ths following script details the code to generate the receptor potential traces produced by the final model in Ch. 2.

```
function output = crayfishsim()

    k1=400; % spring constant for linear spring
    k2=2200; %   "        "    "   nonlinear spring
    n=1.5; % power constant    "       "       "
    B=12; % Dashpot constant
    kb=106; % linear Boltzmann constant
%     kb2=18.9; % square   "         "
    s=0.00277; % linear sensitivity constant
%     s2=0.995*10^-6; % square  "
    q=1; % power constant (q=1 or 2)
    m=25; % tension conversion factor, between 20 and 30
    k0=12; % MSC adaptation constant
    tau0=100; % MSC adaptation time constant
    Ismax=-200; % saturated MSC current at large extension
    Esrev=15; % MSC reversal potential
    Cm=4.3; % membrane capacitance
    gleak=0.56; % leak conductance
    Erest=-65; % resting membrane potential between -55 and
    -70
    Eleak=Erest; % leak current reversal potential
    e0=0; % initial extension
    a=0.08:0.001:0.08; % rate of extension.
    b=-0.08:-0.001:-0.08; % rate of relaxation.
    g=Ismax/(Erest-Esrev); % conductance
    NaAct=-50; % VNaC activation potential
    kNa=6; % VNaC activation constant
    Narev=50; % VNaC reversal potential
    tauNa=10; % VNaC time constant
    Naleak=0.000008; % VNaC leak conductance
    Kleak=0.002; % K channel leak conductance
    Kact=5; % K channel activation potential
    kK=5; % K channel activation constant
    Krev=-100; % K channel reversal potential
    tauK=10; % K channel time constant
    kMSK0=12;
    kMSK=120;
    tauMSK=100;
    IMSKmax=-200;
    EMSKrev=-100;
    gMSK=IMSKmax./(Erest-EMSKrev);
    gKleak=0.7;


%       set initial conditions for stretch protocol

    temp=100;
    temp2=0;
    e=e0+a;

%       initiate dynamic stretch phase
```

```
    for i=0:100

        e=e+a;
        k=(e-e0).*B*k1+k2.*(e-e0).^n;
        sigm=k.*(e-e0);
        sig=sigm./m;
        sig0=k0*(1-exp(-i/tau0));
        P0=1./(1+kb.*exp(-s.*(sig-sig0).^q));
        Is=P0.*g*(Erest-Esrev);

%         var1=-10;
%         var2=10;
%         noise=var1+(var2-var1)*rand(1);
%         Isnoise=Is+noise;

        Emem=Erest-(((1+kb.*exp(-s.*(sig-sig0).^q)).^-
        1).*Is+gleak*(Erest-Esrev))./Cm;

%       conditional statements encode voltage-gated channels

        if Emem>-50

            if temp2==0
                temp=i;
                temp2=1;
            end

            sigNa=1-exp(-i/tauNa);
            PV=1./(1+exp(((Emem-NaAct).*sigNa)./kNa));
            gNa=(PV.*(Narev-Emem)+Naleak.*(Eleak-
            Emem))./Cm.*Emem);
            sigK=1-exp(-i./tauK);
            PK=1./(1+exp(((Emem-Kact).*sigK)./kK));
            gK=(PK.*(Krev-Emem)+Kleak.*(Eleak-
            Emem))./Cm.*Emem);
            g=Ismax./(Erest-Esrev)+gNa+gK;

        end

        if i>=(temp+tauNa)

            g=Ismax./(Erest-Esrev)+gK;

        end


        if i>(temp+tauK)

           g=Ismax./(Erest-Esrev);
```

```
        end
%
% %       A stretch-activated potassium channel activates
          here, when the tension is sufficient.
%
%         if sigm>66000
%
%             gK2=-1;
%             g=Ismax./(Erest-Esrev)+gK2;
%
%         end

        result(i+1,1,:) = e;
        result(i+1,2,:) = k;
        result(i+1,3,:) = sigm;
        result(i+1,4,:) = P0;
        result(i+1,5,:) = Is;
        result(i+1,6,:) = Emem;

    end

%       hold phase

    for i=101:200

        k=((e-e0).*B*k1+k2.*(e-e0).^n)-(k1.*(e-e0).^n);
        sigm=k.*(e-e0);
        sig=sigm./m;
        sig0=k0*(1-exp(-i/tau0));
        P0=1./(1+kb.*exp(-s.*(sig-sig0).^q));
        Is=P0.*g*(Erest-Esrev);

%         var1=-10;
%         var2=10;
%         noise=var1+(var2-var1)*rand(1);
%         Isnoise=Is+noise;

        Emem=Erest-(((1+kb.*exp(-s.*(sig-sig0).^q)).^-
        1).*Is+gleak.*(Erest-Esrev))./Cm;

        if Emem>-50

            if temp2==0
                temp=i;
                temp2=1;
            end

            sigNa=1-exp(-i./tauNa);
            PV=1./(1+exp(((Emem-NaAct).*sigNa)./kNa));
            gNa=(PV.*(Narev-Emem)+Naleak.*(Eleak-
            Emem))./Cm.*Emem);
```

```
            sigK=1-exp(-i./tauK);
            PK=1./(1+exp(((Emem-Kact).*sigK)./kK));
            gK=(PK.*(Krev-Emem)+Kleak.*(Eleak-
            Emem))./Cm.*Emem);
            g=Ismax./(Erest-Esrev)+gNa+gK;

        end

        if i>=(temp+tauNa)

            g=Ismax./(Erest-Esrev)+gK;

        end


        if i>(temp+tauK)

           g=Ismax./(Erest-Esrev);

        end


%         if sigm>66000
%
%             gK2=-1;
%             g=Ismax./(Erest-Esrev)+gK2;
%
%         else sigm<50000;
%
%                 sigMSK=kMSK0.*(1-exp(-i./tauMSK));
%                 PMSK=1./(1+kMSK*exp(-s.*(sig-sigMSK).^q));
%                 IMSK=PMSK.*gMSK.*(Erest-Esrev);
%
%
%                 Emem=Erest+(((1+kb.*exp(-s.*(sig-
                  sig0).^q)).^-1).*Is+gleak.*(Erest-Esrev))+
                  (((1+kMSK.*exp(-s.*(sigMSK-sig0).^q)).^-
                  1).*IMSK+gKleak.*(Erest-EMSKrev))./Cm;
%
%         end

        result(i,1,:) = e;
        result(i,2,:) = k;
        result(i,3,:) = sigm;
        result(i,4,:) = P0;
        result(i,5,:) = Is;
        result(i,6,:) = Emem;

    end

%       release phase
```

```
    for i=201:300

        e=e+b;
        k=((e-e0).*B*k1+k2.*(e-e0).^n)-(k1.*(e-e0).^n);
        sigm=k.*(e-e0);
        sig=sigm./m;
        sig0=k0*(1-exp(-i/tau0));
        P0=1./(1+kb*exp(-s.*(sig-sig0).^q));
        Is=P0.*g*(Erest-Esrev);

%         var1=-5;
%         var2=5;
%         noise=var1+(var2-var1)*rand(1);
%         Isnoise=Is+noise;

        Emem=Erest-(((1+kb.*exp(-s.*(sig-sig0).^q)).^-
        1).*Is+gleak.*(Erest-Esrev))./Cm;

        if Emem>-50

            if temp2==0
                temp=i;
                temp2=1;
            end

            sigNa=1-exp(-i./tauNa);
            PV=1./(1+exp(((Emem-NaAct).*sigNa)./kNa));
            gNa=(PV.*(Narev-Emem)+Naleak.*(Eleak-
            Emem))./Cm.*Emem);
            sigK=1-exp(-i./tauK);
            PK=1./(1+exp(((Emem-Kact).*sigK)./kK));
            gK=(PK.*(Krev-Emem)+Kleak.*(Eleak-
            Emem))./Cm.*Emem);
            g=Ismax./(Erest-Esrev)+gNa+gK;

        end

        if i>=(temp+tauNa)

            g=Ismax./(Erest-Esrev)+gK;

        end


        if i>(temp+tauK)

           g=Ismax./(Erest-Esrev);

        end
```

```
%         There needs to be some balance between the two
          following features
%         to account for the release phase hyperpolarisation.
          There is some
%         initial K component and then a secondary K
          component.
%
%         if sigm>66000
%
%             gK2=-1;
%             g=Ismax./(Erest-Esrev)+gK2;
%
        if sigm<50000;

                sigMSK=kMSK0.*(1-exp(-i./tauMSK));
                PMSK=1./(1+kMSK*exp(-s.*(sig-sigMSK).^q));
                IMSK=PMSK.*gMSK.*(Erest-Esrev);


                Emem=Erest+(((1+kb.*exp(-s.*(sig-sig0).^q)).^-
                1).*Is+gleak.*(Erest-Esrev))+(((1+kMSK.*exp(-
                s.*(sigMSK-sig0).^q)).^-
                1).*IMSK+gKleak.*(Erest-EMSKrev))./Cm;

        end

        result(i,1,:) = e;
        result(i,2,:) = k;
        result(i,3,:) = sigm;
        result(i,4,:) = P0;
        result(i,5,:) = Is;
        result(i,6,:) = Emem;

    end


    for K=6:6
        output=result;
        figure;

        for L=1:1

        plot(result(:,K,L))
        hold on

        end

    end

end
```

Appendix i.i. - Model constants

[Swerup & Rydqvist, 1996]

Parameter	Description	Value	Units
Visco-elastic elements			
k_1	linear spring constant	400	kPa
k_2	non-linear spring constant	2200	kPa
n	non-linear spring power constant	1.5	-
B	Dashpot constant	12	kPas
MSCs			
k_b	linear Boltzmann constant	106	-
	non-linear Boltzmann constant	18.9	-
s	linear sensitivity constant	0.00277	Pa^{-1}
	non-linear sensitivity constant	$0.995x10^{-6}$	Pa^{-1}
q	Power constant	1 or 2	-
m	Tension conversion factor	20-30	-
k_0	MSC adaptation constant	12	kPa
τ_0	MSC adaptation time constant	100	ms
I_{smax}	Saturating current for large extension	-200	nA
E_{srev}	MSC reversal potential	$+10^6$	mV
Electrical parameters of the neuron			
C_m	membrane capacitance	4.3	nF
g_{leak}	leak conductance	0.56	μS
E_{rest}	resting membrane potential	-55 to -70	mV
E_{leak}	leak current reversal potential	E_{rest}	mV

Table 1: Constants employed in the original stretch-receptor neuron model [Taken from Swerup & Rydqvist, 1996]

6 Ascribed a new value of +15mV in new version of model given here. New value deemed more physiologically consistent.

Appendix i.ii. - Model constants (voltage-activated components)

Parameter	Description	Value	Units
VNaC properties			
NaE_{rev}	VNaC reversal potential	+70	mV
E_{act}	VNaC activation potential	-50	mV
Nag_{leak}	VNaC leak conductance	8[7]	pS
k_{Na}	VNaC adaptation constant	6	mV^{-1}
τ_{Na}	VNaC time constant	10	ms
VK channel properties			
KE_{rev}	K channel reversal potential	-100	mV
K_{act}	K channel activation potential	+5	mV
Kg_{leak}	K channel leak conductance	2[8]	nS
k_K	K channel adaptation constant	5	mV^{-1}
τ_K	K channel time constant	10	ms

Table 2: Additional constants for voltage-activated components

7 From Berntson & Walmsley, 2008
8 From Conti *et al.*, 1976

Appendix ii. - Raw data for *in situ* hybridisation studies

The following data comprise the results of the *in situ* hybridisation screen for expression of *ppk* genes in *dbd* neurons. These data were summarised in **Table 1**. For each gene, sample images of stained embryos are presented (as per the *in situ* hybridisation protocol, detailed in CH6: Materials and methods), alongside corresponding modENCODE expression data, where available [Graveley *et al.*, 2011]. Additionally, the data for each gene are accompanied by the sequences of the primers used in the corresponding assays, as well as an image of the electrophoresis gel, run to confirm the successful manufacture of each *in situ* probe.

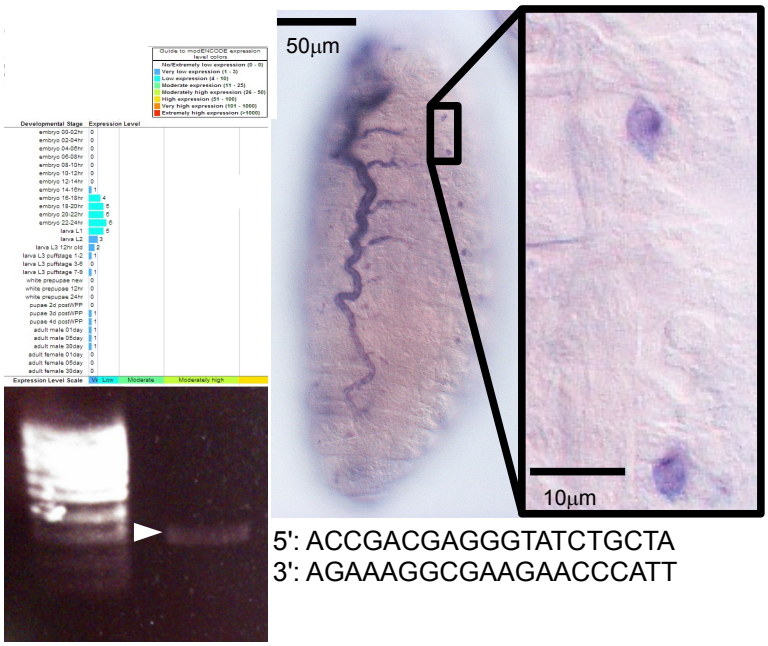

Supplementary Figure 1: *ppk1* expressed in late embryonic dorsal sense organs. Current data for the expression of *ppk1* during embryonic development was retrieved from the modENCODE database (top-left), showing this gene to be expressed in late embryogenesis. An *in situ* RNA probe was generated (bottom-left, sequence: bottom-right), and expression was confirmed in late embryonic trachea (top-centre) and a peripheral sensory neuron (known to be *md* – see Table 1). However, this gene is not expressed in *dbd* neurons.

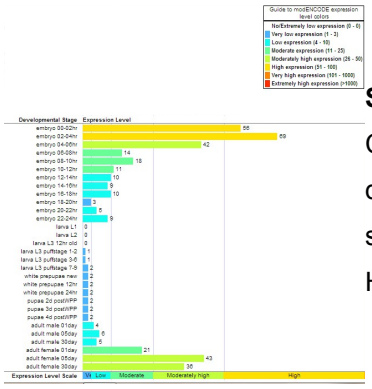

Supplementary Figure 2: *ppk2* expressed in late embryos. Current data for the expression of *ppk2* during embryonic development was retrieved from the modENCODE database, showing this gene to be expressed in late embryogenesis. However, this gene is known not expressed in *dbd* neurons.

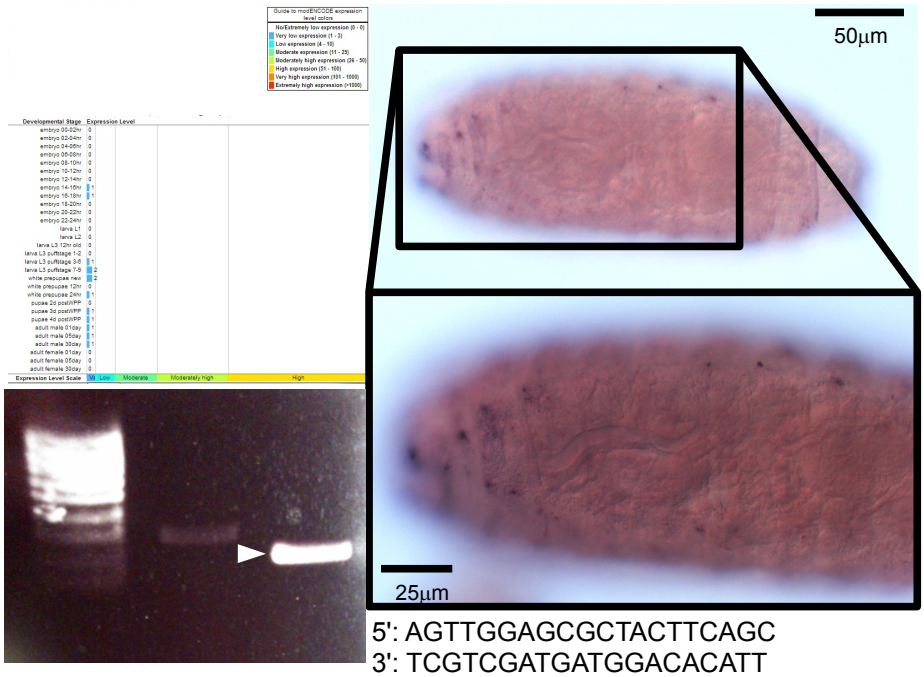

5': AGTTGGAGCGCTACTTCAGC
3': TCGTCGATGATGGACACATT

Supplementary Figure 3: *ppk3* expressed in late embryonic anterior sensory cells. Current data for the expression of *ppk3* during embryonic development was retrieved from the modENCODE database (top-left), showing this gene to be slightly expressed in late embryogenesis. An *in situ* RNA probe was generated (bottom-left, sequence: bottom-right), and low expression was seen in late embryos (top-right), with small pucta apparent in the head (possibly staining anterior sensory cells – see Table 1). However, this gene is not expressed in *dbd* neurons.

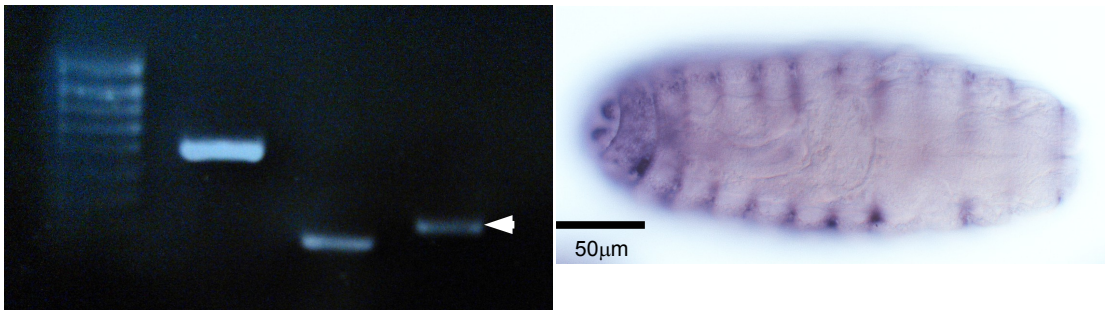

5': CCAAGACGTTTTTCGGTCAT
3': AAAGGCARCRGCTTCTTGG

Supplementary Figure 4: *ppk4* is not expressed in late embryos. An *in situ* RNA probe was generated for *ppk4* (top-left, sequence: bottom-left). However, *in situ* hybridisation for this gene in late embryos was negative (right), thus this gene is not expressed in *dbd* neurons.

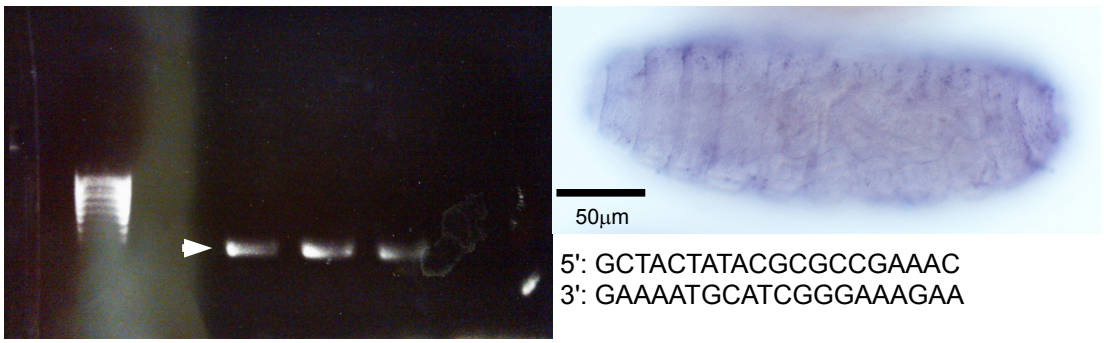

Supplementary Figure 5: *ppk5* is not expressed in late embryos. An *in situ* RNA probe was generated for *ppk5* (top-left, sequence: bottom-left). However, *in situ* hybridisation for this gene in late embryos was negative (right), thus this gene is not expressed in *dbd* neurons.

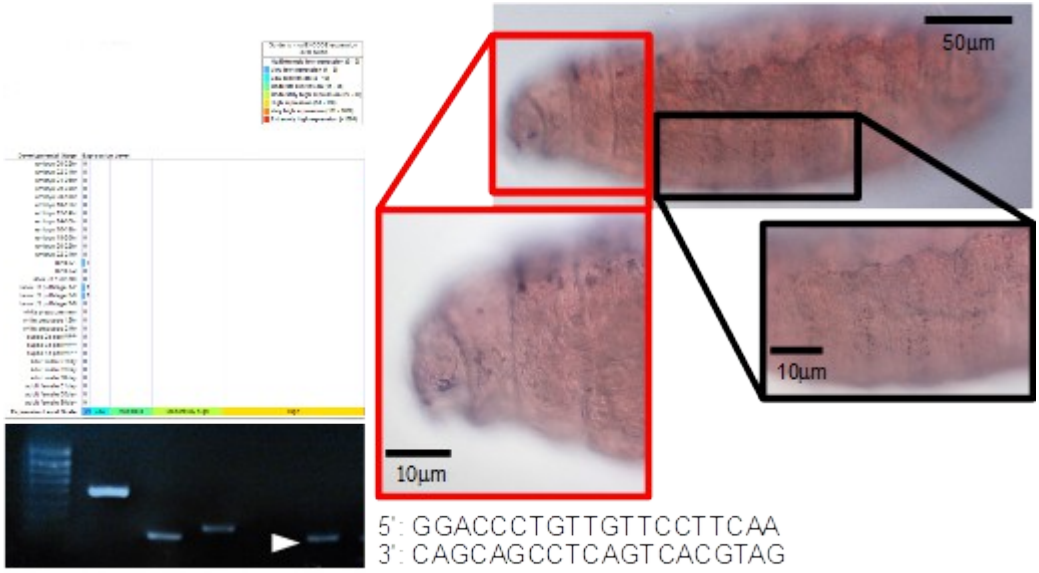

Supplementary Figure 6: *ppk6* expressed in late embryonic anterior sensory cells. Current data for the expression of *ppk6* during embryonic development was retrieved from the modENCODE database (top-left), showing this gene to be slightly expressed in late embryogenesis. An *in situ* RNA probe was generated (bottom-left, sequence: bottom-right), and low expression was seen in late embryos (top-right), with small pucta apparent in the head (inset:red) and abdomen (inset: black), possibly staining anterior sensory cells – see Table 1. However, this gene is not expressed in *dbd* neurons.

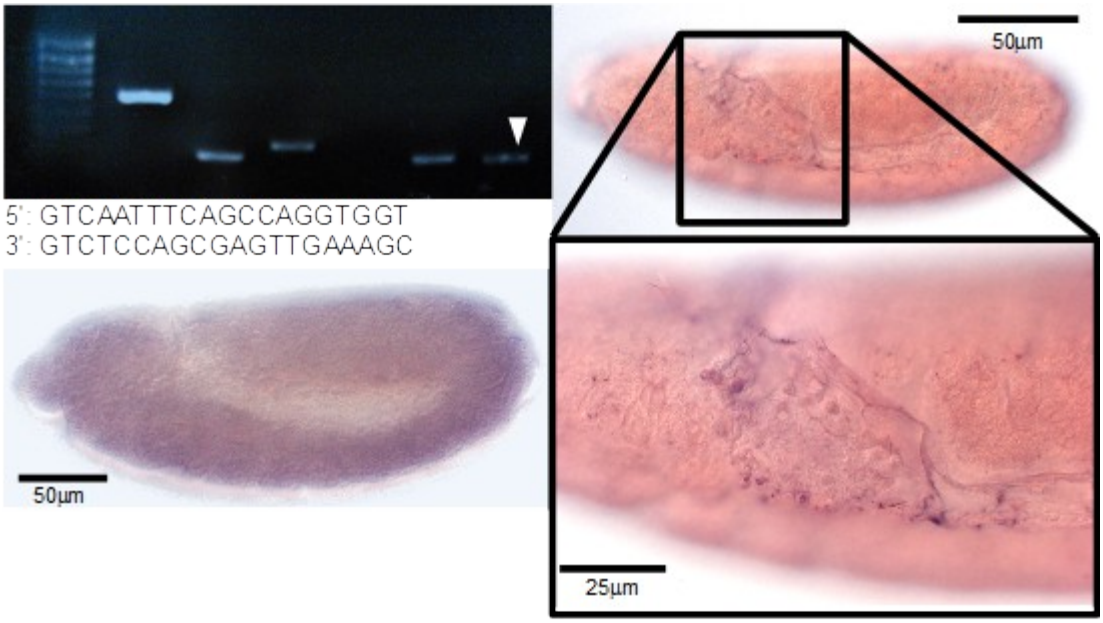

Supplementary Figure 7: *ppk7* expressed in early and late embryos. An *in situ* RNA probe was generated (top-left, sequence: middle-left), and some expression was seen in the late embryonic abdomen (top-right). Whilst the exact areas stained are difficult to characterise (see inset), this gene is clearly not expressed in *dbd* neurons. *ppk7* is also more generally expressed in earlier embryogenesis (bottom-left).

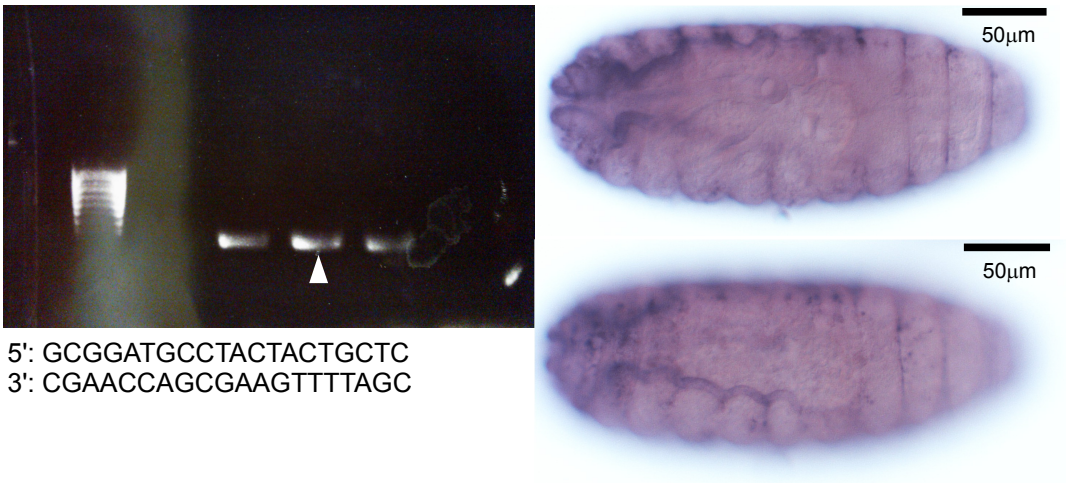

Supplementary Figure 8: *ppk8* expressed in late embryonic trachea. An *in situ* RNA probe was generated (top-left, sequence: bottom-left), and expression was seen in late embryonic trachea (top-right & bottom-right). However, this gene is not expressed in *dbd* neurons.

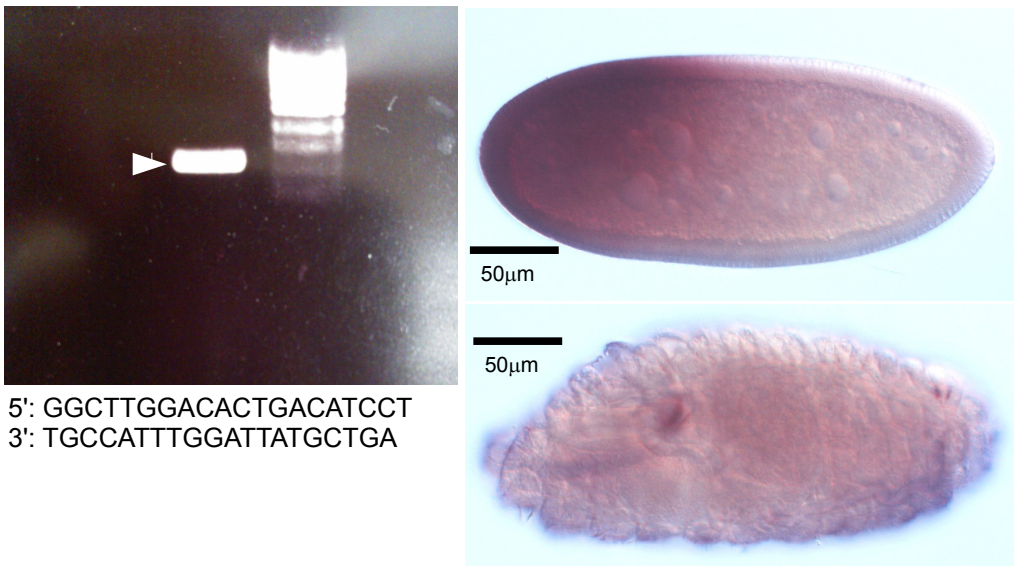

Supplementary Figure 9: *ppk9* not expressed in late embryos. An *in situ* RNA probe was generated (top-left, sequence: bottom-left), and expression was seen in early anterior embryos (top-right). However, expression is completely absent from late-stage embryos and thus, this gene is not expressed in *dbd* neurons.

Supplementary Figure 10: *ppk10* is not expressed in late embryos. Current data for the expression of *ppk10* during embryonic development was retrieved from the modENCODE database (top-left), showing this gene not to be expressed in late embryogenesis. An *in situ* RNA probe was generated (bottom-left, sequence: bottom-right), and non-expression was confirmed in late embryos (top-right). The irregular aggregations of staining (see inset) are likely artefacts, as they are irregularly arranged and inconsisten. Additionally, this gene is not expressed in *dbd* neurons.

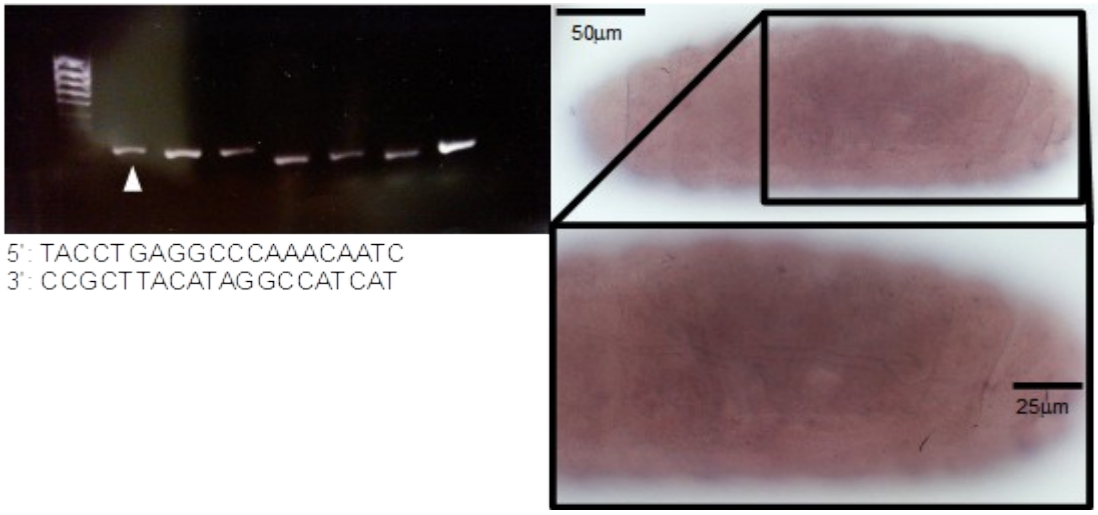

Supplementary Figure 11: *ppk11* expressed in late embryonic dorsal sense organs. An *in situ* RNA probe was generated (bottom-left, sequence: bottom-left), and no expression was observed in late embryos (top-right). The irregular aggregations of staining (see inset) are likely artefacts, as they are irregularly arranged and inconsisten. Additionally, this gene is not expressed in *dbd* neurons.

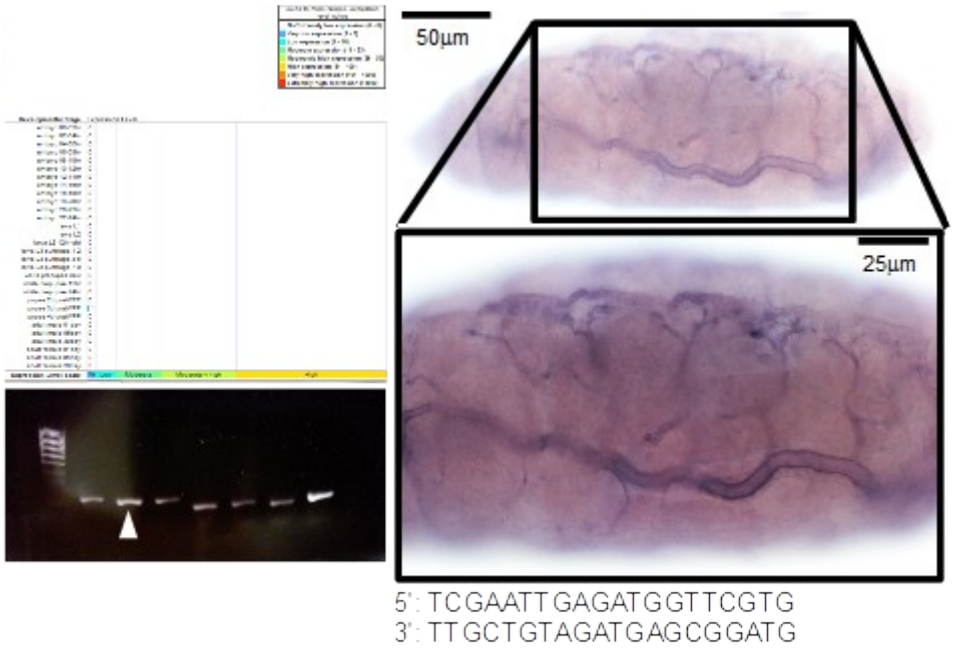

Supplementary Figure 12: *ppk12* expressed in late embryonic trachea. Current data for the expression of *ppk12* during embryonic development was retrieved from the modENCODE database (top-left), showing this gene not to be expressed in late embryogenesis. An *in situ* RNA probe was generated (bottom-left, sequence: bottom-right), and expression was confirmed in late embryonic trachea (top-right). However, this gene is not expressed in *dbd* neurons (see inset).

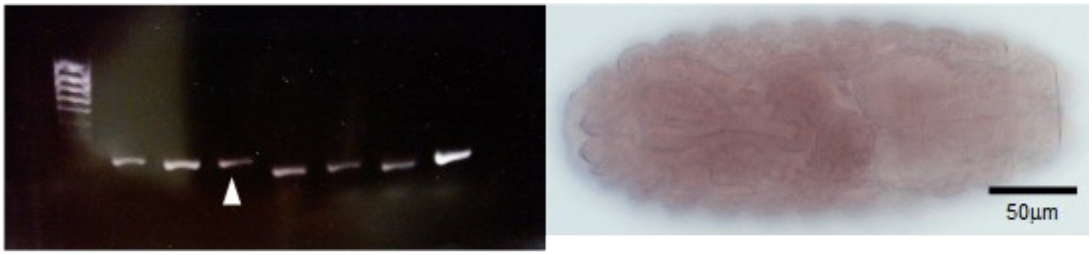

5': AACATGGAGGGTCTGGAGTG
3': TATGAGGCCCACTTCGATTC

Supplementary Figure 13: *ppk13* is not expressed in late embryos. An *in situ* RNA probe was generated for *ppk13* (top-left, sequence: bottom-left). However, *in situ* hybridisation for this gene in late embryos was negative (right), thus this gene is not expressed in *dbd* neurons.

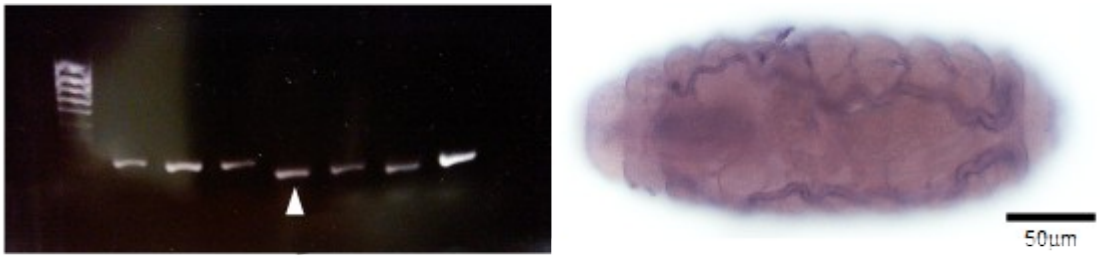

5': CTGTCGGCTAAAGGATCTGC
3': TATCGGTCAGCAGGGTTAGG

Supplementary Figure 14: *ppk14* expressed in late embryonic trachea. An *in situ* RNA probe was generated (top-left, sequence: bottom-left), and expression was seen in late embryonic trachea (right). However, this gene is not expressed in *dbd* neurons.

Supplementary Figure 15: *ppk15* is not expressed in late embryos. Current data for the expression of *ppk15* during embryonic development was retrieved from the modENCODE database (top-left), showing this gene not to be expressed in late embryogenesis. An *in situ* RNA probe was generated (bottom-left, sequence: bottom-right), and non-expression was confirmed in late embryos (top-right). Additionally, this gene is not expressed in *dbd* neurons.

Supplementary Figure 16: *ppk16* may be expressed in late embryonic trachea. An *in situ* RNA probe was generated (top-left, sequence: bottom-left), and faint expression was seen in late embryonic trachea (right). However, this gene is not expressed in *dbd* neurons.

Supplementary Figure 17: *ppk17* expressed in late embryonic trachea. Current data for the expression of *ppk17* during embryonic development was retrieved from the modENCODE database (top-left), showing this gene to be expressed at very low levels in late embryogenesis. An *in situ* RNA probe was generated (bottom-left, sequence: bottom-right), and expression was confirmed in late embryonic trachea (top-right). However, this gene is not expressed in *dbd* neurons.

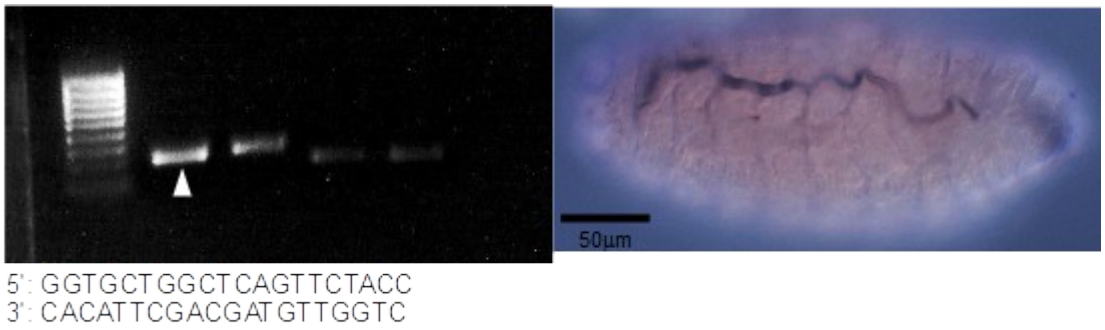

Supplementary Figure 18: *ppk18* is expressed in late embryonic trachea. An *in situ* RNA probe was generated (top-left, sequence: bottom-left), and expression was seen in late embryonic trachea (right). However, this gene is not expressed in *dbd* neurons.

Supplementary Figure 19: *ppk19* expressed in late embryonic trachea. Current data for the expression of *ppk19* during embryonic development was retrieved from the modENCODE database (top-left), showing this gene not to be expressed in late embryogenesis. An *in situ* RNA probe was generated (bottom-left, sequence: bottom-right), and expression was observed in late embryonic trachea (top-right). However, this gene is not expressed in *dbd* neurons.

Supplementary Figure 20: *ppk20* expressed in late embryonic trachea. Current data for the expression of *ppk20* during embryonic development was retrieved from the modENCODE database (top-left), showing this gene not to be expressed in late embryogenesis. An *in situ* RNA probe was generated (bottom-left, sequence: bottom-right), and expression was observed in late embryonic trachea (top-right). However, this gene is not expressed in *dbd* neurons.

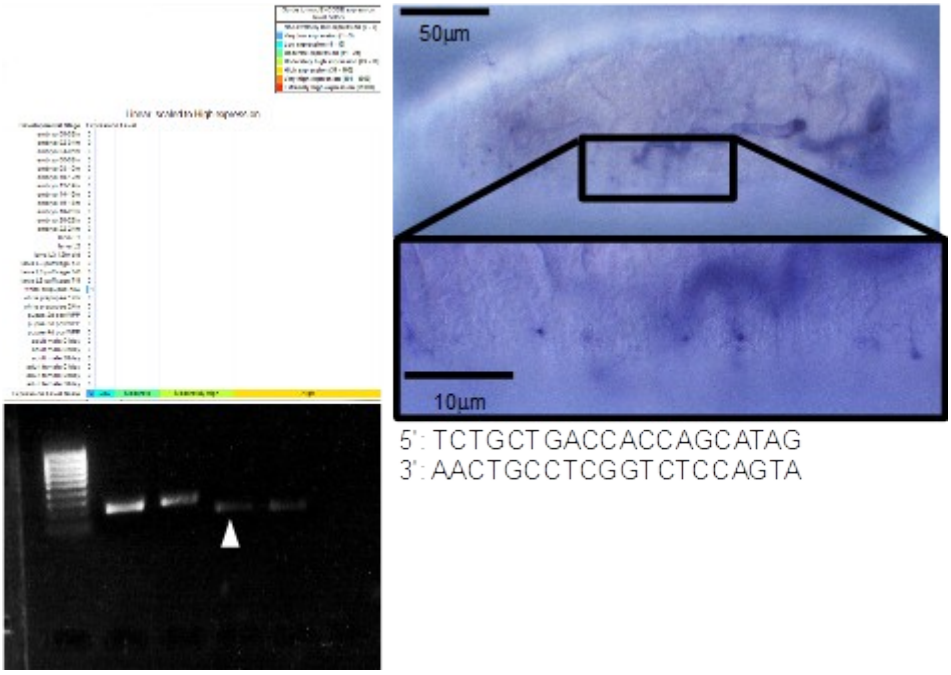

Supplementary Figure 21: *ppk21* expressed in late embryonic trachea. Current data for the expression of *ppk21* during embryonic development was retrieved from the modENCODE database (top-left), showing this gene not to be expressed in late embryogenesis. An *in situ* RNA probe was generated (bottom-left, sequence: bottom-right), and expression was observed in late embryonic trachea (top-right). However, this gene is not expressed in *dbd* neurons. The puncta observed in here are part of the tracheal system (see inset).

Supplementary Figure 22: *ppk22* is not expressed in late embryos. Current data for the expression of *ppk22* during embryonic development was retrieved from the modENCODE database (top-left), showing this gene not to be expressed in late embryogenesis. An *in situ* RNA probe was generated (bottom-left, sequence: bottom-right), and non-expression was confirmed in late embryos (top-right). Additionally, this gene is not expressed in *dbd* neurons.

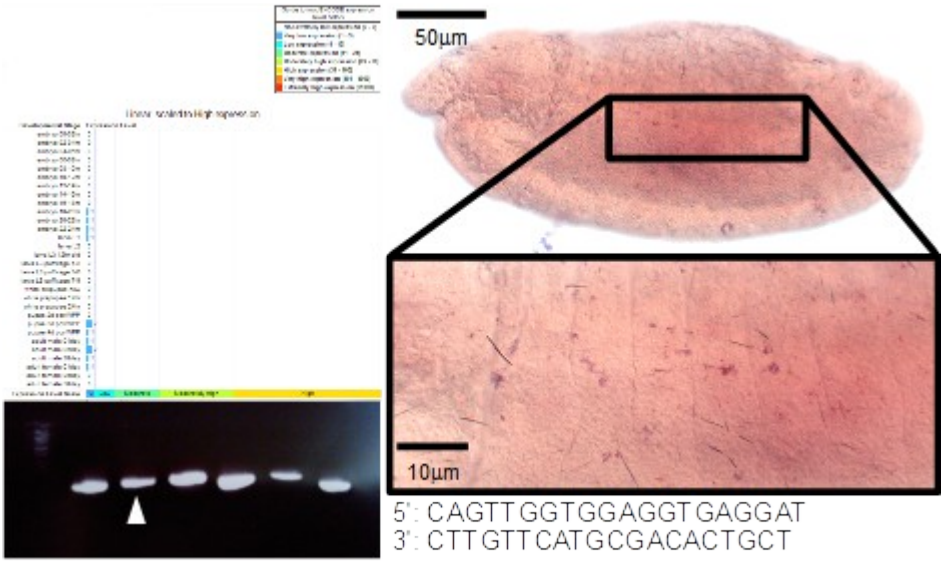

Supplementary Figure 23: *ppk23* may be expressed in late embryos. Current data for the expression of *ppk23* during embryonic development was retrieved from the modENCODE database (top-left), showing this gene to be expressed in late embryogenesis. An *in situ* RNA probe was generated (bottom-left, sequence: bottom-right), and punctate staining was seen in late embryonic abdomen (top-right and inset). However, this gene is not expressed in *dbd* neurons.

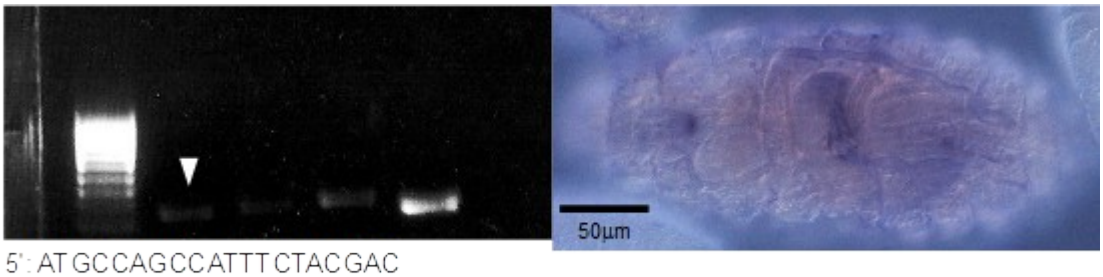

5': ATGCCAGCCATTTCTACGAC
3': CACTCATGCGATTCCTGGTA

Supplementary Figure 24: *ppk24* is not expressed in late embryos. An *in situ* RNA probe was generated for *ppk24* (top-left, sequence: bottom-left). However, *in situ* hybridisation for this gene in late embryos was negative (right), thus this gene is not expressed in *dbd* neurons.

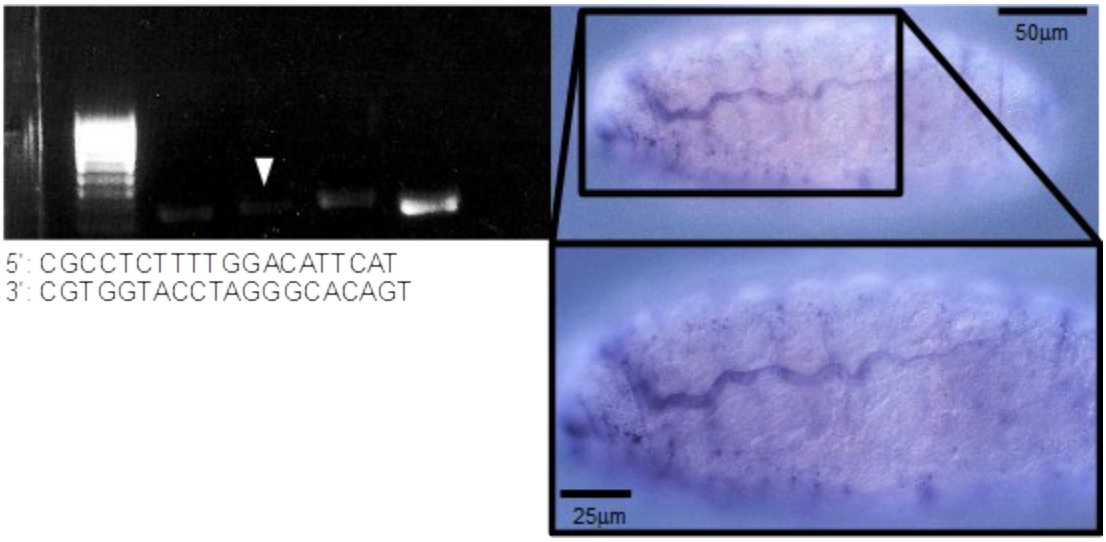

5': CGCCTCTTTTGGACATTCAT
3': CGTGGTACCTAGGGCACAGT

Supplementary Figure 25: *ppk25* is expressed in late embryonic trachea. An *in situ* RNA probe was generated (top-left, sequence: bottom-left), and expression was seen in late embryonic trachea (right). However, this gene is not expressed in *dbd* neurons (see inset).

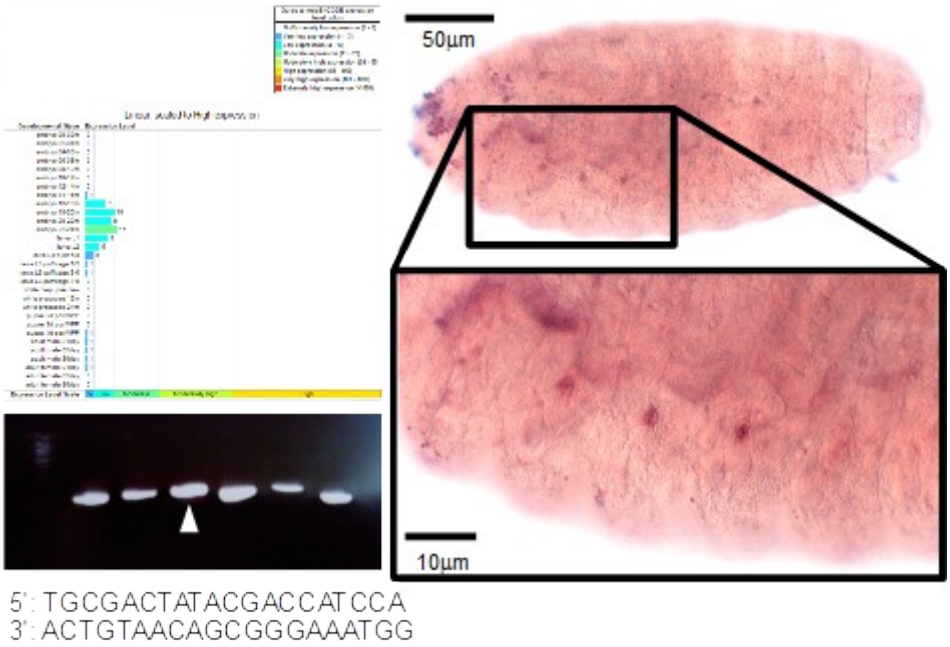

Supplementary Figure 26: *ppk26* is expressed in late embryonic sensory cells. Current data for the expression of *ppk26* during embryonic development was retrieved from the modENCODE database (top-left), showing this gene to be expressed in late embryogenesis. An *in situ* RNA probe was generated (middle-left, sequence: bottom-left), and punctate staining was seen in late anterior embryonic (top-right and inset). However, this gene is not expressed in *dbd* neurons.

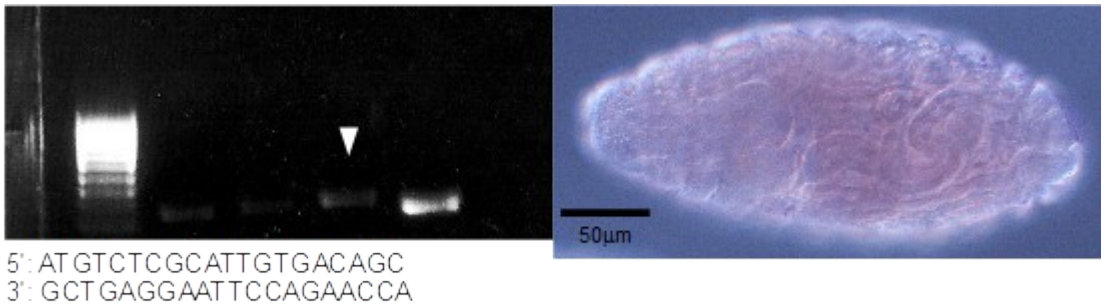

Supplementary Figure 27: *ppk27* is not expressed in late embryos. An *in situ* RNA probe was generated for *ppk27* (top-left, sequence: bottom-left). However, *in situ* hybridisation for this gene in late embryos was negative (right), thus this gene is not expressed in *dbd* neurons.

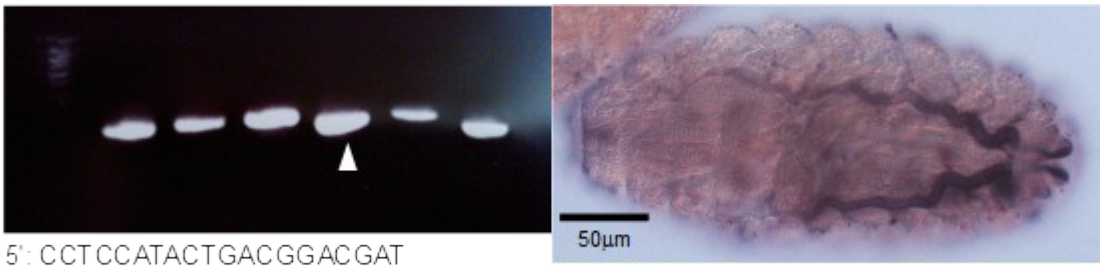

Supplementary Figure 28: *ppk28* is expressed in late embryonic trachea. An *in situ* RNA probe was generated (top-left, sequence: bottom-left), and expression was seen in late embryonic trachea (right). However, this gene is not expressed in *dbd* neurons.

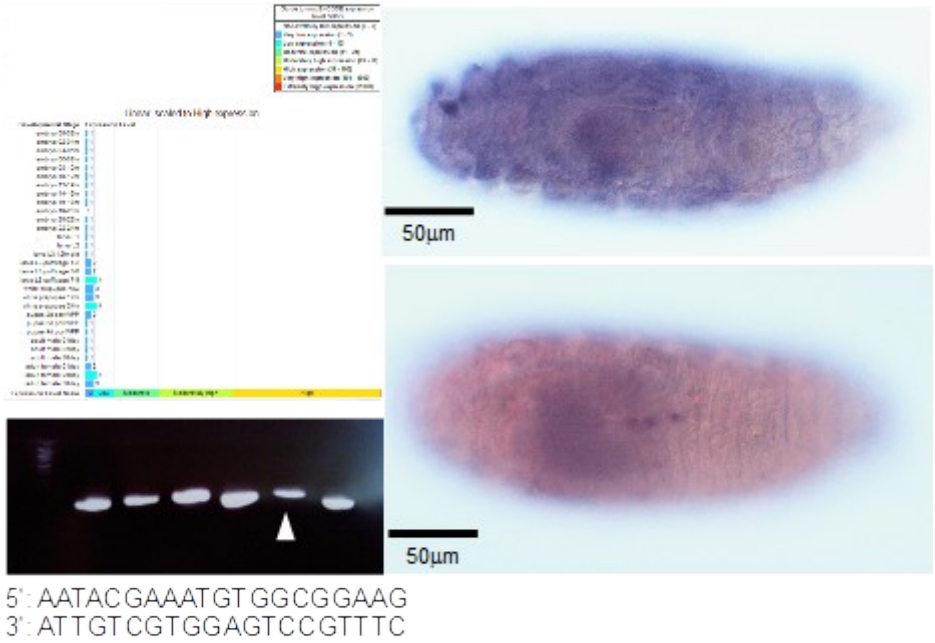

Supplementary Figure 29: *ppk29* is not expressed in late embryos. Current data for the expression of *ppk29* during embryonic development was retrieved from the modENCODE database (top-left), showing this gene to be slightly expressed in late embryogenesis. An *in situ* RNA probe was generated (middle-left, sequence: bottom-left), and non-expression was confirmed in late embryos (right). Additionally, this gene is not expressed in *dbd* neurons.

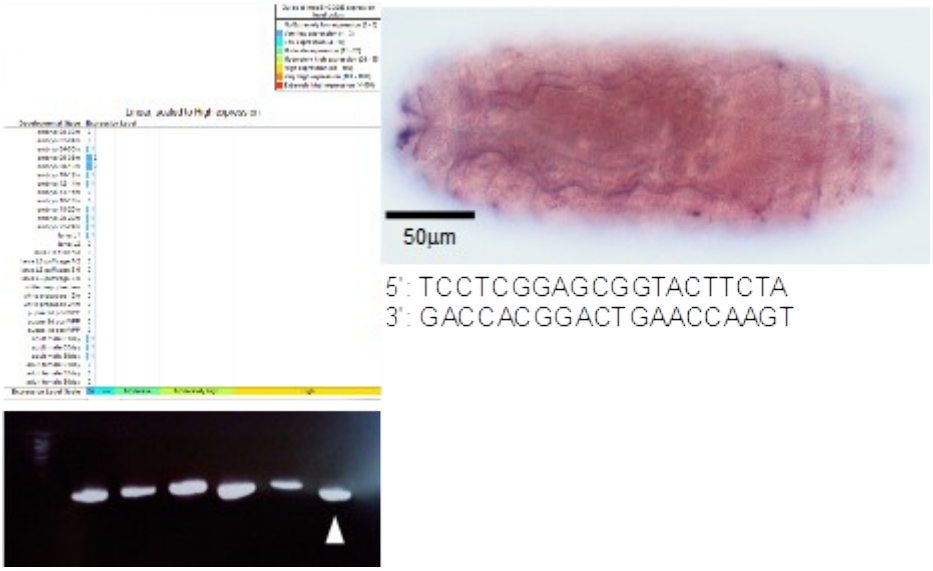

Supplementary Figure 30: *ppk30* is not expressed in late embryos. Current data for the expression of *ppk30* during embryonic development was retrieved from the modENCODE database (top-left), showing this gene to be slightly expressed in late embryogenesis. An *in situ* RNA probe was generated (bottom-left, sequence: bottom-right), and non-expression was confirmed in late embryos (top-right). Additionally, this gene is not expressed in *dbd* neurons.

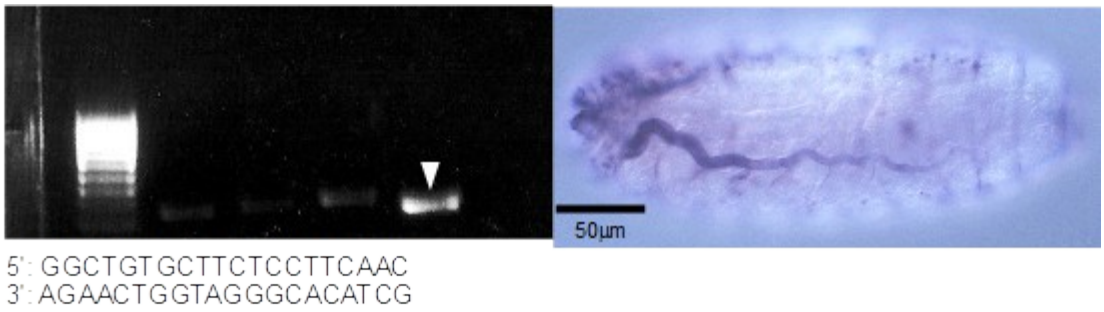

Supplementary Figure 31: *ppk31* is expressed in late embryonic trachea. An *in situ* RNA probe was generated (top-left, sequence: bottom-left), and expression was seen in late embryonic trachea (right). However, this gene is not expressed in *dbd* neurons.

Appendix iii. - Paper: Suslak, TJ., Armstrong, JD. & Jarman, AP., 2011. A general mathematical model of transduction events in mechano-sensory stretch receptors. *Network*. 22(1-4), pp.133-42

This paper summarises the early modifications that were made to the MSc. model, within the early stages of this project, adapting the model to begin to reproduce stretch-evoked receptor potentials of mammalian muscle spindles.

Network: Computation in Neural Systems
March–December 2011; 22(1–4): 133–142

informa
healthcare

A general mathematical model of transduction events in mechano-sensory stretch receptors

T. J. SUSLAK[1], J. D. ARMSTRONG[2], & A. P. JARMAN[3]

[1]*Doctoral Training Centre in Neuroinformatics and Neural Computation,* [2]*Institute for Adaptive and Neural Computation, and* [3]*Centre for Integrative Physiology, University of Edinburgh, 10 Crichton St., Edinburgh, UK*

(Received in final form 3 November 2011)

Abstract
Crayfish (*Astacus astacus*) muscle stretch receptors show strong homology to mammalian muscle spindles and bipolar neurons in *D. melanogaster*. All are typical, non-ciliated, stretch-sensitive, afferent neurons. Such receptors are observed in many species and perform an important sensory role. However, they are poorly characterised. A previous study reported a bio-mechanical and behavioural model of *A. astacus* stretch receptors, which used the principles of elasticity and tension in a spring to describe the adaptation of a mechano-sensory ending. This model described the changing mechano-sensory currents in the receptor when subjected to a stretch protocol. Here, we re-implement and extend this model. Notably, we introduce additional descriptions of voltage-gated channels that are suggested to contribute to stretch receptor mechano-transduction. Our model presents a more complete picture of the initiation of the mechano-receptor potential in response to a stretching stimulus. The inclusion of voltage-dependent sodium and potassium currents in addition to the initial mechano-sensitive sodium current allowed the model to account for most of the initial stretch response of the receptor. This preliminary model has potential for extension to describe fully the behaviour of non-ciliated mechano-sensors across species and predict the molecular mediators of mechano-transduction.

Keywords: *ion channel, mechanosensation, muscle spindle, stretch receptor, modelling*

Introduction

Mechano-sensation plays a key role in the ability of organisms to sense and interact with each other and their environment. Mechano-receptors detect mechanical stimuli such as tension, stretch and pressure. They have obvious roles in many

Correspondence: T. J. Suslak, Thomas Suslak, Informatics Forum, 10 Crichton St., Edinburgh, UK, EH8 9AB. E-mail: T.J.Suslak@sms.ed.ac.uk

ISSN 0954-898X print/ISSN 1361-6536 online/01/01-04000133–142
DOI: 10.3109/0954898X.2011.638967

forms of touch sensation, as well as proprioception and internal regulation (Hunt *et al.* 1978; Carr *et al.* 2001; Calabrese *et al.* 2002). Mechano-receptors are also involved in hearing, and they form an integral part of vertebrate auditory hair cells (Corey *et al.* 2004; Farris *et al.* 2004). Not only are mechano-sensory endings central to sensory modalities, but they also show a large degree of conservation between diverse animals.

Here we consider the non-ciliated stretch receptors, represented by type II sensory neurons in arthropods and muscle spindle cells in vertebrates. Such mechano-sensory endings have been studied in *Caenorhabditis elegans*, *Drosophila melanogaster*, *Astacus astacus*, *Trachemys scripta elegans* and *Rattus norvegicus*, amongst others (Rydqvist and Swerup 1991; Goodman and Schwarz 2003; Farris *et al.* 2004; Goodman *et al.* 2004; Simon *et al.* 2010). In all of these species, whilst individual stretch receptors are specialised for specific functions, there are underlying anatomical commonalities. These anatomical similarities suggest an evolutionary relationship between them, which in turn underpins the hypothesis that these endings share a common physiological mechanism (Bewick *et al.* 2005; Hamill, 2006). Nonetheless, beyond a couple of candidates for a primary mechano-transducer, little is currently known about the underlying physiology of stretch-sensitive endings.

An alternative approach to understanding stretch receptor function involves computational modelling. Predictions from modelling can be compared with experimental data recorded from stretch receptors. This approach has produced a model of the electrical behaviour of the mechano-sensitive response of type-II, non-ciliated stretch receptors of the crayfish *A. astacus* and *Pacifastacus leniusculus* (Swerup and Rydqvist 1996). This model was a significant step in understanding mechano-transduction.

Whilst an important first step, the model for crayfish stretch receptors was limited to describing the initial processes of mechano-transduction. The model described the contribution of a mechano-sensory sodium channel (MSC) in relation to the electrical adaptation of the afferent ending. It did not have the ability to describe any further components of this complex system, such as other ion channels known to be essential in mammalian spindle cells. As a result, the model had limited application in stretch receptors more generally.

In order to explore the utility of a mathematical model in describing the full response of a mechano-sensory ending, the mathematical relationships used in the original model were used to build a new model of a stretch-sensitive ending. Subsequently, extensions to the model were implemented to encode voltage-activated channels, which are also present in mechano-sensory endings.

Methods

Modelling stretch

The principle relationships used to model a stretch receptor are based on the model of Swerup and Rydqvist (1996). The equations below are numbered to correspond to the stages detailed in the accompanying diagram (Figure 1). The crayfish stretch receptor was mathematically described as an adapting spring, with a linear

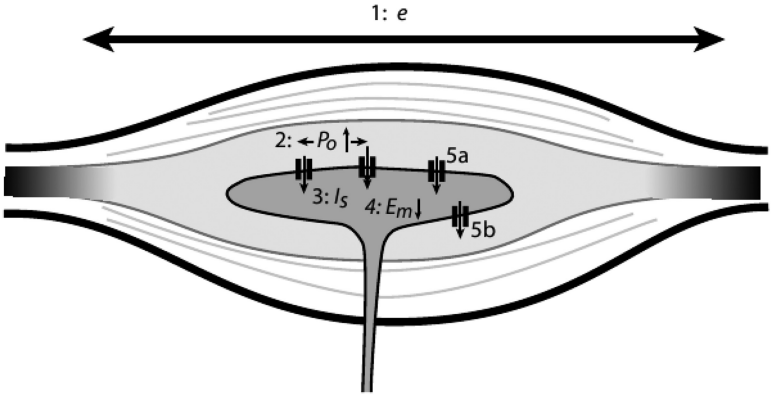

Figure 1. Diagrammatic representation of the stretch receptor model.
When a stretch stimulus is applied, the muscle extends by length e (1) and the afferent ending experiences a proportional tensile force. Mechano-sensory sodium channels (MSCs) in the ending are gated according to this tension, with higher tensions increasing MSC open probability. As the open probability increases, more MSCs are likely to be open (2). As more MSCs open, sodium enters the ending generating a mechano-sensory current (3) and depolarising the ending, (4). This depolarisation activates voltage-gated sodium channels in the ending (5a) and voltage-dependent potassium channels (5b), which are later components of the stretch-initiated response.

component in series with a Kelvin-Voigt element (Swerup and Rydqvist 1996). These were mathematically linked to the open probability of a mechanically-gated sodium channel (MSC). Principally, the tension in the receptor (σ_m) varies with the extension (e), given by:

$$\sigma_m = k \cdot e_2 = k_2 \cdot e_2^{n+1} = k_1 \cdot e_1 + B \cdot \frac{\mathrm{d}e_1}{\mathrm{d}t} \tag{1}$$

where e_1 is the linear component of the extension, representative of the tension in the inelastic, tendinous capsule of the receptor, e_2 is non-linear, representing the elastic components of the receptor, such as the membrane and muscle [$e = e_{linear} + e_{non\text{-}linear}$, k] is a non-linear parameter relating tension and extension, k_2 is a non-linear spring constant (2,200 kPa), k_1 is a linear spring constant (400 kPa), B is the Dashpot constant of the Kelvin-Voigt element (12kPas) and n is a power constant for the non-linear spring (1.5).

Modelling the MSC adaptation

Within the ending, the open probability (P_0) of the MSCs is dependent on the tension in the muscle according to the following:

$$P_O = \frac{1}{\left(1 + k_b \cdot \exp\left[-s \cdot \left(\frac{\sigma_m}{m}\right)^q\right]\right)} \tag{2}$$

where k_b is a Boltzmann constant of the MSC (106), s is the MSC sensitivity constant (0.00277 Pa-1) and m is a tension conversion factor (25). This relationship

describes the likelihood of MSCs being open for a given extension of the receptor. The current flowing through these channels is therefore:

$$I_s = P_O \cdot g \cdot (E_{rest} - E_{srev}) \tag{3}$$

where g is the maximum channel conductance (2.5mS) E_{rest} is the resting membrane potential (−65 mV) and E_{srev} is the MSC reversal potential (10 mV). Finally, the membrane potential can be calculated as:

$$E_m = E_{rest} - \frac{[(\{1 + k_b \cdot \exp[-s \cdot (\sigma - \sigma_0)^q]\}^{-1}) \cdot I_s + g_{sleak} \cdot (E_{rest} - E_{srev})]}{C_m} \tag{4}$$

where q is a power constant (1) and C_m is the membrane capacitance (4.3nF).

Modelling voltage-gated channels

All the above equations and constants are as stated by Swerup & Rydqvist (1996). In order to determine whether voltage-gated channels could be incorporated into this model, mathematical descriptions of neuronal, voltage-gated sodium channels (VNaCs) and potassium channels (VKs) (Angelino and Brenner 2007; Platkiewicz and Brettle 2010) were incorporated. Specifically:

$$g_{Na} = \frac{P_V \cdot (NaE_{rev} - E_m) + g_{leak} \cdot (E_{leak} - E_m)}{C_m \cdot E_m} \tag{5}$$

where NaE_{rev} is the VNaC reversal potential (50 mV), g_{leak} is the VNaC leak conductance (8pS), E_{leak} is the membrane leak potential (−75 mV) and P_V is the VNaC open probability, *i.e.,* the likelihood of a voltage-gated channel opening at a particular membrane potential, which is:

$$P_V = \frac{1}{1 + \exp\left(\frac{(E_m - E_{act}) \cdot \sigma_{Na}}{k_{Na}}\right)} \tag{6}$$

where E_{act} is the VNaC activation potential (−50 mV), k_{Na} is a VNaC activation constant (6) and σ_{Na} is a function of the VNaC time constant, expressed as:

$$\sigma_{Na} = 1 - \exp\left(\frac{-t}{\tau_{Na}}\right) \tag{7}$$

where τ_{Na} is the VNaC time constant (10) and t is time. The VK channels were modelled similarly with corresponding constants ($KE_{rev} = -100$ mV, $K_{leak} = 2$nS, $K_{act} = 5$ mV, $k_K = 5$, $\tau_K = 10$).

Implementation of the model

Mathematical descriptions of the crayfish stretch receptor were encoded in Matlab®. All constants required for the simulation were established at the start of the programme. The stretch protocol was simulated as an incremental increase in receptor length (extension) over 100 iterations. The extension-dependent relationships were encoded within a *for* loop that updated the extension and all of the dependent relationships, at every iteration. Conditional statements added within

this loop encoded the voltage-dependent components, with these items becoming activated if the model should enter a pre-defined condition. These conditions may be set by the experimenter within the model. The hold and relaxation phases are similarly modelled over 100 iterations and contain identical instructions with the exception of the commands pertaining to the extension of the receptor. All variables, including time, extension rate and the value of all other parameters, are fully modifiable using a standard text editor.

Results

Initially, we reproduced the model of Swerup and Rydqvist (1996) using Matlab®, although we incorporated a modified representation of the stretch stimulus (see below). This model demonstrated the key features of the original model (Figure 2). It exhibited the stretch-induced depolarisation in the receptor, the post-stretch repolarisation observed in the hold phase, and the full repolarisation consistent with the relaxation response, restoring the receptor to its resting potential. However, we also observed closer correspondence with the original, physiological recordings with our model than the previous model. For the stretch rates simulated ($a = 0.01{:}0.03$) depolarisation of the modelled ending is observed from rest in accordance with that seen in the original model (our model: 0–45 mV; original model: 0–60 mV; recordings: 0–40 mv). Upon entering the hold phase, the dynamic component of the stretch is removed and the potential declines with the tension until it reaches the hold potential (new model: consistent -2 mV to -3 mV; old model: scaled between -15 mV at long stretch, -2 mV to -3 mV at short stretch; recordings: consistently *c.*-5 mV). This may be due to our modified method used to simulate the stretch length. Whilst the original model used a percentage increase in receptor length to simulate stretch, we modelled the stretch as a constant rate of length increase. Therefore, unlike the original, the absolute stretch is the same for all initial receptor lengths. This method may be more readily applicable to different receptors in different-sized organisms, allowing a single stretch value to be applied to data from a variety of receptors.

The experimental data used to characterise the original model was obtained from crayfish stretch receptors in the presence of TTX and TEA to abolish voltage-gated currents (Rydqvist and Swerup 1991). This allowed MSC-dependent depolarisation to be targeted for analysis and modelling. However, under normal conditions (in the absence of TTX and TEA), a voltage-gated component of receptor adaptation can be observed (Ottoson and Swerup 1984). This component presents itself as a sharp, rapid depolarisation (20 mV) in addition to the initial MSC-dependent depolarisation (30–40 mV). This inward current then rapidly inactivates and the membrane potential returns to the level mediated by MSC-dependent depolarisation alone (Figure 3, left). Therefore, we extended the model to include terms describing neuronal VNaCs and VKs, based on known physiological characteristics (Angelino and Brenner 2007; Platkiewicz and Brettle 2010). This augmentation of the model enabled it to mimic previously recorded electrophysiological data from the crayfish receptor, determined in the absence of TTX and TEA (Figure 3, right). In addition to the mechano-sensory depolarisation (for $a = 0.025$), the augmented model suggests that voltage-gated channels can be activated by the MSC-mediated

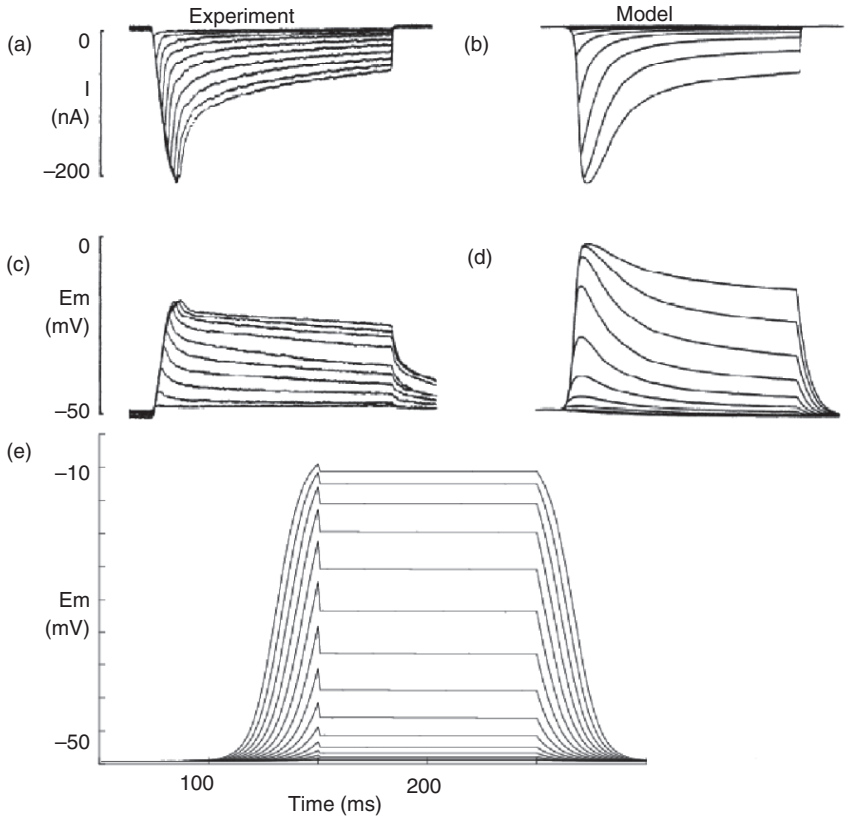

Figure 2. The model accurately reflects *in vivo* recordings.
Experimental recordings from the same receptor cell (*a* and *c*) were originally modelled (*b* and *d*), accurately reproducing the behaviour observed *in vivo* (Swerup and Rydqvist 1996). These traces were mimicked in the re-implementation (*e* – current data not shown). The re-implementation was achieved in Matlab® through the use of the original equations and the same empirically derived constants used to produce the original model (Swerup and Rydqvist 1996). Stretches are between 10 and 30 μm/ms.

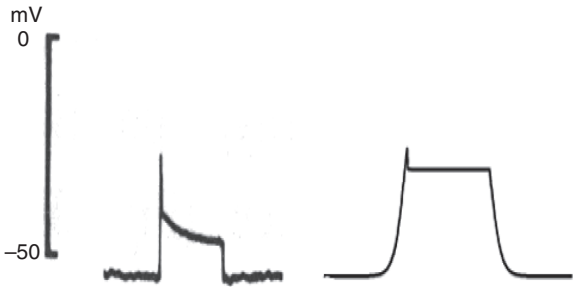

Figure 3. The bio-mechanical model of stretch receptors was expanded to include voltage-gated channels.
Experimental recordings from crayfish stretch receptors, in the absence of voltage-gated channels (a) demonstrate the electrically dependent response of the receptor following stretching (stretches of 25 μm/ms) (Ottoson and Swerup 1985). This is mimicked in the implementation of voltage-gated channel components in addition to the initial bio-mechanical model (b).

depolarisation. This results in an initial overshoot with a depolarisation of 25 mV, which subsequently falls off, following VNaC inactivation, to the level of the sustained MSC potential (−40 mV) for the duration of the hold phase (Figure 3).

We then explored whether this model could be expanded to address the mammalian muscle spindle system. This receptor expresses certain differences in its physiology compared to its crustacean counterpart. In particular, mammalian muscle spindle cells operate under different environmental conditions. This was addressed by employing a longer stretch protocol (0.1 mm/ms) to resemble more closely the mammalian system. Previous studies in the electrical behaviour of mammalian muscle spindles have demonstrated that the ending initially depolarises, as with the crayfish, but this is not then followed immediately by a return to the hold potential. Instead, the initial depolarisation is followed by a subsequent after-repolarisation and after-depolarisation (Hunt *et al.* 1978). Using the modified stretch protocol, we were able to model the initial depolarisation, as expected. In addition, the model exhibited subsequent, smaller depolarisations from the hold potential occur (+15mV from hold), resulting in a potentiated supra-hold potential (Figure 4)

Discussion

Previously, it was shown that the bio-mechanical properties of crayfish stretch receptor mechano-transduction could be modelled with respect to the MSCs within these afferent endings (Swerup and Rydqvist 1996). This was the first attempt to simulate the actual events of transduction as opposed to using a simple input-output approach (Borsellino *et al.* 1965). We recreated the bio-mechanical model of the crayfish stretch receptor in a new format and extended it. The original model had

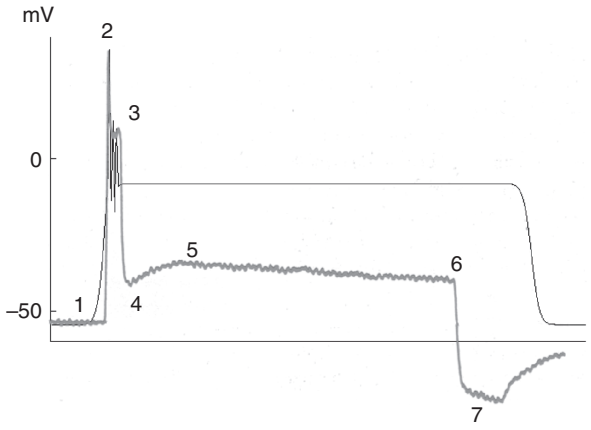

Figure 4. Adapting the model with mammalian-like parameters accurately reflects mammalian recordings.
Recording of a mammalian muscle spindle preparation shows a characteristic depolarisation (2), after-repolarisation and after-depolarisation (3) (grey, adapted from Hunt et al. 1978). The model (black) reproduces this. However, the model currently lacks accurate characterisation of the hold and release phases (4–7) and so these phases of the trace differ (for example, the higher-than-normal plateau in the hold phase).

been shown to be an accurate model of the initial transduction events within the crayfish stretch receptor. By including terms describing neuronal voltage-gated channels, it has been possible to reproduce further events in the primary mechano-transduction process. Nevertheless, electrophysiological studies suggest that mechano-transduction is a complex process involving many more mediators in addition to those modelled here. We anticipate that our model will be suitable for adaptation in the future to accommodate these. By utilising the empirically derived constants that were originally used to parameterize a similar model and incorporating them appropriately into the relationships given, it is possible to produce accurate representations of the mechano-sensitive stretch response observed in the crayfish stretch receptor. Future work will also be aimed at exploring these parameters further to determine their effect on the model's performance.

There are two key differences in the output of our extended model compared with the original, MSC-centred model. First, we note that the new model focuses primarily on the initiation of the stretch response and hence there is a sharp drop in the potential at the beginning of the hold phase, as approximations are used to frame the rest of the model. Nonetheless, the new model reports a similar hold potential to the original for equivalent stretches. Therefore it is reasonable to maintain that, with additional tuning of this phase of the model, it would behave as the original in this regard. However, the new model appears to represent the original physiological data better in terms of the depolarisation values and the drop-off in potential following the end of the first dynamic phase. We suggest that this is due to new means of implementing the simulated stretch. Secondly, the original model effectively employs an instantaneous stretch stimulus, whereas we used a stimulus that operates over a period of time steps. Consequently, there is a delay in depolarisation apparent in the new model (*cf.* Figure 2d) that is not present in the original. However, the potential reported at the end of the dynamic phase is similar in both the new model and the original recordings.

Likewise, when a VNaC component is added to the model, the results mimic the observed physiological data. From the model, the post-stretch voltage-dependent depolarisation can be seen as an initial sharp voltage increase, and this is clearly also present *in vivo*.

With a small modification, the model was also able to produce key qualitative features of electrophysiological recordings in mammalian muscle spindles. The model demonstrates the presence of the initial stretch- and voltage-mediated depolarisation of comparable amplitude with the *in vivo* recordings of Hunt *et al.* (1978). Additionally, the model shows other characteristic features of the muscle spindle electrical profile, namely the after-repolarisation and after depolarisation (Figure 4, points 2–3).

Of note in all of the model predictions is the higher-than-expected plateau potential during the hold phase of the simulation. We postulate that this is due to the presence of additional ion channels in the afferent ending that our model does not currently include. In particular, we anticipate a mechano-sensory potassium channel or other voltage-gated potassium channel that is active during the hold phase, which results in this reduced hold potential. This high hold potential is also present in the mammalian simulation. The results here indicate a holding potential approximately 20 mV higher than is recorded in the muscle spindle and 10 mV higher than the crayfish recordings (immediately after cessation of dynamic stretching).

Compared with our current model, stretch receptors therefore exhibit an increase in potassium conductance approaching an additional 50%. However, it is also clear from further simulations that this phenomenon is a separate entity to the existing potassium components of this model (data not shown). We also note that crayfish and muscle spindle recordings both show a decay in the hold potential with time, which our model does not yet account for.

Therefore our model currently suggests that it is likely that further potassium components are present *in vivo*, mediating the lower hold potential as well as a post-release hyper-polarisation. In addition, experimental studies suggest a role for calcium in the stretch response (Hunt *et al*. 1978 Ottoson and Swerup 1984; Bewick *et al*. 2005; Simon *et al*. 2010). These processes are yet to be modelled. In summary, our model, although preliminary and requiring more extensive validation especially against other species, demonstrates the potential ability to describe a general class of model for mechano-transduction events in non-ciliated, primary, stretch-sensitive afferent neurons across different species. Moreover, it supports the hypothesis that these receptors may indeed share a common physiological mechanism.

Acknowledgements

Many thanks to B. Rydqvist for supplying the material used in the original paper which formed the basis of this work. This research was carried out with funding from EPSRC as part of the Doctoral Training Centre at the University of Edinburgh.

References

Angelino E, Brenner MP. 2007. Excitability constraints on voltage-gated sodium channels. PLoS. Comput Biol 3:1751–60.

Bewick GS, Reid B, Richardson C, Banks RW. 2005. Autogenic modulation of mechano-receptor excitability by glutamate release from synaptic-like vesicles: evidence from the rat muscle spindle primary sensory ending. J Physiol 562:381–94.

Borsellino A, Poppele RE, Terzuolo CA. 1965. Transfer functions of the slowly adapting stretch receptor organ of Crustacea. Cold Spring Harb Symp Quant Biol 30:581–6.

Calabrese B, Tabarean IV, Juranka P, Morris CE. 2002. Mechanosensitivity of N-type calcium channel currents. Biophys J 83:2560–74.

Carr MJ, Gover TD, Weinreich D, Undem BJ. 2001. Inhibition of mechanical activation of guinea-pig airway afferent neurons by amiloride analogues. Br J Pharmacol 133:1255–62.

Corey DP, García-Añoveros J, Holt JR, Kwan KY, Lin SY, Vollrath MA, Amalfitano A, Cheung ELM, Derfler BH, Duggan A, et al. 2004. TRPA1 is a candidate for the mechanosensitive transduction channel of vertebrate hair cells. Nature 432:723–30.

Goodman MB, Lumpkin EA, Ricci A, Tracey WD, Kernan M, Nicolson T. 2004. Molecules and mechanisms of mechano-transduction. J Neurosci 24:9220–2.

Goodman MB, Schwarz EM. 2003. Transducing touch in *Caenorhabditis elegans*. Ann Rev Physiol 65:429–52.

Hamill OP. 2006. Twenty odd years of stretch-sensitive channels. Pflugers Arch -Eur J Physiol 453:333–51.

Hunt CC, Wilkinson RS, Fukami Y. 1978. Ionic basis of the receptor potential in primary endings of mammalian muscle spindles. J Gen Physiol 71:683–98.

Ottoson D, Swerup C. 1985. Ionic dependence of early adaptation in the crustacean stretch receptor. Brain Res 336:1–8.

Platkiewicz J, Brette R. 2010. A threshold equation for action potential initiation. PLoS Comput Biol 6:e1000850.

Rydqvist B, Swerup C. 1991. Stimulus-response properties of the slowly adapting stretch receptor neuron of the crayfish. Acta Physiol Scand 143:11–9.

Simon A, Shenton F, Hunter I, Banks RW, Bewick GS. 2010. Amiloride-sensitive channels are a major contributor to mechano-transduction in mammalian muscle spindles. J Physiol 588:171–85.

Swerup C, Rydqvist B. 1996. A Mathematical Model of the Crustacean Stretch Receptor Neuron. Biomechanics of the Receptor Muscle, Mechanosensitive Ion Channels, and Macrotransducer Properties. J Neurophysiol 76:2211–20.